APPLICATION OF LOCAL POROSITY TO DEFINE PORE NETWORKS AND PORE GEOMETRY IN SOILS: A CASE STUDY ALONG A CARBON DIOXIDE AND TEMPERATURE GRADIENT

by

HYEN CHUNG CHUN

A dissertation submitted to the

Graduate School-New Brunswick

Rutgers, The State University of New Jersey

In partial fulfillment of the requirements

For the degree of

Doctor of Philosophy

Graduate Program in Environmental Sciences

Written under the direction of

Dr. Daniel Giménez

And approved by

_____

_____

_____

_____

New Brunswick, New Jersey

May, 2009

ABSTRACT OF THE DISSERTATION

Application of Local Porosity to Define Pore Networks and Pore

Geometry: A Case Study of Pore Morphology Along A Carbon Dioxide

and Temperature Gradient

By HYEN CHUNG CHUN

Dissertation Director:

Dr. Daniel Giménez

Pore network models are useful tools to investigate soil pore geometry. These models provide quantitative information of pore geometry from 3D images. However, there are limitations in image sizes and resolutions to extract networks. This study presents a modified pore network model to characterize large images with local porosity. The objectives of this work were to apply the modified model to characterize pore structure from large images at different scales (aggregate and soil column), image sizes, and resolutions and to characterize changes in pore structure induced by different levels of CO_2 and temperature. Soil samples were taken from three sites (urban site with the highest, suburban with intermediate and rural with the lowest CO_2 concentration and temperature). Undisturbed columns (5.5 cm in diameter and 12 cm in height) and aggregate samples were taken from each site and scanned with a computer tomographer at resolutions of 22 (column) and 6 microns (aggregates).

Pore networks were extracted by medial-axis transformation from local porosities at a unit cell and were used to measure pore geometry from aggregates and bulk soils. Three image volumes and 12 cell sizes were used to define image and cell size scaling effects. The configuration entropy and universal multifractals were employed to characterize pore spatial distributions, and water retention and hydraulic conductivity were measured on bulk soils.

Pore numbers and pore volumes measured in soil columns and aggregates had a linear relationship in log-log plots across cell sizes, while pore length and tortuosity did not show any specific trend. These results imply that some properties cannot be accurately projected to different scales within aggregate and laboratory scales.

Pore spatial distribution in bulk soils from all three sites and pore geometry information from aggregates and bulk soils of urban and rural site showed that different level of CO_2 and temperature affected pore structure formations. Pores from urban site were more widespread and were greater than rural site. Hydraulic properties confirmed that urban soil had more connected and less tortuous pores than rural soil.

The modified pore network model is a powerful tool to characterize pore properties from large size images.

Acknowledgments

First, I would like to thank my mentor and advisor, Professor Daniel Gimenez, for his support and scientific encouragement during my doctoral studies. He has trained and guided me to achieve my goals in this study. I have been inspired by his wide range of knowledge and experience, and I hope that I continue to learn from him as a scientist.

Next, I am very grateful to the members of my committee, Drs. Ying Fan Reinfelder, Weilin Huang, and Richard Heck. I appreciate the time spent by them on my dissertation and their valuable remarks.

I thank my family. My parents and husband, Jiwhan, have been patient and silently supporting me over years. I am grateful to their unconditional love and support.

I would like to thank all laboratory members who became my friends, especially, SungWon. I also wish to acknowledge Dr. Lewis Ziska and Kate George from Agricultural Research Service, United States Department of Agriculture, for providing soil samples and sampled site data for this study.

Table of Contents

vi

List of Tables

List of Figures

List of Symbols

Chapter 1 : Introduction

1.1 Climate Change

The carbon dioxide (CO_2) concentration of the atmosphere has been steadily rising due mainly to burning of fossil fuels (International Panel on Climate Change, IPCC, 200). Furthermore, global warming seems to be an inevitable consequence of increasing concentrations of greenhouse gases in the atmosphere. Depending on scenarios of energy use coupled with population growth, prediction are that CO_2 concentration could increase up to 940 parts per million by 2100, which could lead to a mean surface global warming up to 5.8 °C (IPCC, 2007).

A large number of studies have been conducted to assess responses of various types of ecological systems to elevated CO_2 concentration and temperature.

1.2 Effects of Climate Change

Increase in emission of greenhouse gases has raised atmospheric CO_2 concentration and temperature, which, in turn, have affected entire ecosystems (Niklause et al., 2001). Figure 1.1 summarizes the effects of elevated CO_2 concentration and temperature on soil systems and Table 1.1 describes changes of ecological components under elevated CO_2 concentration and temperature. If atmospheric CO_2 concentration and temperature were to increase as climate models predict, soil C input would increase while plant transpiration rate would decrease (De Graff et al., 2004). This would lead to increases in soil moisture and microbial activity (Morgan et al., 2004). Under these conditions, plant roots and soil microbes are stimulated, which would prompt responses in mineralization and decomposition of C and N in soil (Zak et al., 2000).

However, inhibitions of root growth and microbial activity have been reported under elevated CO_2 concentration and temperature (Arnon et al., 2000; Barnard et al.,

2004; Wan et al, 2004). One explanation for these contradictory responses is that different species of plant roots and microbes react differently to climate change (King et al., 1996). Increases in CO_2 concentration and temperature stimulate microbial N consumption. This leaves less N for plant uptake, so plant growth will be limited (Zak et al., 2000).

Soil biota, microbes and roots affect processes of aggregation and aggregate stability. So far, soil aggregate stability and aggregate sizes have been investigated under elevated CO_2 concentration or temperature separately. Under warming condition, a decrease in biological activity results in decrease of aggregate stability and under elevated CO_2 concentration, aggregate sizes shifted to smaller sizes (Rillig et al., 2001; Rillg et al., 2002; Eviner and Chapin, 2002). However, this changes in soil properties may be caused by other factors in soil than the climate change. For example, the partial pressure of CO_2 in the soil air may differ greatly from that in the atmosphere. Plant roots and soil biota respiration can induce a 2 to 3 fold increase in CO_2 concentration over the level found in the atmosphere (Davison et al., 2004). However, Amundson and Davidson (1990) found that there is correlation between soil CO_2 concentration and atmospheric CO_2 concentration. They also reported that soil CO2 concentration variations are the smallest near soil surface. In this study, concentrations of soil CO_2 were not measured, but soil samples were taken from the surface where concentrations of soil CO_2 are more likely to mirror the concentrations in the atmosphere. Moreover, since changes in soil CO_2 concentration occur in response to changes in plant root or soil biota induced by climate change (Fig. 1.1), it is reasonable to assume that changes in soil properties are

caused directly and indirectly by changes in atmospheric CO_2 concentration and temperature.

Based on previous studies, it is reasonable to expect changes in pore structure induced by changes in the amount and activity of roots and soil biota. For instance, soil aggregate stability would increase if the levels of soil moisture are enough to sustain root and microbial growth. In turn, this would lead to more development of inter- and intra-aggregate pores. To date, there has been no report of soil pore structure changes under enriched CO_2 concentration and higher temperature. To find changes in soil structure induced by climate change, soil structure should be characterized by image analyses, since image analyses provide relatively accurate and quantitative descriptions of soil structure and pore geometry. However, image analyses have been performed at pore scale from small sizes of soil samples. VandenByganrt and Protz (1999) tested representative image size for image analyses and found that image areas of less than 7 cm^2 are sufficient to characterize pore parameters. Soil properties measured from small samples or images should represent properties of larger areas. To solve this problem, scaling of soil properties should be considered.

1.3 Scales and Scaling

Soil structure is heterogeneous across a wide range of scales (Dexter, 2002). Therefore, any measurement of soil structure should consider sample size, since soil structure and properties have variations across scales. Practical concerns regarding soil properties, such as water movement or contaminant transport through soil, are typically at the field or regional scales (Dane and Hopmans, 2002) (Fig.1.2), but measurements to characterize soil properties are made on relatively small samples (aggregates or small

columns). Soil properties measured on aggregate or small column (laboratory scale) are relatively accurate and cheaper to make than measurements at the field scale (Hopmans et al., 2002). Changes in ecological components have been observed at laboratory or aggregate scale (Table 1.1). There has been no report of climate effects on soil structure measured at micro scale.

Observations at the micro scale can be useful to estimate measured properties at larger scale, in particular if those observations could be scaled. The term scaling refers to using information from one scale to infer information at another scale (Fig. 1.2). Scaling implies that there is a relationship among the values of measured properties across scales.

1.4 Morphological Image Analyses

Morphological analyses from three dimensional images have been developed recently as computer tomography developed. Pore network models are used to quantify pore geometry from three dimensional porous images (Taina et al., 2008). Pore network models were introduced by Fatt (1956) who considered pore-body objects and linking channels (throats) between those pores to describe connectivity. Each pore-body object was considered as spheres and throats as cylinders to calculate length and diameter. Although a network model can be developed in two- or three- dimensions, two-dimensional networks cannot provide a good representation of three-dimensional systems, such as soil, because of their inability to provide a complete representation of the connectivity of pores (Chatzis and Dullien, 1977).

Pore network models represent pore space with simplified geometries (skeletons) and there are two ways to extract skeleton structure (Luo et al., 2008). One is the thinning algorithm and the other is the medial-axis transformation (Fig. 1.3).

The thinning algorithm is obtained by a successive erosion of pixels from the boundary of each slice (Vogel and Roth, 2003; see Fig. 1.3). Subsequently, the skeleton structure is constructed by connecting the center nodes (pixels remaining after thinning) in each slice. The thinning algorithm has been applied to measure volume (Langmaack et al., 1999), length (Bastardie et al., 2003), tortuosity (Langmaack et al., 2002), and continuity (Capowiez et al, 1998) of soil pores. The thinning algorithm is a useful tool to measure properties of pores, but it considers every node as a pore-body node without considering throats, possibly resulting in incorrect measurements of pore properties.

The alternative method to thinning is the medial-axis transformation (Fig. 1.3). One of its characteristics is the measurement of the distance from the pore boundaries as thinning occurs (Al-Roush and Willson, 2005). Computation starts from the boundary to the center of a pore assigning distance information to each voxel (Lindquist et al., 1996). The medial-axis algorithm allows a pore to be separated into pore-body and throat based on distance information during the thinning and provides accurate geometry of natural pore system (Al-Roush and Willson, 2005; Peth et al., 2008).

The size and resolution of the images that can be resolved with either pore network model are limited because the techniques are computationally demanding. To overcome these limitations, pore network models need to be improved.

1.5 Concept of Local Porosity Distribution Analysis

Pore structure can also be characterized by measuring the porosity in cells of a regular shape and various sizes (Hilfer, 1992). Commonly, cubic shape cells are imposed on three dimensional images and the porosity of each cell is collected. The distribution

of local porosities is affected by cell size (Lin and Hourng, 2005), with greater variation at small cell sizes than at larger ones.

Local porosity has been used to characterize spatial distribution of inter-aggregate pores (Wong and Wibow, 2000; Cislerova and Votrabova, 2002) and to simulate pore structure of soil (Masad and Muhunthan, 1997). Hu and Stroeven (2005) used distributions of local porosity to measure connectivity of pores in three dimensional images of cement material. They calculated local porosity at a series of cell sizes and defined a pore by connecting two or more adjacent cells having porosity greater than 45%.

The spatial distribution of local porosity can provide an accurate representation of three dimensional pore spaces in soil (Biswal et al., 1998). Local porosity can also be a useful tool to define scaling effects on pore system (Hilfer, 1992). Pore network models applied to local porosities rather than to individual voxels would make possible to measure pore geometry in large images because it would reduce the number of data point to handle and the local porosity distribution itself was proven effective to quantify pore geometry (Hu and Stroeven, 2005).

1.6 Hypotheses and Objectives

There is a need to calculate pore morphological properties from three dimensional images with less demanding techniques than presently available, therefore in this study, medial-axis transformation was applied to local porosity calculated at a series of cell sizes. In addition, medial–axis transformation was used to define networks of soil pores. This modification would minimize time and computer capacity needed to measure pore morphological properties from large size images. Moreover, medial–axis algorithm

would provide more complete analyses of pore morphology than other pore network models such as the thinning algorithm.

As discussed above, while other ecological components have been investigated (Table 1.1) soil structure has not been studied under conditions of atmospheric CO_2 concentration and temperature gradients,. The study of soil structure would help understand changes in soil properties, such as soil moisture or conductivity. These properties are directly related to plant water in soil and water transport through soil, and eventually to processes that affect land managements and human lives. Therefore, it is important to find climate effects on soil structure and related soil properties. The first hypothesis of this work was a gradient in atmospheric CO_2 concentration and temperature would induce changes of spatial distributions of pores. The second hypothesis was that gradient in atmospheric CO_2 concentration and temperature would result in changes of pore morphological properties. This hypothesis was tested using aggregate and column (bulk) soil samples. Hydraulic properties were measured in greatersoil sample sizes than the sample size for image analyses. To compare and match the properties from measurement of hydraulic properties and image analyses, it is critical to find scaling effects on so pore geometry. However, scaling effects have not been studied vigorously, because there are limitations in obtaining various scales of soil samples. This study applied local porosities on soil images to overcome these limitations and define detailed scaling across the aggregate and laboratory scales. The third hypothesis was that soil structure and pore geometry would have vary at different scales. The second hypothesis was

The primary objectives of this study were

1.   Developing a pore network model coupled with local porosity to measure pore morphological properties.

2.   Characterization of pore spatial distributions in soils sampled along a gradient in atmospheric CO_2 concentration and temperature.

3.   Characterization of pore morphologies and hydraulic properties in soils sampled along atmospheric CO_2 concentration and temperature gradient.

4.   Characterization of pore geometry at 12 cell sizes and 3 image volumes to define scaling effects on pore properties

1.7 Thesis Outline

In Chapter 2, characterizations of pore distributions were performed to find climate effects on soil pore structure (objective 2). Statistical analyses (configuration entropy and structure function) were applied to obtain quantitative information of pore spatial distribution from bulk soils along atmospheric CO_2 concentration and temperature gradient.

In Chapter 3, observation of climate effects on pore structure extended by measuring pore morphological and hydraulic properties from soils along a CO_2 concentration and temperature gradient were measured (objective 1 and 3). Aggregate samples and bulk soil samples from two sampled sites exhibiting the greatest difference in CO_2 concentration and temperature would define climatic effects on pore structures at two structural scales. Fortran codes were developed to calculate a pore network model coupled with local porosity calculation (modified pore network) for measuring pore geometry from large size images.

In Chapter 4, pore morphological properties from a bulk soil and an aggregate sample were investigated to define scaling effects of image volumes and resolutions (objectives 4).

References

Al-Raoush, R.I. and C.S. Willson. 2005. Extraction of physically realistic pore network properties from three-dimensional synchrotron X-ray microtomography images of unconsolidated porous media systems. *J. Hydrol*. 300(1-4): 44-64.

Amundson, R.G. and E.A. Davidson. 1990. Carbon dioxide and nitrogenous gases in the soil atmosphere. *J. Geochem*. Explor. 38:13-41.

Arnon, J.A., J.G. Zaller, E.M. Spehn, P.A. Niklaus, C.E. Wells, and C. Korner. 2000. Dynamics of Root Systems in Native Grasslands: Effects of Elevated Atmospheric CO_2. *New Phytol.* 147(1): 73-86.Bastardie. F., Y. Capowiez , J.R. de Dreuzy and D. Cluzeau. 2003. X-ray tomographic and hydraulic characterization of burrowing by three earthworm species in repacked soil cores. *Appl. Soil Ecol.* 24(1): 3-16.

Barnard, R., L. Barthes, X. Le Roux, H. Harmens, A. Raschi, J.F. Soussana, B. Winkler, and P.W. Leadley. 2004. Atmospheric CO_2 elevation has little effect on nitrifying and denitrifying enzyme activity in four European grasslands. *Global Change Biol.* 10: 488–497.

Berntson, G.M. and F.A. Bazzaz. 1998. Regenerating temperate forest mesocosms in elevated CO2: belowground growth and nitrogen cycling. *Oecologia* 113: 115-125.

Biswal, B., C. Manwart, R. hilfer, S. Bakke, and P.E. Oren. 1999. Quantitative analysis of experimental and synthetic microstructures for sedimentary rock. *Physica A*. 273: 452-475.Capowiez, Y., A. Pierret, O. Daniel, P. Monestiez, and A. Kretzschmar. 1998. 3D skeleton reconstructions of natural earthworm burrow systems using CAT scan images of soil cores. *Biol. Fert. Soils*. 27(1): 51-59.

Capowiez, Y., A. Pierret, and C. J. Moran. 2003. Characterization of the three dimensional structure of earthworm burrow systems using image analysis and mathematical morphology. *Biol. Fertil. Soils* 38:301–310.

Chatzis, I. and F. A. L. Dullien, 1975. Modelling pore structure by 2-D and 3-D networks with application to sandstones, *J. Can. Pet. Technol*. 16(1): 97-108.

Cıslerova, M. and J. Votrabova. 2002. CT derived porosity distribution and flow domains. *J. Hydrol*. 267: 186-200.

Curtis, P.S. and X. Wang. 1998. A meta-analysis of elevated CO_2 effects on woody plant mass, form and physiology. *Oecologia.* 113: 299–313.

Curtis, P.S., C.S. Vogel, X.Z. Wang, K.S. Pregitzer, D.R. Zak, J. Lussenhop, M. Kubiske, and J.A. Teeri. 2000. Gas exchange, leaf nitrogen, and growth efficiency of Populus tremuloides in a CO_2-Enriched Atmosphere. *Ecol. Appl.* 10 (1): 3-17.

Dai, A., K.E. Trenberth, and T. Qlan. 2004. A Global Dataset of Palmer Drought Severity Index for 1870–2002: Relationship with Soil Moisture and Effects of Surface Warming. *J. Hydrometorol.* 5 (6): 1117-1130.

Dane, J.H., and J.W. Hopmans. 2001. Water Retention and Storage, Chapter 3.3.1 Introduction, in Methods of Soil Analysis, Part 1, Physical Methods, (*eds*) Dane, J.H. and G.C.Topp, Agronomy 9. Madison, WI, 2002.

Davidson EA, Y.I. Francoise,and D.C. Nepstad. 2004. Effects of an experimental drought on soil emissions of carbon dioxide, methane, nitrous oxide, and nitric oxide in a tropical forest. *Glob. Change Biol*. 10:718–730.

De Graff, M., J. Six, D. Harris, H. Blums, and C. Van Kessel. 2004. Decomposition of soil and plant carbon from pasture systems after 9 years of exposure to elevated CO2: impact on C cycling and modeling. *Global Change Biol*. 10: 1922–1935.

Eviner, V. T. and F.S. Chapin. 2002. The influence of plant species, fertilization and elevated CO2 on soil aggregate stability. *Plant. Soil*. 246 (2): 211-219.

Fatt, I., 1956. The network model of porous media, I: Capillary pressure characterizations. *Trans. AIME*. 207: 144.

Fitter, A.H., A. Heinemeyer, and P.L. Staddon. 2000. The impact of elevated CO_2 and global climate change on arbuscular mycorrhizas: a mycocentric approach. *New Phytol*. 147 (1): 179-187.

Hilfer, R. 1992. Local porosity theory for flow in porous media. *Phys. Rev. B*. 45: 7115-7121.

Hopmans, J. W., D.R. Nielsen, and K. L. Bristow. 2002. How useful are small-scale soil hydraulic property measurements for large-scale vadose zone modeling? In: Smiles, D., P.A.C. Raats, and A. Warrick (*eds.*). Heat and mass transfer in the natural environment. The Philip Volume. Geophysical Monogr. Ser.129. pp. 247–258. AGU, Washington, DC.

Hu, J. and P. Stroeven. 2005. Local porosity analysis of pore structure in cement paste. *Cen. Concr. Res*. 35(2): 232-242.

Hungate, BA, E.A. Holland, R.B. Jackson, F.S. Chapin, H.A. Mooney and C.B. Field. 1997. The fate of carbon in grasslands under carbon dioxide enrichment. *Nature*. 388: 576-579.

IPCC. 2007. Summary for policymakers: Climate change 2007: The physical science basis. Contribution of working group I to the fourth assessment report of the Intergovernmental Panel on Climate Change. Paris, February 2007.

Janus, L. R., N. L. Angeloni1, J. McCormack, S. T. Rier, N. C. Tuchman, and J. J. Kelly. 2005. Elevated atmospheric CO_2 alters soil microbial communities associated with trembling Aspen (Populus tremuloides) roots. *Microb. Ecol*. 50: 102–109.

Jastrow, J., Miller, R., Owensby, C., 2000. Long-term effects of elevated atmospheric CO2 on below-ground biomass and transformations to soil organic matter in grassland. *Plant. Soil* 224, 8597.

Jucevica, E.and V. Melecis. 2006. Global warming affects Collembola community: A long-term study. *Pedobiologia*. 50: 177-184.

Kandeler, E., D. Tscherko, R.D. Bardgett, P.J. Hobbs, C. Kanpichler, and T.H. Jones. 1998. The response of soil microorganisms and roots to elevated CO_2 and temperature in a terrestrial model ecosystem. *Plant. Soil*. 202 (2): 251-262.

King, J.S., K.S. Pregitzer, D.R. Zak, W.E. Holmes, and K. Schmidt. 2005. Fine root chemistry and decomposition in model communities of north-temperate tree species show little response to elevated atmospheric CO2 and varying soil resource availability. *Oecologia*. 146: 314–328.

Klironomos, J.N., M.F. Allen , M.C. Rillig , J. Piotrowski , S. Makvandi-Nejad , B.E. Wolfe , and J.R. Powell. 2005. Abrupt rise in atmospheric CO_2 overestimates community response in a model plant-soil system. *Nature*. 433: 621-624

Ladeau,S.L. and J.S. Clark. 2006. Pollen production by Pinus taeda growing in elevated

atmospheric CO2. *Funct. Ecol.* 20: 541–547.

Langmaack, M., S. Schrader, U. Rapp-Bernhardt, and K. Kotzke. 1999. Quantitative analysis of earthworm burrow systems with respect to biological soil-structure regeneration after soil compaction. *Biol. Fert. Soils.* 28(3): 219-229.

Langmaack, M., S. Schrader, U. Rapp-Bernhardt, and K. Kotzke. 2002. Soil structure rehabilitation of arable soil degraded by compaction. *Geoderma.* 105(1-2): 141-152.

Lagomarsino, A., M.C. Moscatelli, P. De Angelis, and S. Grego. 2006. Labile substrates quality as the main driving force of microbial mineralization activity in a poplar plantation soil under elevated CO_2 and nitrogen fertilization. *Sci. Total. Environ.* 372: 256–265.

Lin, T.L. and L.W. Hourng. 2005. Determination of applicable local porosity distributions in a powder bed by the maximum entropy method. *Adv. Powder Technol.* 16 (3): 231-246.

Lindquist, W.B., S.M. Lee, D.A. Coker , K.W. Jones, and P. Spanne. 1996. Medial axis analysis of void structure in three-dimensional tomographic images of porous media. *J. Geophys. Res.* 101(B4): 8297-8310.

Luo, L.F., H. Lin, and P. Halleck. 2008. Quantifying soil structure and preferential flow in intact soil using x-ray computed tomography. *Soil Sci. Soc. Am. J.* 72(4): 1058-1069.

Morgan, J.A., D. E. Pataki, C. Körner, H. Clark, S.J. Del Grosso, J. M. Grünzweig, A. K. Knapp, A. R. Mosier, P. C. D. Newton, P. A. Niklaus, J. B. Nippert, R. S. Nowak, W. J. Parton, H. W. Polley, and M. R. Shaw. 2004. Water relations in grassland and desert ecosystems exposed to elevated atmospheric CO2. *Oecologia.* 140: 11–25.

Masad, E. and B. Muhunthan. 1997. Three-dimensional characterization and simulation of anisotropic soil fabric. *J. Geotech. And Geoenvir. Engrg.* 126(3): 199-207.

Morgan, J. A.. D. E. Pataki, C. Körner, H. Clark, S. J. Del Grosso, J. M. Grünzweig, A. K. Knapp, A. R. Mosier, P. C. D. Newton, P. A. Niklaus, J. B. Nippert, R. S. Nowak, W. J. Parton, H. W. Polley, and M. R. Shaw. Water relations in grassland and desert ecosystems exposed to elevated atmospheric CO_2. 2004. *Oecologia.* 140: 11–25.

Niklaus, P.A., M. Wohlfender, R. Siegwolf, C. Korner. 2001. Effects of six years atmospheric CO2 enrichment on plant, soil, and soil microbial C of a calcareous grassland. *Plan. Soil.* 233 (2): 189-202.

Pajari, B. 1995. Soil respiration in a poor upland site of scots pine stand subjected to elevated-temperatures and atmospheric carbon concentration. *Plant. Soil.* 168: 563-570.

Pendall, E., S. Bridgham, P.J. Hanson, B. Hungate, D.W. Kicklighter, D.W. Johnson , B.E. Law, Y.Q. Luo, J.P. Megonigal , M. Olsrud, M.G. Ryan, and S.Q. Wan . 2004. Below-ground process responses to elevated CO_2 and temperature: a discussion of observations, measurement methods, and models. *New Phytol.* 162:311–322.

Peth, S., R. Horn, F. Beckmann, T. Donath, J. Fischer, A.J.M. Smucker. 2008. Three-dimensional quantification of intra-aggregate pore-space features using synchrotron-radiation-based microtomography. *Soil Sci. Soc. Am. J.* 72(4): 897-907.

Rillig, M.C., S.F. Wright, B.A. Kimball, P.J. Pinter, G.W. Wall , M.J. Ottman, and S.W. Leavitt. Elevated carbon dioxide and irrigation effects on water stable aggregates in a

Sorghum field: a possible role for arbuscular mycorrhizal fungi. *Global Change Biol*. 9: 333-337.

Rillig, M.C., S. F. Wright, M. R. Shaw, and C. B. Field. 2002. Artificial climate warming positively affects arbuscular mycorrhizae but decreases soil aggregate water stability in an annual grassland. *Oikos*. 97: 52-58.

Taina, I.A., R.J. Heck, and T. R. Elliot. 2008. Application of X-ray computed tomography to soil science: A literature review. *Can. J. Soil Sci*. 88(1):1-20.Treseder, K. K. and M. F. Allen. 2000. Mycorrhizal fungi have a potential role in soil carbon storage under elevated CO2 and nitrogen deposition. *New Phytol.* 147: 189-200.

VandenBygaart, A. J. and R. Protz. 1999. The representative elementary area REA in studies of quantitative soil micromorphology. *Geoderma.* 89: 333–346.

Vogel, H.J. and K. Roth. 2003. Moving through scales of flow and transport in soil. *J. Hydroal.* 272(1-4): 95-106.

Volk, M., P.A. Niklaus, and C. Körner. 2000. Soil moisture effects determine CO_2 responses of grassland species. *Oecologia.* 125:380-388.

Wan, S.Q., R.J. Norby, K.S. Pregitzer, J. Ledford, and E.G. O'Neill. 2004. CO2 enrichment and warming of the atmosphere enhance both productivity and mortality of maple tree fine roots. *New Phytol.* 162 (2): 437-446.

Ward, J.K. and J.K. Kelly. 2004. Scaling up evolutionary responses to elevated CO_2: lessons from Arabidopsis. *Ecol. Lett.* 7: 427- 440.

Whitmore, A.P. 2006. Determination of the mineralization of nitrogen from composted chicken manure as affected by temperature. *Nutr. Cycl. Agroecosyst.* 77(3): 225-232.

Wong, R.C.K. and R. Wibowo. 2000. Tomographic evaluation of air and water flow patterns in soil column. *Geotech. Test. J.* 23(4): 413-422.

Zak, D.R., K.S. Pregitzer, J.S. King, and W.E. Holmes. 2000. Research review: Elevated atmospheric CO2, fine roots and the response of soil microorganisms: A review and hypothesis. *New Phytol.* 147 (1): 201-222.

Table 1.1 Summary of the effects of elevated CO_2 concentration and temperature on selected ecosystems properties.

Ecosystem component	Authors	Observation	Property being altered	Duration of exposure	Results
Plant	Curtis & Wang (1997)	Plant growth	CO_2	1 year	Increased
	Curtis et al (2000)	Photosynthesis and growth	CO_2	2 years	Increased
	Ziska et al (2004)	Productivity	CO_2 & Temperature	2 years	Increased
	Ladeau & Clark (2006)	Productivity	CO_2	10 years	Increased
C/N cycle	Jastrow et al (2000)	C/N stock & C/N ratio	CO_2	8 years	Increased
	Wan et al (2004)	Fine root N concentration	CO_2	3 years	Decreased
			Temperature		Increased
	Pendall et al (2004)	C/N ratio	CO_2	4 years	Increased
	Lagomarsino et al (2006)	C/N ratio	CO_2	5 months	Increased
	Whitmore (2006)	N mineraliazation	Temperature	2 years	Increased
	Berntson & Bazzaz (1998)	Fine root N concentration	CO_2	2 years	Decreased
Root	King et al (1996)	Fine root biomass of Loblolly pine seedling	CO_2 & Temperature	160 days	Increased
	King et al (1996)	Fine root biomass of Pnderosa pine seedling	CO_2 & Temperature	160 dayss	No difference
	Soussana et al (1996)	Root biomass	CO_2 & Temperature	2 years	Decreased
	Kandeler et al (1998)	Root biomass	CO_2 & Temperature	9 months	Decreased
	Fitter et al (1999)	Root turnover rate	Temperature	10 months	Increased
	Pendall et al (2004)	Root biomass	CO_2	5 years	Increased
	Wand et al (2004)	Root productivity & motality	CO_2 & Temperature	1year	Increased

	Wand et al (2004)	Root productivity & motality	CO_2	3years	No difference
			Temperature		Decreased
	King et al (2005)	Fine root growth	CO_2	2.5years	Increased
Microbes	Hungate et al (1997)	Microbial biomass	CO_2	3years	Decreased
	Zak et al (2000)	Fungi community	CO_2	1year	No difference
	Treseder & Allen (2000)	Mycorrhizal fungi community	CO_2	2 years	Increased
	Gavito et al (2003)	Mycorrhizal fungi community	CO_2	2 years	No difference
			Temperature		Increased
	Ebersberger et al (2003)	Soil enzymes activity	CO_2	6 years	Increased
	Barnard et al (2004)	Soil enzymes activity	CO_2	7 years	No difference
	Janus et al (2005)	Fungi community	CO_2	5 years	Increased
	Klironomus et al (2005)	Mycorrhizal fungi community	CO_2	6 years	Increased
Soil moisture	Pajari(1995)	Soil moisture	CO_2		Increased
			Temperature		Decreased
	Volk et al (2000)	Soil moisture	CO_2	1 year	Increased
	Morgan et al (2004)	Soil moisture	CO_2	4 years	Increased
	Dai et al (2004)	Soil moisture	Temperature	10 years	Decreased
	Jucevica & Melecis (2006)	Soil moisture	Temperature	11 years	Decreased
	Leipprand & Gerten (2006)	Soil moisture	CO_2	29 years	Increased
Aggregates	Rillig et al (1999)	Aggregate sizes	CO_2	1 year	Decreased
	Rillig et al (2001)	Stability	CO_2	1 year	Increased
	Niklaus et al (1999)	Aggregate sizes	CO_2	5 years	Decreased
	Eviner & Chapin (2001)	Stability	CO_2	4 years	Increased
	Rillig et al (2002)	Stability	Temperature	1 year	Decreased
	Niklaus et al (2003)	Aggregate sizes	CO_2	1 year	Decreased
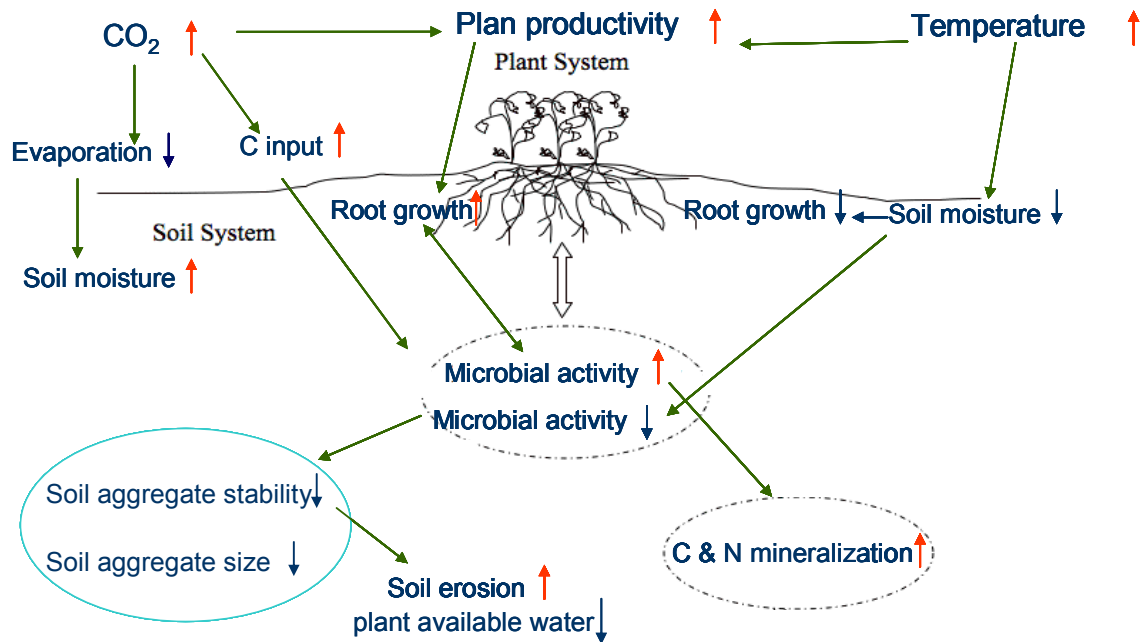
Figure 1.1 Direct and indirect effects of elevated CO_2 concentration and temperature in soil systems. Red arrows indicate increase, blue arrows indicate decrease and green arrows indicate interactions between ecological components.
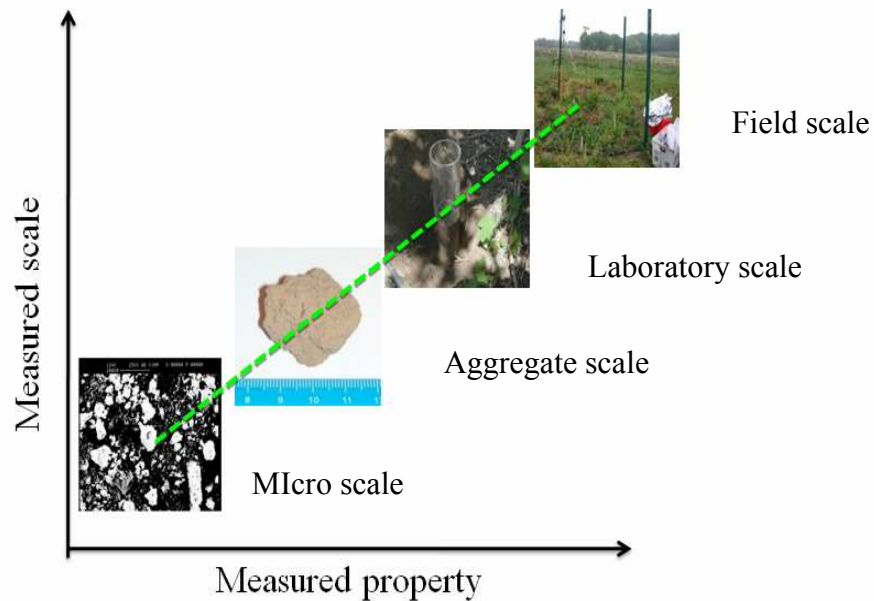
Figure 1.2 Diagram of different scales in soil sampling and scaling. The image at the field scale is an example of a plot image for soil samples in Buckeystown, Maryland. The size of the plot is 2m ×2m. The image at the laboratory scale is an example of a bulk soil sample from the plot. The sample size in the picture is 5 cm in diameter and 12 cm in height. The image at the aggregate scale is an example of an aggregate and the image at the micro scale is an example of soil particles. The green line represents the relationship of measured properties across scales.

A   B
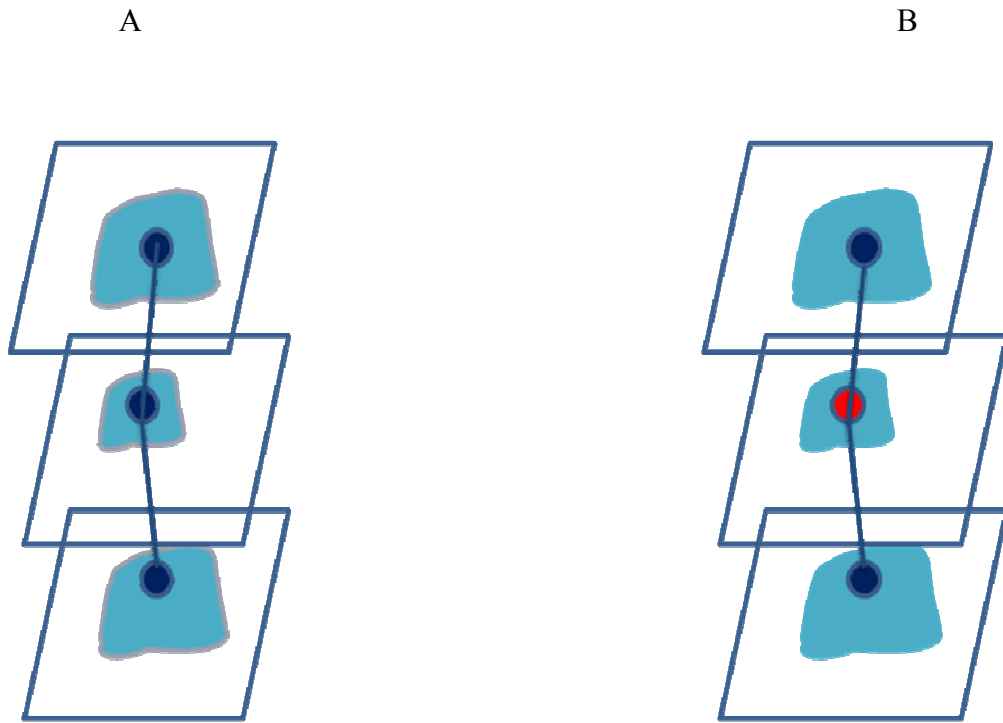
Figure 1.3 Simplified diagrams of algorithms to generate pore network models. A. Thinning and B. Medial-axis transformation. Blue object represent a pore from each slice. Dark blue circles and line represent center node of each slice and networks. Colors of center nods in B mean different burning numbers.

Chapter 2 : Characterization of Soil Pore Structure along an Urban-Rural CO_2 / Temperature Gradient

2.1 Introduction

The concentration of atmospheric CO_2 and temperature has increased, for the last two centuries, due to industrial development and land use change (International Panel on Climate Change (IPCC, 2007). The IPCC report predicted that the concentration of atmospheric CO_2 will double by the end of 21st century. The average global temperature has increased by 0.6 °C during the 20th century, and an additional increase is expected during the 21st century. These increases are likely to affect ecosystems directly and indirectly (Koca et al, 2006). Elevated CO_2 concentration and warming affect soil directly and indirectly and consequently changes in soil affect other components of terrestrial ecosystems (Rounsevell et al., 1996) (Fig. 1.2). Research in soil responses under enriched CO_2 concentration and/or temperature have been mainly focused on root dynamics (Norby and Jackson, 2000) and on the composition of soil microbial communities (Heinemeyer and Fitter, 2004).

2.1.1 Effects of Elevated CO_2 Concentration

Plant productivity and fine root biomass growth typically increases with increased CO_2 concentration, due to the stimulated photosynthesis and increase in soil moisture by reduced water uptake by plants (Pajari, 1995; Volk et al., 2000; Leipprand and Gerten, 2006) (Table 1.1). However, microbial biomass sometimes increases (Ebersberger et al., 2003), stay the same (Zak et al., 2000; Bernard et al., 2004) or decreases (Hungate et al., 1996) (Table 1.1). An increase in CO_2 concentration alone causes increases in microbial biomass (Ebersberger et al., 2003) and fungi biomass (Treseder & Allen, 2000; Janus et al., 2005). One explanation for these contradictory reactions under enriched CO_2

concentration is that different types of microbes react differently by the plant/root types, soil nutrient and soil water availability (King et al., 1996).

2.1.2 Effects of High Temperature

Warming increases root productivity, root and microbial biomass by increasing photosynthesis and the days of the growing season. However, high temperature also has negative effects on root biomass and microbial activities because of soil moisture deficiency in the soil and atmosphere (Soussana et al., 1996; Kandeler et al., 1998; Koch et al., 2007; Sardans et al., 2008) (Table 1.1). High temperature causes draught in soil and increases in fungi community, because they are more favorable to dry environment and became dominant in soil microbial community (Treseder and Allen, 2000; Gavito et al., 2003).

2.1.3 Effects of Elevated CO_2 Concentration and High Temperature

Responses of ecological systems to combined changes of elevated atmospheric CO_2 concentration and high temperature have not shown a clear trend. Ziska et al. (2004) found increases in plant productivity with increases in both atmospheric CO_2 concentration and temperature. However, under these conditions fine root biomass could; increase (King et al., 1996), stay the same (King et al., 1996) or decrease (Kandeler et al., 1998) (Table 1.1). In addition, Soussana et al. (1996) reported that increases in temperature under elevated CO_2 concentration did not affect soil moisture. Therefore, effects from high temperature are compensated by effects of elevated atmospheric CO_2 concentration in ecological system. Since atmospheric CO_2 concentration and temperature could increase simultaneously, it is critical to elucidate the ecological responses under CO_2 concentration and temperature increases in order to predict changes of ecological or soil system.

2.1.4 Soil Physical Properties

Soil physical properties will be influenced by elevated CO_2 concentration and warming. Soil interacts with all ecological components and changes of one component in soil may have a domino effect in ecological systems (Niklaus et al., 2003; Pendall et al., 2004). For example, the activity of soil enzymes is regulated by temperature and soil moisture (Koch et al., 2007; Sardans et al., 2008). As atmospheric CO_2 concentration increases, soil moisture increases by reducing plant water consumption (Volk et al., 2000; Morgan et al., 2004; Leipprand and Gerten, 2006) (Table 1.1). However, increases in air temperature alone would result in drier soil due to increase of evaporation rate (Dai et al., 2004) (Table 1.1). Therefore, it is difficult to predict responses of soil moisture in the future since the soil moisture deficit by warming may be alleviated by elevated CO_2 and changes in precipitation (Pajari, 1995; Olsrud et al., 2004; Pendall et al., 2004b).

Another important factor is soil temperature that controls soil processes. Changes of soil temperature affect the rate of biological processes (Rounsevell et al., 1999). Most studies focused on regions containing permafrost because warming is directly related to thawing and freezing of snow/ice in those regions. Waelbroeck (1993) reported that soil temperature could increase up to 75% in an depth of 7.5 cm (active layer) of permafrost soil if air temperature increases by 3 °C. However, the increase of soil temperature predicted by the Global Climate Model (GCM) may not be as great as 3 °C, if the model would consider excessive soil moisture from thawing in cold area. Soil moisture would inhibit heat transfer from air temperature to soil, and, for this reason, soil temperature would not increase as much as climate models predicted under high air temperature.

Climate change also alter the transport and storage of water or nutrients in soil. These changes are directly related to soil structure. There are reports of increases in saturated hydraulic conductivity and of decreases in bulk density under elevated atmospheric CO_2 concentration (Prior et al., 2004). Rillig et al. (2001) found that higher CO_2 concentrations increased arbuscular mycorrhizal fungi (AMF) in soil aggregates; which, in turn, increased aggregate stability of aggregates smaller than 125 μm in diameter. As a result, aggregate sizes shifted to smaller sizes (Rillig et al., 1999; Niklaus et al., 2003). As warming progresses, aggregate stability decreases, because higher temperatures stimulate the decomposition of AMF (Rillig et al., 2002). Based on the contrasting predictions of soil physical properties, it is important to perform direct observations on soil pore structure under different levels of atmospheric CO_2 concentration and temperature. This analysis will help to predict changes of soil structure and soil processes accurately.

Analyses of spatial distribution of solid-pore arrangements are relatively simple and powerful tools to characterize pore structure from soil images. The configuration entropy and universal multifractal analyses (structure function) which are spatial distribution analyses have been proven to be sensitive enough to characterize heterogeneous structures or distributions (Pozdnyakova et al., 2005; Chun et al., 2008).

The hypothesis of this study was that there would be changes in soil pore structure under elevated CO_2 concentration and warming because pore structure synthesizes influences of soil biota, microbes and roots.

The objectives of this work were 1) to characterize pore structural changes by spatial analyses of three dimensional images of soil, sampled from sites located along a

natural gradient of both CO_2 concentration and temperature, and 2) to define

environmental variables that affect soil structure changes under these conditions.

2.2 Materials and Methods

2.2.1 Soil

The sites selected for this study were along an urban- rural gradient: a site at an

organic farm near Buckeystown, Maryland approximately 87 km west of Baltimore

(rural), a site at the Carrie Murray Nature Center on the outer edge of the Baltimore city

(suburban), and a site at the Baltimore science center, which is located inside of the city

(urban) (Fig. 2.1). In 2002, the top 20 cm of a fallow soil that did not had any fertilizer

applications for 5 years was removed from the Beltsville experimental farm over a 6×9 m.

These soils were sieved to remove rhizomes, stolons and corms, and then mixed

uniformly with seeds of 30 species. Then from the 6×9 m area of the Beltsville

experimental farm, soils were excavated up to 110 cm (B and C horizons) and mixed well.

Four plots with size of 2 × 2 m were established at each site in 2002. All plots were

excavated to a depth of 110 cm and filled with the lower horizon soils first and soils with

seeds were placed on top (Ziska et al., 2004). Soil samples were then taken at each site to

a depth of 30 cm and analyzed at the University of Maryland Soil Testing Laboratory at

College Park, Maryland (Table 2.1). At each site, a weather station was established to

collect environmental variables such as atmospheric CO_2 concentration and temperature,

and soil temperature and moisture. The average concentration of CO_2 and temperature

during the period 2002 to 2006 was the highest for the urban site (488 ppm and 14.8 ºC)

and the lowest for the Rural site (422 ppm and 12.7 ºC), while the suburban site was

intermediate between the other two sites (442 ppm and 13.6 ºC) (George et al., 2007).

An undisturbed bulk soil (5.5 cm in diameter and 12 cm in height) was sampled from each of the three plots by excavating a sample carefully (see Fig. 1.2). The outside of each sample was covered by cheesecloth with saran to harden the surface of the sample. The cheesecloth was soaked lightly to prevent infiltration of saran solution (mixing of saran powder in methyl ethyl keton) into pores, but thickened enough to harden the surface of the sample. Aggregate samples (less than 2 cm in diameter) were hand-picked from all plot surfaces in 2007. Both aggregates and the bulk soil samples were sealed in plastic bags and transported to a laboratory in an icebox to prevent the loss of moisture. Once in the lab, the soil samples were stored in a refrigerator. In this chapter, one sample from each of three plots at each site was used for image analyses. A total of nine bulk soil samples (5.5 cm in diameter and 12 cm in height) were analyzed.

2.2.2 Soil Moisture and Temperature Data

Soil moisture and temperature data were reported by George et al. (2007). Daily soil moisture and temperature data were collected from 2002 to 2006. Soil moisture was measured with a sensor from Decagon Devices (USA) and temperature with a probe from, Campbell Scientific (USA). Both properties were measured at 10 cm depth. In this study, data covering the period from 2004 to 2006 were used for analyses.

Soil temperature data were fitted with a sinusoidal function (Hillel, 1982):

$$T(z,t) = T_A + A\exp(z\sqrt{2K_T/(2\pi/\tau)})\sin((2\pi/\tau)*t + z/\sqrt{2K_T/(2\pi/\tau)}) \quad -\infty < z < 0 \qquad (1)$$

where $T(z,t)$ is the soil temperature at time t (day) and depth z (m-in this case $z = 0.1$ m), T_A is an annual mean temperature (ºC), A is the amplitude of the surface fluctuations (ºC), τ is the period of the wave (day), and K_T is the thermal diffusivity ($m^2 day^{-1}$). When heat penetrates into a soil from the surface, the amplitude decreases with depth. Damping

depth is the depth at which the amplitude is 37% the amplitude at the soil surface. From

Eq.(1), damping depth (zd) can be calculated as $\sqrt{2K_T/\omega}$, where $\omega = 2\pi/ 365(\text{day}^{-1})$.

2.2.3 Computer Tomography (CT) and Image Processing

An axial X-ray micro computer tomographer (model MS, General Electric

Medical Systems, London, ON, Canada) located at the University of Guelph (ON,

Canada) was used to scan the soil samples. The X-ray source was set at 120 kV and the

current at 160 mA. Two small tubes with water and air were scanned with soil samples

for density calibration of air and water in the samples. A bulk soil sample was placed

into a sample holder (5.5 cm in diameter by 12.5 cm in height) and placed inside the

tomographer. The resolution of the scans was 22 μm for the bulk soil samples. The

aggregate sample was placed inside a tube (2 cm in diameter by 5 cm in height) and

scanned at a resolution of 6 μm. Series of two dimensional cross sectional images were

reconstructed into three dimensional images by Microview software (GE Healthcare

Biosiences).

After reconstruction of three dimensional images, gray images were converted to

binary images using a Java program in Image J (Research Services Branch, National

Institute of Health, Bethesda, MD) developed by Elliot and Heck (2007). The

thresholding algorithm was the local thresholing process based on indicator kriging (Oh

and Lindquist, 1999). Briefly, two threshold values (TH1 and TH2) were chosen from

the grey color intensity histogram. The lower threshold value (TH1) became a cut-off

value for a solid voxel and all voxels with grey intensity value below TH1 were

converted to the value of 0. The greater threshold value (TH2) was a cut-off value for a

pore voxel and voxels with greater intensity values than TH2 were converted to the value

of 1. Voxels with gray intensity values between TH1 and TH2 were assigned to either phase value (0 or 1) using indicator kriging which provides the probability of each voxel based on neighboring voxels. This thresholding algorithm was proven to be a better technique than traditional algorithms such as global thresholding although it requires more time to complete (Oh and Linquist, 1999; Al-Raoush and Wilson, 2005). The original image size for the bulk soil sample was about $2000 \times 2000 \times 1500$ voxels. After thresholding, the image size was reduced to $1000 \times 1000 \times 1000$ voxels (10648 mm^3). The aggregate image size was $546 \times 395 \times 231$ voxels (10.76 mm^3). The threshold process was based on a two stage threshold application. Detailed information of the threshold theory is in Elliot and Heck (2007). This thresholding method was different to the 3DMA program used in Chapter 3 and 4. The basic algorithm is the same for these two programs, but the criteria for deleting noise from images is different. However, we tested the effects of the thresholding procedure (Java *vs.* 3DMA code) and found no difference in results of the spatial distribution analysis (Appendix A).

2.2.4 Image Analyses

The configuration entropy and universal multifractal analyses were written in Fortran codes to characterize pore structure from three dimensional soil images. Both measurements apply a box-counting technique by repeatedly covering an image with different size cubes (L^3) and evaluating the number of cubes having a common property. The technique was modified from the 2D version of the algorithm (Andraud et al., 1997; Gimenez et al., 2002; Gibson et al., 2006).

The configuration entropy H*(L^3), proposed by Andraud *et al*. (1994, 1997), was measured as:

$$p_k(\mathrm{L}) = \frac{\mathrm{N}_k(\mathrm{L}^3)}{\mathrm{N}} \tag{2}$$

and

$$H^*(\mathrm{L}^3) = \frac{H(\mathrm{L}^3)}{H_M(\mathrm{L}^3)} = -\frac{1}{\log(\mathrm{L}^3+1)} \sum_{k=0}^{1} p_k(\mathrm{L}^3) \log p_k(\mathrm{L}^3) \tag{3}$$

where N is the total number of cells and N_k is the number of cells with k number of pores. $\mathrm{H_M}(\mathrm{L}^3) = \log(\mathrm{L}^3+1)$ is the maximum possible entropy for cells of volume, L^3 (i.e., all possible states k are equiprobable). Each binary image was divided into square cells of size L =1 to L=100 and in each cell the number of states k was counted. The $H^*(\mathrm{L}^3)$ function is concave downward showing a more or less defined peak (Fig.2.2.b). When $H^*(\mathrm{L}^3)$ equals to 0, all cells have the same number of pores or porosity and the pore structure is homogeneous. When $H^*(\mathrm{L}^3)$ is equal to 1, all possible states k or porosities are equiprobable. The $H^*(\mathrm{L}^3)$ function was characterized by the entropy value at the peak (Emax) and by the characteristic cell size ($\mathrm{L_o}$) at which the peak is observed (Chun et al. 2008).

Local porosities were estimated at the characteristic cell sizes ($\mathrm{L_o}$) of 25 (voxels) and 32 (voxels) for the urban and suburban/rural sites (the $\mathrm{L_o}$ values of the urban and suburban were not significantly different). A three dimensional images was divided in cells of size $\mathrm{L_o}$ and the porosity of each cell was computed as (see Fig.2.2.c);

$$\phi(L_o^3) = \frac{VP(L_o^3)}{V(L_o^3)} \tag{4}$$

where $\mathrm{V}(\mathrm{L_o}^3)$ is total number of voxels from a cell and $\mathrm{VP}(\mathrm{L_o}^3)$ is the number of pore voxels from a cell.

A universal multifractal model was used to describe the statistical behavior or trend of local porosity (ϕ) across various moments (q) (Liu and Molz, 1997). The universal multifractals model is defined as

$$\sum_{i=1}^{n} \left\langle \left| \phi_x - \phi_{x+h} \right|^q \right\rangle \propto h^{\varsigma(q)} \tag{5}$$

where x is a distance, h is a lag and the brackets indicate statistical average. In this study, q ranged from 0 to 4 with 0.1 intervals. Results from Eq. (5) for each q were plotted against lag (h) in a log-log plot (Fig. 2.2.d). The linear range was selected in the log-log plots and the values of the slopes from the linear range were applied to calculate the structure function (Fig. 2.2.e).

The scale invariant structure function exponent ζ (q) was defined as (Liu and Molz, 1997);

$$\varsigma(q) = qH - \frac{C}{\alpha - 1}(q^\alpha - q) \qquad \alpha \neq 1 \tag{6}$$

where H is the degree of scale dependency, C is the mean singularity of process, and α is degree of multifractality bounded between 0 and 2. The parameter H characterizes the spatial correlation of the average absolute value increment; H equals to 0 means the field variations are scale independent and H greater than 0 means the variations are scale dependent. The C parameter ranges from 0 (homogeneous process) to the value of the Euclidean dimension of the observation space (3 in this study) which means that the changes of pattern is heterogeneous. The parameter α indicates how far a distribution is from a monofractal type of scaling; α being equals to 0 means single scaling and 2 means the log-normal multifractal case (Pozdnyakova et al., 2005).

2.2.5 Statistical analyses

An ANOVA test was performed at 95% significant level for the configuration entropy parameters and porosity. The *F*-test was used to reveal differences in fractal dimensions across sites (Neter *et al*., 1990). A paired *t*-test was conducted at 95% to determine statistical differences among fitted parameters from soil temperature distributions across sites. Soil moisture data were separated by two seasonal groups: within and outside the plant growing season.The plant growing season dates for each year were defined as the period between the last frost after winter and the first frost prior to the onset of the following winter (George et al., 2007). Frost was defined as temperatures reaching below 0 °C for at least an hour. Seasonally separated soil moisture data were grouped into 12 classes based on ranges of soil moisture data and the frequencies of each class were calculated. Chi-square test at 95% was used to determine statistical differences among the frequencies among sites. These analyses were performed by SPSS (Statistical Package for the Social Sciences, SPSS Inc.).

Principal component analysis (PCA) was performed to investigate correlation among environmental variables and parameters from image analyses. PCA is a mathematical way of determining a linear transformation of a sample of points in N-dimensional space which exhibits the properties of the sample most clearly along the coordinate axes (Konovalov et al., 2003). From linear combinations of the original axes, PCA constructs a new coordinate system by aligning the samples along their major dimensions or axes of variation. The new axes are called principal components (PC) or factors and the amount of variance explained by each PC is expressed as its eigenvalue. The greatest variance is considered as the first principal component and the immediately smaller value becomes the second principal component and so on. Classification analysis

was performed to separate three sites based on factor loading and eigenvalues of variables from PCA. The PCA and classification analysis was done with Statistica (Statsoft.Inc).

2.3 Results and Discussion

2.3.1 Characterization of Sampled Sites

George et al. (2007) reported atmospheric CO_2 concentration and air temperature, soil temperature and moisture, and precipitation data from the urban, suburban, and rural sites during the period 2002 to 2006. Over these five years, the average atmospheric CO_2 concentration and air temperature were significantly different among sites (George et al. 2007). The concentration of CO_2 at the urban site was 16% greater than the rural site during five years. Average air temperature at the urban site was the highest (14.84 °C) followed by suburban (13.60 °C) and rural (12.66 °C). Precipitation over the five years was not significantly different across sites, while soil moisture and temperature data were different ($p=0.01$). In addition, Ziska et al. (2004) working on the same plots in 2002, reported changes of plant productivity (above ground), biomass and plant height along atmospheric CO_2 and temperature gradient in 2002. Plant biomass and height showed significant difference among sites and had strong positive correlation with CO_2 concentration ($r^2=0.86$) and soil temperature ($r^2=0.98$) changes from the first year of observation.

Average soil moisture values from 2004 to 2006 were 11.11(%) ± 4.7, 10.67 (%) ± 2.7, and 13.87(%) ± 5.3 for the rural, suburban and urban sites, respectively and significantly different ($p=0.04$). There was no significant difference in histogram distributions of soil moisture within or outside the growing season (Fig. 2.3), except for the suburban site outside the growing season ($p=0.01$). George et al. (2007) found that average soil moisture values from each year were significantly different. However, this difference was caused by data from 2004, while there was no difference during other

years. George et al. (2007) speculated that the greater soil moisture values in the urban site were induced by additional watering to meet high demand of evapo-transpiration in 2004. In addition, soil moisture measurements were performed at 10 cm depth from the surface of each site. One depth of measurements (close to the surface) and additional water inputs may affect soil moisture data and prevent from finding differences across sites.

Soil temperature data collected from 2004 to 2006 were fitted with Eq (1) (Fig. 2.4). Average temperatures were 13.22 °C± 0.80 for the rural site, 13.29 °C ± 0.35 for the suburban site and 14.13 °C ± 0.54 for the urban site, respectively. There was significant difference between the urban site and other two sites in mean temperature (Ta) (p=0.04), but not between the rural and the suburban site (Table 2.2). In addition, amplitude (A) and damping depth (d) from each year showed significant differences across sites (p=0.01). The urban site had the greatest A values and the smallest values of the damping depth d and thermal diffusivity. In relation to heat transfer, the damping depth and thermal diffusivity results suggest that the higher air and surface temperature at the urban site did not penetrate as deeply as in the rural site.

2.3.2 Configuration Entropy and Local Porosity Analyses

Configuration entropy analysis was used to quantify spatial arrangements of pore voxels across various cell sizes. The Emax and Lo values of the urban site were different than in the other two sites (p=0.00) while total porosity were not significantly different (p>0.05) among the three sites (Table 2.1 and Fig. 2.5). The urban site had the greatest average Emax value (0.86) and the lowest Lo value (25 voxels), while rural had the lowest Emax value (0.78) and the greatest Lo value (35 voxels). Chun et al. (2008) found

that pore structure with more scatterings of pores across an image had greater Emax

values and smaller Lo values. If pores were spread out across an image, the possibility of

having cells with various porosities would increase and heterogeneity of pore structure

would increase. Based on these definitions, pore structure at the urban site was more

heterogeneous by having more spread out pore distributions within images than other

sites.

The universal multifractal model had been used to characterize soil and hydraulic

properties (Liu and Molz, 1995; Seuront et al, 1999; Pozdnyakova et al., 2005). In this

study, local porosity distributions at cell size Lo were characterized by the universal

multifractal model and the three parameters from the structure function. Average Lo size

of 25^3 voxels was used to calculate all soil images from urban site and Lo of 32^3 voxels

were applied to all images from suburban and rural site (Fig. 2.6). According to the *t*-test,

all three parameters from the urban site had statistically different values than the other

two sites (*p*=0.00) (Table 2.1). The urban site had greater average H and C values and

lower average α value than the other two sites. This implies that the spatial arrangements

of local porosities from the urban site soils were more heterogeneous with larger

variations (Pozdnyakova et al., 2005). The more heterogeneity of local porosity

arrangements from the urban site was supported by configuration entropy analysis.

Greater widespread pores across an image increased the values of Emax and C. On the

other hand, the suburban and rural soils had relatively more homogeneous and less

variation in local porosity arrangements. The log-log plot of structure function (Eq. (6))

for the urban soil fitted to the log-log plot of measured ζ(q) from Eq. (5) against q values

reasonably well until q ≈ 2 (Fig. 2.7). The multifractal model fitted the other two soils

very well across all q values . Liu and Molz (1997) explained the type of misfit found in

the urban soil as the transition of a multifractal phase. In another words, soil samples

from the urban sites required larger image sizes to get accurate parameters of the

structure function due to greater errors in greater q (moment) values. The log-log plot of

structure function from the urban site had greater values of ζ (q) across q values. Van

Opheusden et al. (1996) found artificial particles with small pores had smaller values or

lower distribution in a structure function plot compared to aggregated particles with

greater pores.

Results from image analyses of pore structure showed that different levels of

temperature and CO_2 concentration along with soil moisture and temperature differences

induced differences in spatial distribution of pores. Based on entropy and

characterization of local porosity with universal multifractal, the urban soil had a more

heterogeneous and clustered pore structure than the other two sites (Fig. 2.5 and Fig. 2.7).

2.3.4 Environmental Variables

A PCA was performed to determine correlation among environmental variables

and parameters from image analyses. A total of 16 variables were used in the PCA

(Table 2.3). From the PCA analysis, factors 1, and 2 explained 100% of the variability

among variables.

Factor 1 explained more than 82% of the variability from the variable

distributions and included biomass, CO_2 concentration, nighttime temperature, Ta and A

from soil temperature fitting, slopes from the structure function at q=0.5, H, C from the

structure function, Lo, and Emax from the entropy analysis. Factor 2 had greater

eigenvalues for damping depth, slopes from the structure function at q=1 and 2, α from

the structure function and daytime temperature. The main contributions of factor 1 formation were Emax, Lo, biomass, and nighttime temperature, while the factor 2 was determined mostly by damping depth, α, and daytime temperature (Table 2.3 and Fig. 2.8). The three sites were classified by the urban site and the suburban or the rural site by eigenvalues of the variables (Fig. 2.9). Factor 1 separated the urban site and the suburban or the rural site, while factor 2 separated between the suburban and the rural site. Since factor 1 covered 80% of variability, the greatest separation was between the urban site and the suburban or the rural site.

The PCA and site classification analysis confirmed that parameters from image analyses were greatly correlated to plant biomass, CO_2 concentration and atmospheric/ soil temperature. Moreover, these results confirmed that soils from the urban site had different pore structures than other two sites and this difference may have resulted from warmer temperature (higher nighttime temperature) and plant activity.

Much research that has investigated soil property changes by higher CO_2 concentration or temperature have predicted degradation of soil structure and increase of soil erosion and runoff (Wang et al., 2007; Aydin et al., 2008). Previous studies assumed that higher atmospheric temperature will cause drier condition in soil and major negative effects will be occurred by drier condition. Based on this study, warmer condition without enough soil moisture may cause the opposite results in a soil system. Although climate models predict future climate changes as increase of atmospheric temperature and decrease of rainfall globally, ICPP (2007) reported that annual precipitation increases over most of the northern Europe, the northeastern United States, and high-latitude regions. For example, cold areas may benefit by warmer and wetter condition since these

conditions stimulate root growth and microbial activity in soil. In consequence, stimulated root and microbial activity will induce physical and biological processes of soil structure formation. As a result, soil structure will not be degraded in regions with enough levels of soil moisture (Sombroek, 1990).

2.4 Conclusions

Analyses of spatial distribution of solid-pore arrangements, from three dimensional images, provided important information of soil structural changes induced by greater atmospheric CO_2 concentration, high temperatures, soil moisture and plant biomass. Entropy and the universal multifractal model revealed that the soil from the urban site, which had more complex and clustered pore structure, may have resulted from higher temperature and ambient moisture in soil. Parameters from image analyses had strong correlation with plant biomass, air temperature and atmospheric CO_2 concentration. Therefore, atmospheric CO_2 and temperature affected pore structure formation. However, it is difficult to describe changes in pore structure based only on spatial distribution analyses. There should be more detailed information of pore properties such as pore geometry. Furthermore, aggregate analyses from the sites will reveal more complete information about changes of soil structure and process under elevated CO_2 concentration and warming conditions.

References

Andraud, C., A. Beghdadi and J. Lafait. 1994. Entropic analysis of random morphologies. *Physica A*. 207*:* 208-212.

Andraud, C., A. Beghdadi, E. Haslund, J. Lafait, and B. Virgin. 1997. Local entropy characterization of correlated random microstructures. *Physica A* 235: 307-318.

Aydin, M., T.Yano, F. Evrendilek, and V. Uygur. 2008. Implications of climate change for evaporation from bare soils in a Mediterranean environment. *Environ. Monit. Assess.* 140: 123–130

Barnard, R., L. Barthes, X. Le Roux, H. Harmens, A. Raschi, J.F. Soussana, B. Winkler, and P.W. Leadley. 2004. Atmospheric CO_2 elevation has little effect on nitrifying and denitrifying enzyme activity in four European grasslands. *Global Change Biol.* 10: 488–497.Capowiez, Y., A. Pierret, and C.J. Moran. 2003. Characterisation of the three-dimensional structure of earthworm burrow systems using image analysis and mathematical morphology. *Biol. Fert. Soils.* 38(5):301-310.

D'Acqui, L.P., E. Daniele, F. Fornasier, L. Radaelli, and G.G. Ristori. 1998. Interaction between clay microstructure, decomposition of plant residues and humification. *Eur. J. Soil Sci.* 49 (4): 579-587.

Dai, A., K.E. Trenberth, and T. Qlan. 2004. A Global Dataset of Palmer Drought Severity Index for 1870–2002: Relationship with Soil Moisture and Effects of Surface Warming. *J. Hydrometorol.* 5 (6): 1117-1130.

Ebersberger, D., P. A. Niklaus, and E. Kandeler. 2003. Long term CO_2 enrichment stimulates N-mineralisation and enzyme activities in calcareous grassland. *Soil Bio. Biochem.* 35: 965–972.

Gavito, M.E., P.Schweiger, and I. Jakobsen. 2003. P uptake by arbuscular mycorrhizal hyphae: effect of soil temperature and atmospheric CO_2 enrichment. *Global Change Biol.* 9: 106-116.

George, K., L.H. Ziska, J.A. Bunce, and B. Quebedeaux. 2007. Elevated atmospheric CO2 concentration and temperature across an urban-ls transect.

Gibson, J.R., H. Lin, and M.A. Burns. 2006. A comparison of fractal analytical methods on 2- and 3-dimensional computed tomographic scans of soil aggregates. *Geoderma.* 134: 335–348.

Giménez, D., J. Karmon, A. Posadas, and R. Shaw. 2002. Fractal dimensions of mass estimated from intact and eroded soil aggregates. *Soil Till. Res.* 64:165-172

Heinemeyer, A and A.H. Fitter. 2004. Impact of temperature on the arbuscular mycorrhizal (AM) symbiosis: growth responses of the host plant and its AM fungal partner. *J. Exp. Bot.* 55 (396): 525-534.

Hungate, B.A., J. Canadell, and F. S. Chapin. 1996. Plant species mediate changes in soil microbial N in response to elevated CO_2. *Ecology.* 77(8): 2505-2515.

IPCC. 2007. Summary for policymakers: Climate change 2007: The physical science basis. Contribution of working group I to the fourth assessment report of the Intergovernmental Panel on Climate Change. Paris, February 2007.

Janus, L. R., N. L. Angeloni1, J. McCormack, S. T. Rier, N. C. Tuchman, and J. J. Kelly. 2005.

Elevated atmospheric CO_2 alters soil microbial communities associated with trembling Aspen (Populus tremuloides) roots. *Microb. Ecol.* 50: 102–109.

Kandeler, E., D. Tscherko, R.D. Bardgett, P.J. Hobbs, C. Kanpichler, and T.H. Jones. 1998. The response of soil microorganisms and roots to elevated CO_2 and temperature in a terrestrial model ecosystem. *Plant. Soil.* 202 (2): 251-262.

King, J.S., R.B. Thomas, and B.R. Strain.1996. Growth and carbon accumulation in root systems of Pinus taeda and Pinus ponderosa seedlings as affected by varying CO2, temperature and nitrogen. *Tree Physiol.* 16 (7): 635-642.

King, J.S., K.S. Pregitzer, D.R. Zak, W.E. Holmes, and K. Schmidt. 2005. Fine root chemistry and decomposition in model communities of north-temperate tree species show little response to elevated atmospheric CO_2 and varying soil resource availability. *Oecologia.* 146: 314–328.

Koca, D., B. Smith, and M.T. Ske. 2006. Modeling Regional Climate Change Effects On Potential Natural Ecosystems in Sweden. *Climatic Change.* 78: 381–406.

Koch, O., D. Tscherko, and E. Kandeler. 2007. Temperature sensitivity of microbial respiration, nitrogen mineralization, and potential soil enzyme activities in organic alpine soils. *Global Biogechem. Cy.* 21(4).

Konovalov, A. M., Yu. M. Krynko, Yu. S. Musatenko, and M. G. Nakhodkin. 2003. Analysis of the principal components for REEL spectra of indium. *J. Electron. Spectrosc*. 133: 27–37

Ladeau,S.L. and J.S. Clark. 2006. Pollen production by Pinus taeda growing in elevated atmospheric CO_2. *Funct. Ecol.* 20: 541–547.

Leipprand, A. and D. Gerten. 2006. Global effects of doubled atmospheric CO_2 content on evapotranspiration, soil moisture and runoff under potential natural vegetation. *Hydrolog. Sci. J.* 51(1): 171-185.

Lin, T. L. and L.W. Hourng. 2005. Determination of applicable local porosity distributions in a powder bed by the maximum entropy method. Adv. Powder Technol. 16 (3): 231-246.

Lindquist, W.B. and A. Venkatarangan. 1999. Investigating 3D geometry of porous media from high resolution images. *Phys. Chem. Earth (A)* 25: 593.

Liu, H.H. and F.J. Molz. 1997. Multifractal analyses of hydraulic conductivity distributions. *Water Resour. Res*. 33(11): 2483-2488.

Morgan, J. A., D. E. Pataki, C. Körner, H. Clark, S. J. Del Grosso, J. M. Grünzweig, A. K. Knapp, A. R. Mosier, P. C. D. Newton, P. A. Niklaus, J. B. Nippert, R. S. Nowak, W. J. Parton, H. W. Polley, and M. R. Shaw. Water relations in grassland and desert ecosystems exposed to elevated atmospheric CO_2. 2004. *Oecologia.* 140: 11–25

Neter, J., W. Wasserman and M. H. Kutner. 1990. Applied Linear Statistical Models, 3rd edition. Richard D. Irwin, Inc., Burr Ridge, Illinois.

Niklaus, P.A., M. Wohlfender, R. Siegwolf, C. Korner. 2001. Effects of six years atmospheric CO_2 enrichment on plant, soil, and soil microbial C of a calcareous grassland. *Plan. Soil.* 233 (2): 189-202.

Niklaus, P.A., J. Alphei, D. Ebersberger, C. Kampichler, E. Kandeler, and D. Tscherko. 2003. Six years of in situ CO_2 enrichment evoke changes in soil structure and soil biota

of nutrient-poor grassland. *Global Change Biol.* 9: 585–900.

Norby, R.J.and R.B. Jackson. 2000. Root dynamics and global change: seeking an ecosystem perspective. *New Phytol.* 147 (1): 3-12.

Oh, W. and W. B. Lindquist. 1999. Image thresholding by indicator kriging. *IEEE Trans. Pattern Anal. Mach. Intell.* 21: 590-602.

Olsrud, M., J. M. Melillo, T. R. Christensen, A. Michelsen, H. Wallander, and P. A. Olsson. Response of ericoid mycorrhizal colonization and functioning to global change factors. *New Phytol.* 162: 459–469.

Pajari, B. 1995. Soil respiration in a poor upland site of scots pine stand subjected to elevated-temperatures and atmospheric carbon concentration. *Plant. Soil.* 168: 563-570.

Pardini, G., C.V. Guidi, R. Pini, D. Regues, and F. Gallart. 1996. Structure and porosity of smectitic mudrocks as affected by experimental wetting-drying cycles and freezing-thawing cycles. *Catena.* 27 (3-4): 149-165.

Pendall, E., S. Bridgham, P.J. Hanson, B. Hungate, D.W. Kicklighter, D.W. Johnson , B.E. Law, Y.Q. Luo, J.P. Megonigal , M. Olsrud, M.G. Ryan, and S.Q. Wan . 2004. Below-ground process responses to elevated CO_2 and temperature: a discussion of observations, measurement methods, and models. *New Phytol.* 162:311–322.

Posadas, A. N. D., D. Gimenez, M. Bittelli, C. M. P. Vaz, and M. Flury. 2003. Multifractal characterization of soil particle-size distributions. *Soil Sci. Soc. Am. J.* 65(5): 1361-1367.

Pozdnyakova, L, D. Gimenez, and P.V. Oudemans. 2005. Spatial analysis of cranberry yield at three scales. *Agron. J.* 97 (1): 49-57.

Prior, S.A., G.B. Runion, H.A. Torbort, and H.H. Rogers. 2004. Elevated atmospheric CO2 in agroecosystems: Soil physical properties. *Soil Sci.* 196 (6):434-439.

Rillig, MC, S. F. Wright, M.F. Allen, and C. B. Field. 1999. Rise in carbon dioxide changes in soil structure. *Nature.* 400: 628-628.

Rillig, M.C., S.F. Wright, B.A. Kimball, P.J. Pinter, G.W. Wall , M.J. Ottman, and S.W. Leavitt. 2001. Elevated carbon dioxide and irrigation effects on water stable aggregates in a Sorghum field: a possible role for arbuscular mycorrhizal fungi. *Global Change Biol.* 9: 333-337.

Rillig, M.C., S. F. Wright, M. R. Shaw, and C. B. Field. 2002. Artificial climate warming positively affects arbuscular mycorrhizae but decreases soil aggregate water stability in an annual grassland. *Oikos.* 97: 52-58.

Rounsevell, M.D.A., A.P. Brignall, and P. A. Siddons. 1996. Potential climate change effects on the distribution of agricultural grassland in England and Wales. *Soil Use Manage.* 12(1): 44-51.

Sardans, J., J. Penuelas, and M. Estiarte. 2008. Changes in soil enzymes related to C and N cycle and in soil C and N content under prolonged warming and drought in a Mediterranean shrubland. *Appl. Soil Ecol.* 39(2): 223-235.

Sombroek, W.G. 1990. Soils on a warmer earth: the tropical regions. In: (eds.) Scharpenseel, H.W., M. Schomaker, and A. Ayoub. pp. 157-174.

Soussana, J.F., E. Casella, and P. Loiseau. 1996. Long-term effects of CO2 enrichment and temperature increase on a temperate grass sward .2. Plant nitrogen budgets and root

fraction. *Plant. Soil*. 182 (1): 101-114.

Tennekoon, L., M.C. Boufadel, D. Lavallee, and J. Weaver. 2003. Multifractal anisotropic scaling of the hydraulic conductivity. *Water Resour. Res.* 39(7): 1193.

Treseder, K.K. and M. F. Allen. 2000. Black boxes and missing sinks: Fungi in global change research. *Mycol. Res.* 104:1281-1283.

van Opheusden, J.H.J., M.T.A. Bos, and G. van der Kaaden. 1996. Anomalous multifractal spectrum of aggregating Lennard-Jones particles with Brownian dynamics. *Physica A*. 227 (3-4): 183-196.

Volk, M., P.A. Niklaus, and C. Körner. 2000. Soil moisture effects determine CO2 responses of grassland species. *Oecologia*. 125:380-388.

Waelbroeck, C. 1993. Climate soil processes in the presence of permafrost - A systems modeling approach. *Ecol. Model.* 69(3-4): 185-225.

Wand, S.J.E., G.F. Midgley, M.H. Jones, and P.S. Curtis. 1999. Responses of wild C4 and C3 grass (Poaceae) species to elevated atmospheric CO2 concentration: a meta-analytic test of current theories and perceptions. *Global Change Biol*. 5 (6): 723-741.

Wang, H.J., Z.S.Yang, , Y. Saito, J.P. Liu, X.X. Sun, and Y. Wang, 2007. Stepwise decreases of the Huanghe (Yellow River) sediment load (1950–2005): Impacts of climate change and human activities. *Global Planet. Change.* 57: 331–354.

Ziska, L.H., J.A. Bunce, and E.W. Goins. 2004. Characterization of an urban-rural CO2/temperature gradient and associated changes in initial plant productivity during secondary succession. *Oecologia.* 139 (3): 454-458.

Table 2.1 Selected soil physical and chemical data of the soil at the sites. OM is organic matter in soil and CEC is cation exchange capacity. Soil N is soil nitrogen content and Soil C is soil carbon content

Site	Urban	Suburban	Rural
Texture (%)			
Sand		32	
Silt		61	
Clay		7	
OM(%)	1.5	1.4	1.3
pH	6.7	6.8	6.6
CEC (cmolc/kg)	5.85	6.24	6.42
Soil N (kg/ha)	771.8	735.8	783.9
Soil C (kg/ha)	13075.2	12876.5	14063.2

Table 2.2 Summary of porosity and parameters from the entropy and universal multifractal analysis: Emax is the maximum value of entropy, Lo is the cell size (voxels) at which Emax is recorded (Eq. 3), and H, C and α are parameters from structure function (Eq.6).

	Urban	Suburban	Rural
Porosity	0.16 ± 0.02	0.15 ± 0.02	0.13 ± 0.02
Emax	0.86 ± 0.02^a	0.79 ± 0.03	0.78 ± 0.04
Lo	25.00 ± 3.92^a	30.95 ± 2.65	34.67 ± 5.50
H	0.28 ± 0.01^a	0.17 ± 0.04	0.21 ± 0.02
C	0.04 ± 0.01^a	0.02 ± 0.01	0.02 ± 0.01
α	1.53 ± 0.19^a	1.90 ± 0.07	1.97 ± 0.09

The letter 'a' represents statistical difference at 95% across sites

Table 2.3 Parameters of Eq. (1) fitted to data from the urban, suburban and rural sites.

		Urban	Suburban	Rural
	T_A	14.06[a]	12.92	12.76
2004	A	17.51[a]	14.70[a]	12.17[a]
	d	0.22[a]	0.32[a]	0.60[a]
	T_A	13.49[a]	13.19	12.55
2005	A	20.22[a]	15.11[a]	12.87[a]
	d	0.16[a]	0.34[a]	0.44[a]
	T_A	14.82[a]	13.76	14.34
2006	A	17.22[a]	14.03[a]	12.57[a]
	d	0.24[a]	0.37[a]	0.50[a]

The letter 'a' represents statistical difference at 95% across sites

Table 2.4 Eigenvalues and variable contributions from the PCA of environmental
variables and parameters from image analyses: Emax and Lo are parameters from the
configuration entropy (Eq. 3), H, C and α are parameters from the structure function
analysis (Eq. 6), ζ (0.5), ζ (1), and ζ (2) are the slopes of the structure function at q=0.5,
1, and 2 respectively, Biomass is above ground plant biomass, CO2 is the
concentration of atmospheric CO2 and TA, A, and zd were parameters from (Eq. 1)
fitted to data from each site.

	Eigenvalue		Contribution of variables	
	Factor 1	Factor 2	Factor 1	Factor 2
Emax	-0.27	-0.05	0.07	0.00
Lo	0.27	0.15	0.07	0.02
H	-0.25	0.23	0.06	0.05
C	-0.27	0.02	0.05	0.00
α	-0.02	0.60	0.00	0.36
ζ (0.5)	-0.26	0.21	0.07	0.05
ζ (1)	-0.15	0.26	0.01	0.07
ζ (2)	-0.15	0.26	0.01	0.07
biomass	-0.27	0.03	0.08	0.00
CO_2	-0.27	-0.10	0.07	0.01
Daytime temperature	-0.18	0.45	0.03	0.20
Nighttime temperature	-0.27	-0.03	0.08	0.00
T_A	-0.27	-0.03	0.06	0.00
A	-0.26	-0.20	0.05	0.04
zd	0.23	0.33	0.05	0.11
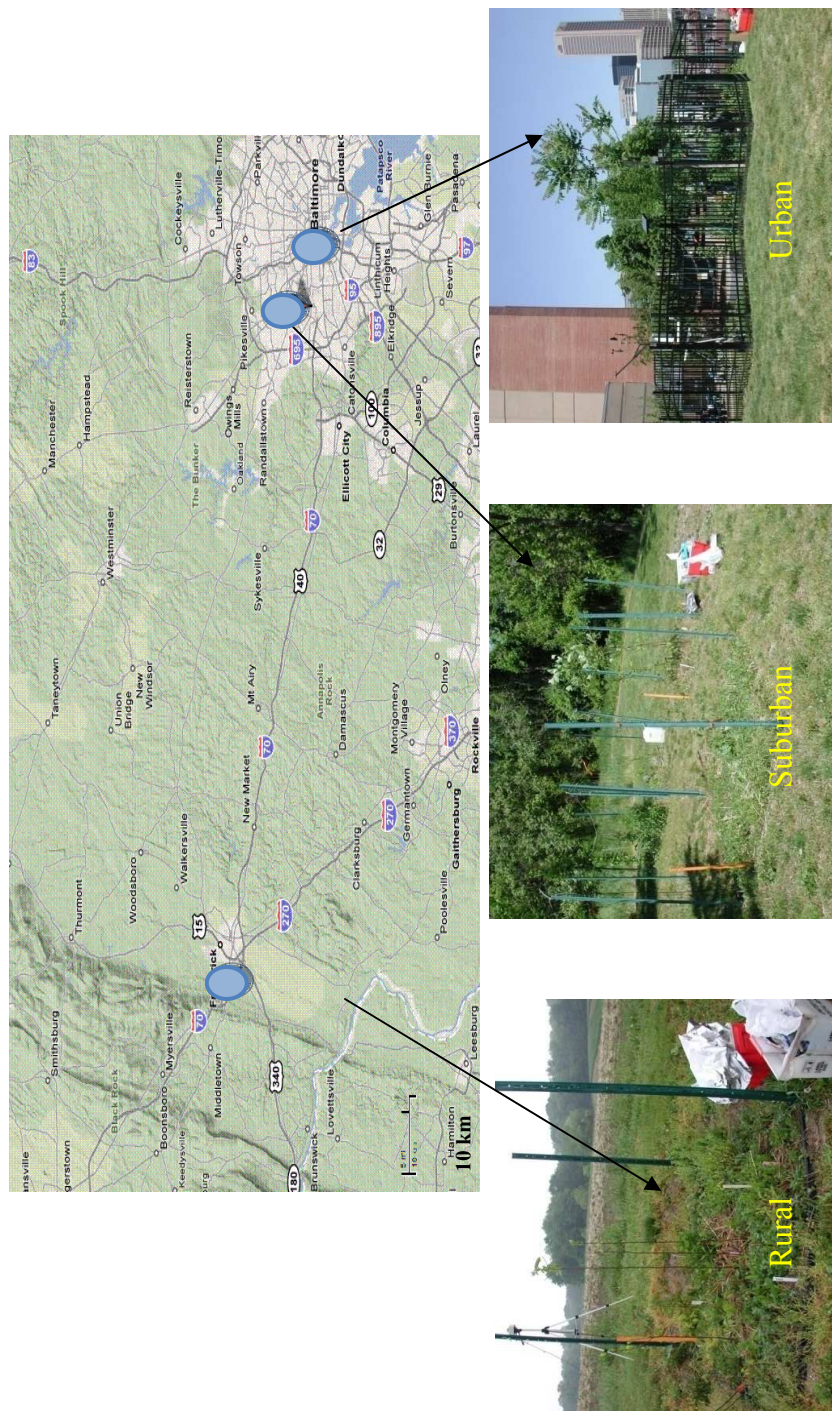
Figure 2.1 Map of Baltimore area and pictures of the sampling areas. The rural site was at an organic farm near Buckeystown, Maryland approximately 87 km west of Baltimore. The suburban site was a site at the Carrie Murray Nature Center on the outer edge of the Baltimore city. The urban site was at the Baltimore science center inside the city.
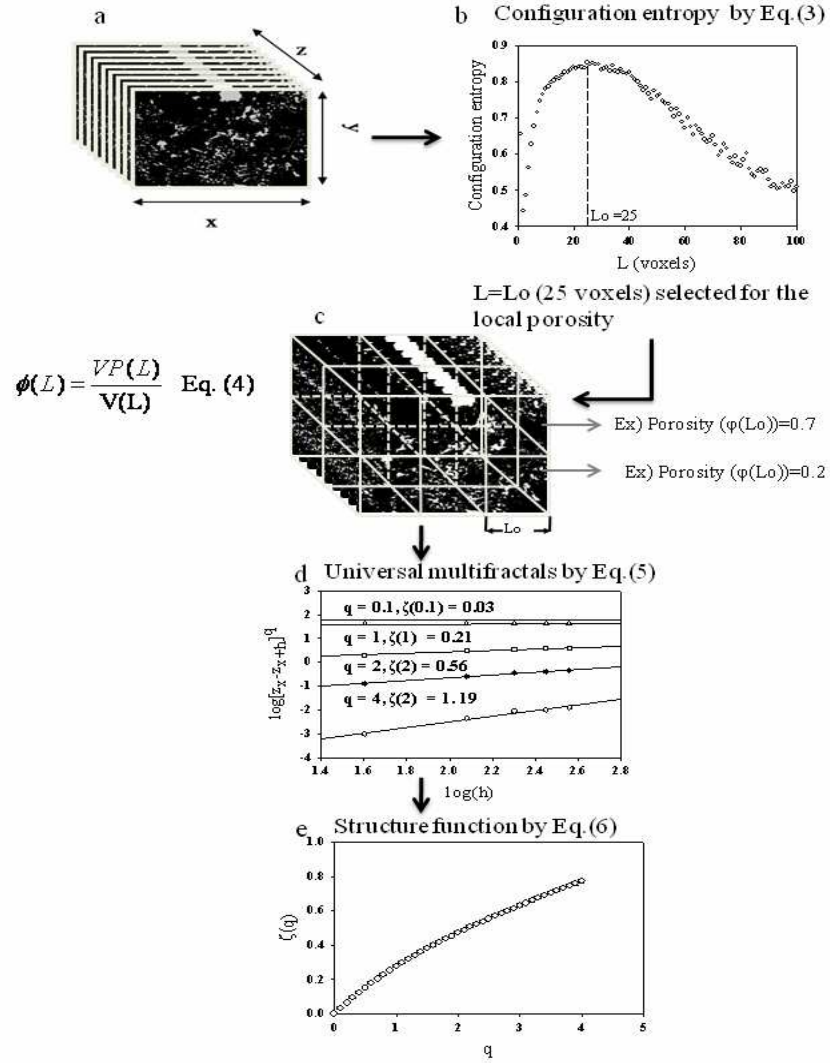
Figure 2.2 Diagram of image processing and pore spatial distribution analyses (entropy and universal multifractals): a. Stack of binary image slices (x=1000 voxels, y=1000 voxels, z (depth) =1000 voxels), b. Configuration entropy calculation, c. Local porosity calculation at cell size, Lo, d. Universal multifractals and and e. Structure function calculation.
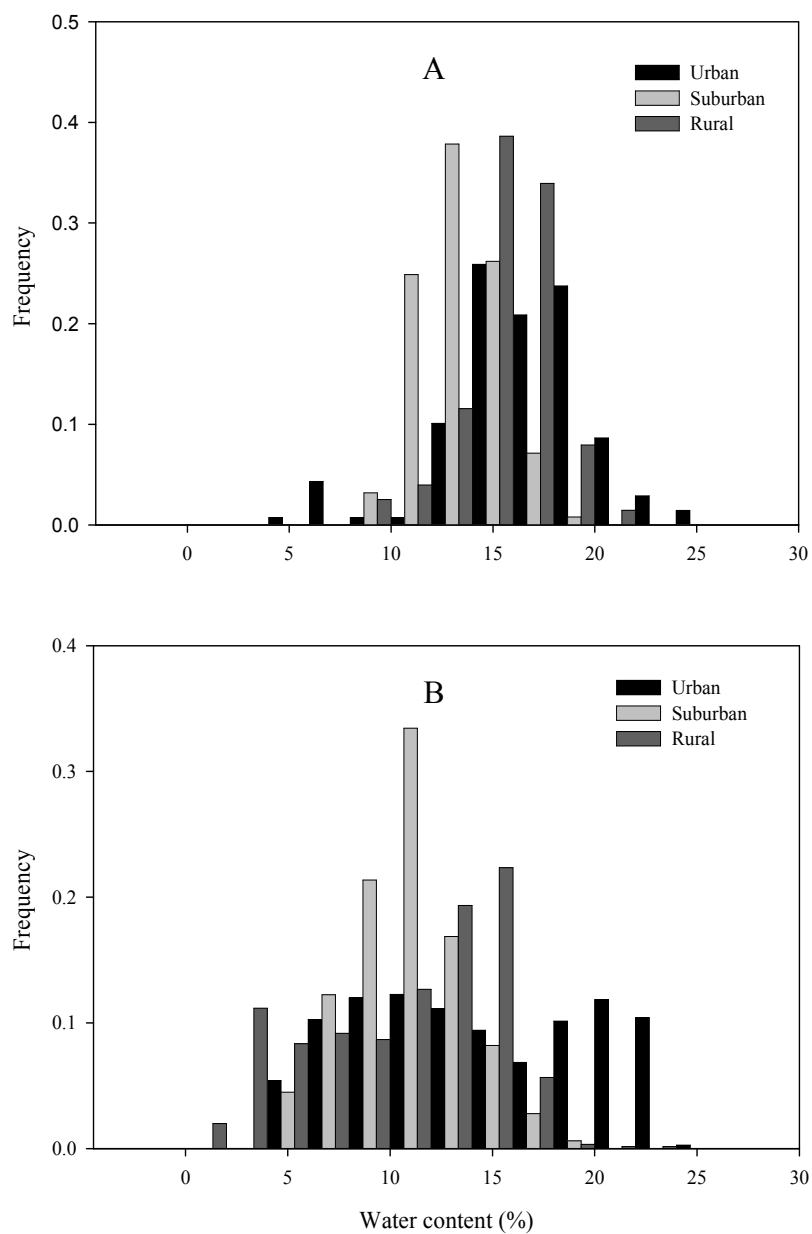
Figure 2.3 Distributions of soil moisture from each site during the period of 2004-2006. A: Soil moisture data during the growing season and B: Soil moisture data outside the growing season.
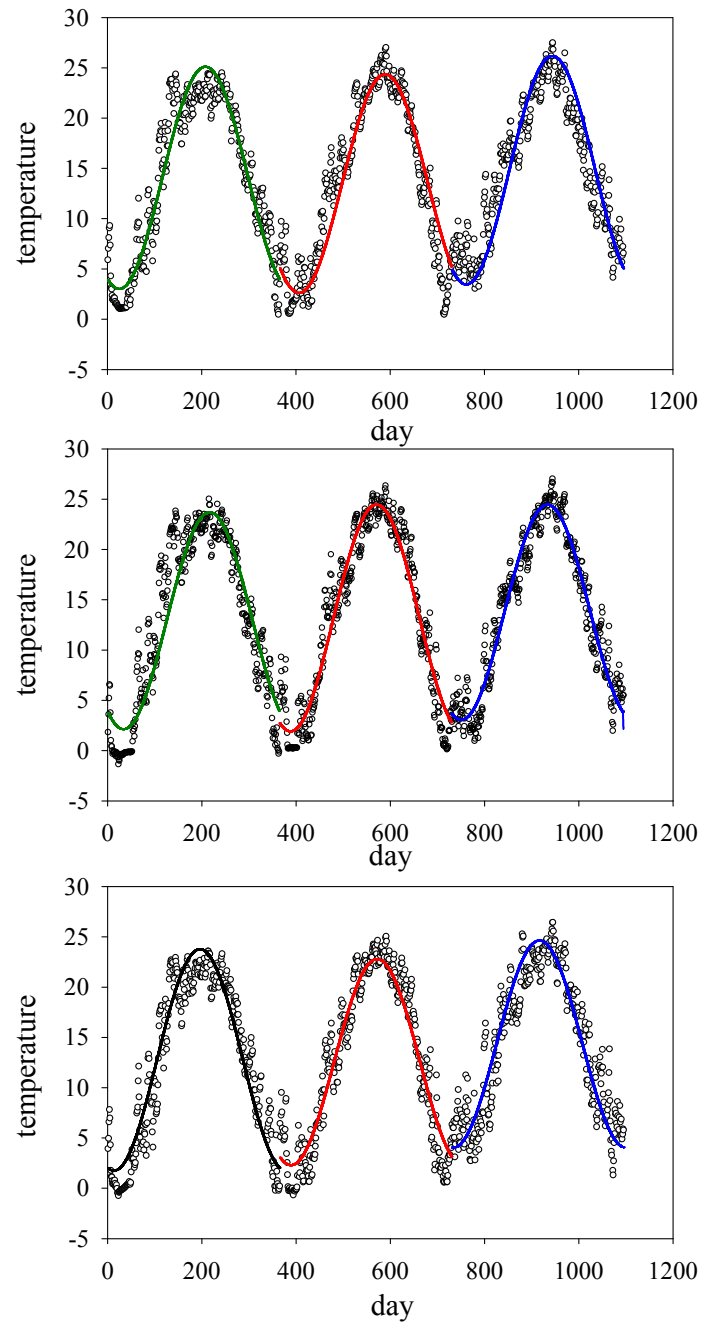
Figure 2.4 Soil temperature data from the urban (top plot), suburban (middle plot) and rural (bottom plot) sites. Lines are fit with Eq. (1) for years 2004 (green), 2005 (red) and 2006 (blue).
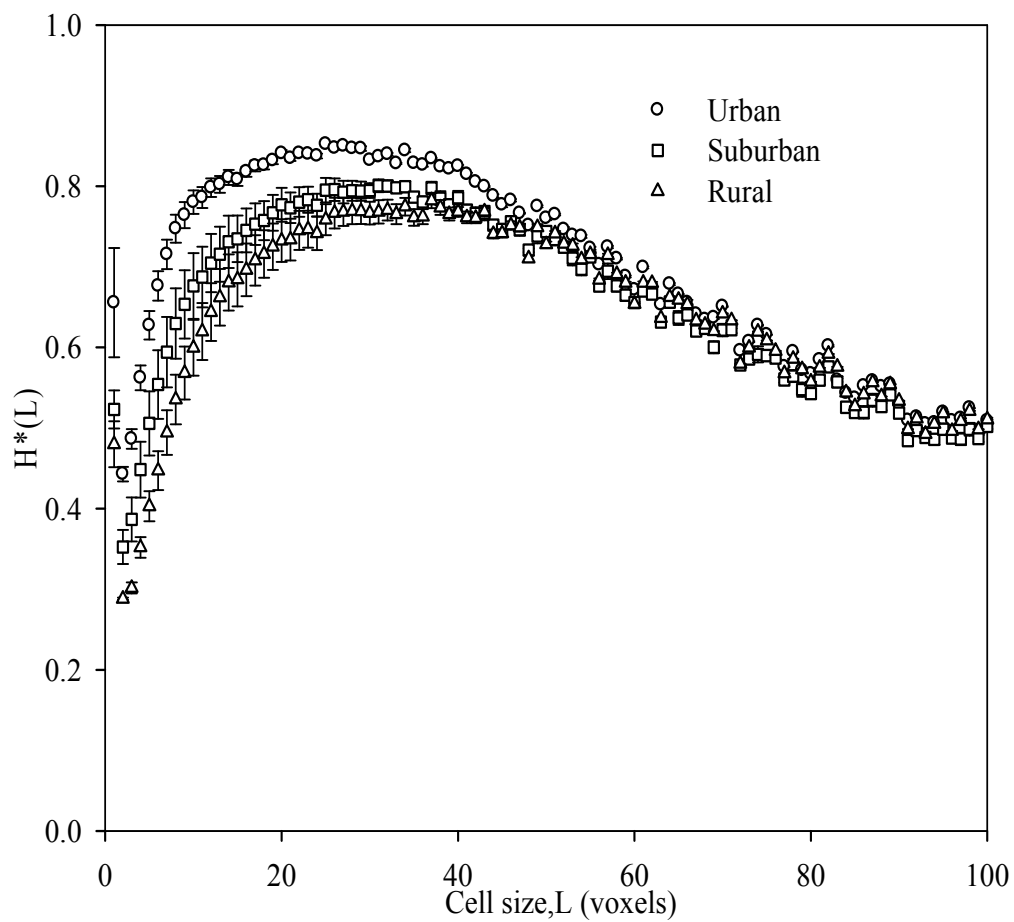
Figure 2.5 Results from the configuration entropy analysis. Values are site averages from three images; bars are standard deviations.
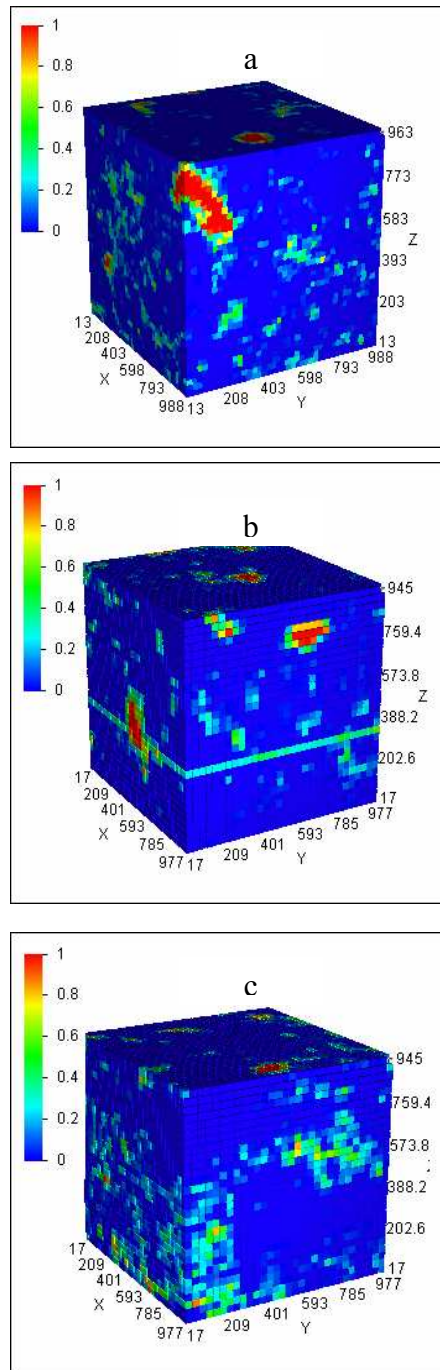
Figure 2. 6 Distributions of local porosity from selected samples at cell sizes; a: Urban soil at cell size of 25^3 voxles, b: Suburban soil at cell size of 32^3 voxels and c: Rural soil at cells size of 32^3 voxles. The legend represents porosity from each cell.
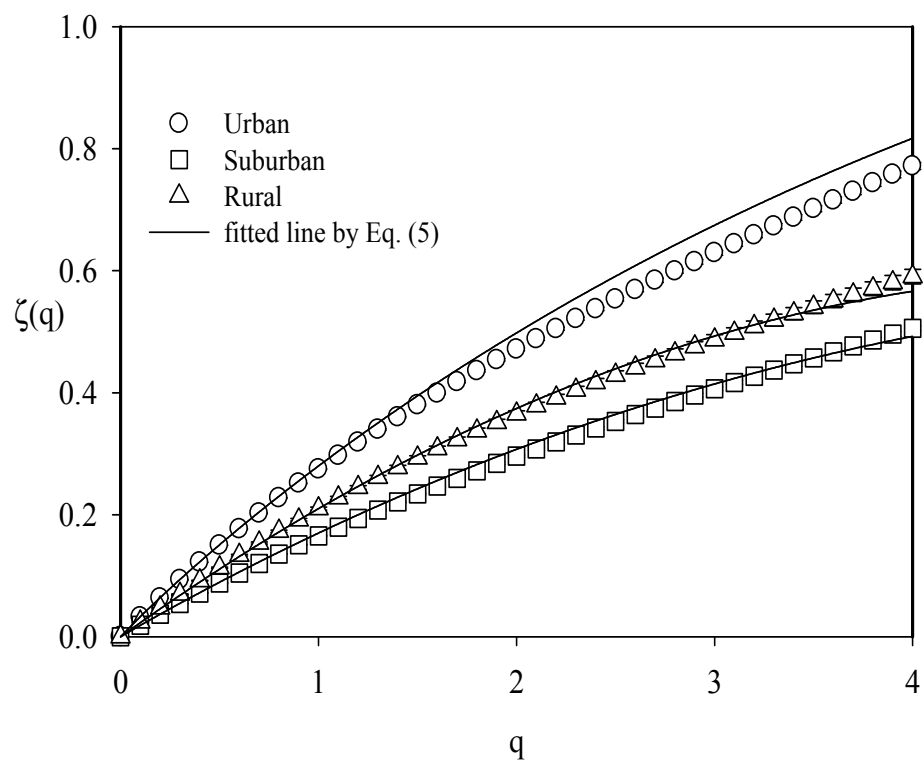
Figure 2. 7 Structure function results from each site calculated with Eq. (4) and fitted line with Eq. (5).
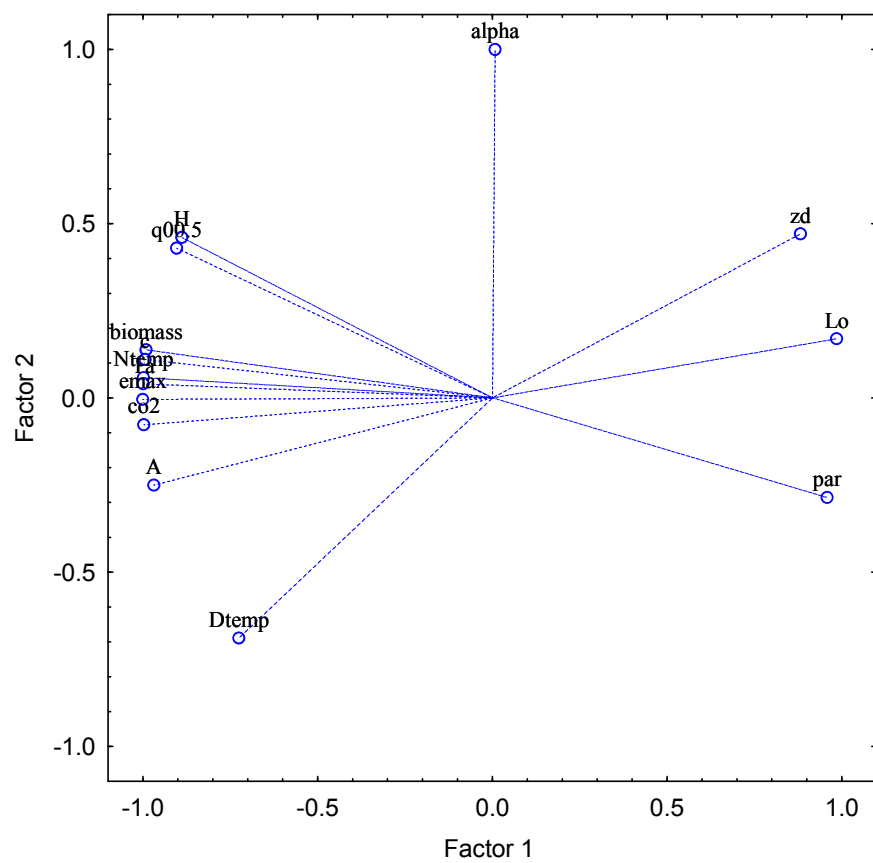
Figure 2. 8 The projection of variables from eigenvalue scores
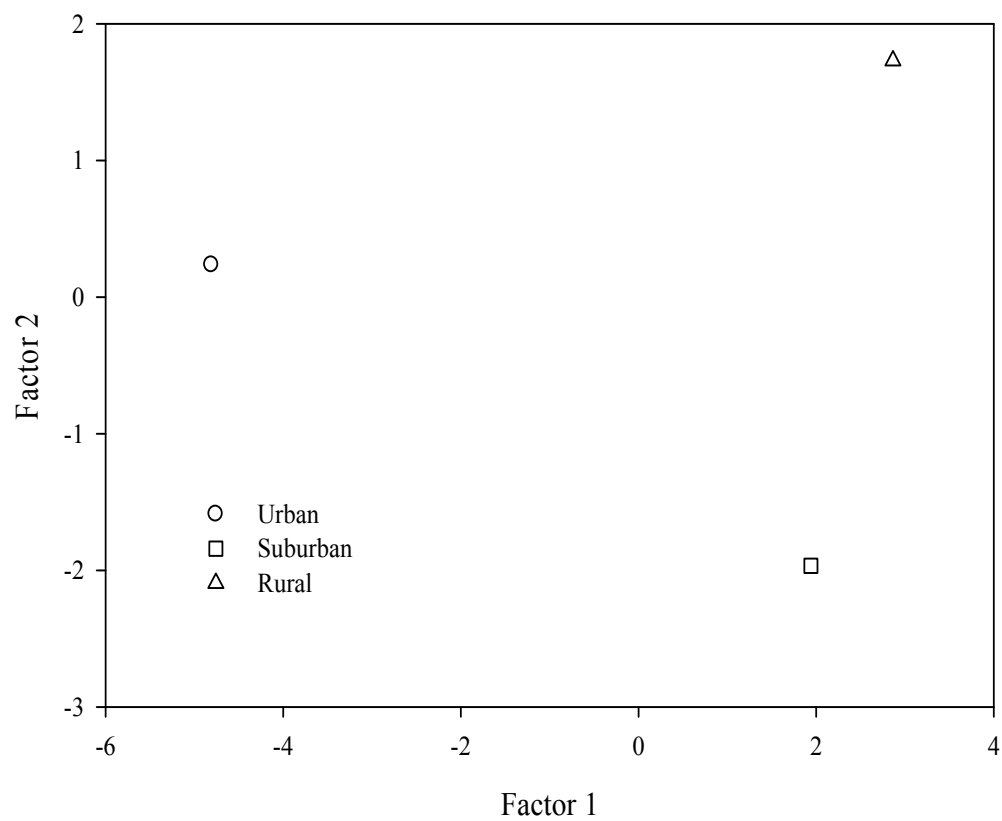
Figure 2. 9 Site classification based on PCA analysis of variables

Chapter 3 : Climate Effects on Pore Morphological and Hydraulic Properties

3.1 Climate Effects on Soil Structure

Increases in atmospheric CO_2 concentration and temperature have been proven to affect different components of ecosystems, such as plant, soil organic matter and microbial community (Zak et al., 2000; King et al., 2005; Koca et al, 2006). Since roots influence soil pore formation, soil organic matter, and soil microbes, changes of atmospheric CO_2 concentration and temperature are likely to affect soil pore formation and pore geometry.

3.1.1 Changes of Inter-Aggregate Pore Formation under Elevated CO_2 Concentration and High Temperature

The formation of inter-aggregate pores in soils is affected by activities of soil fauna, growth of plant roots and physical processes such as dry/wet cycles (Ou et al., 1998). No clear trend has been determined in property or activity changes of soil fauna, root growth or dry/wetting cycle under elevated CO_2 concentration and temperature.

Soil moisture content is an important factor that affects physical and biological activities. Soil moisture increases under enriched CO_2 concentration and decrease under warming condition (Volk et al., 2000; Morgan et al., 2004; Leipprand and Gerten, 2006). If there is no reduction of soil moisture, enriched CO_2 concentration and warming would increase diversity of soil fauna, would stimulate root growth and would enhance earthworm burrowing activity, which in turn, woul create inter-aggregate pores (Couteaux and Bolger, 2000; Pendall et al., 2004). There is no report about dry-wet cycle changes in soil under enriched CO_2 concentration and warming conditions. However, it can be speculated that with sufficient soil moisture, drying/wetting cycles would decrease because soil moisture buffers heat transport and changes in soil temperature (Hollister et

al., 2006). Increase of soil moisture and less dry-wet cycles would prevent development of inter-aggregate pores in soil (Six et al., 2004). Increment in root and soil fauna activities would produce more inter-aggregate pores by void spaces treated by root penetrations and earthworm burrowing, while less drying/ wetting cycles would prevent development of inter-aggregate pores.

3.1.2 Changes of Intra-Aggregate Pore Formation under Elevated CO_2 concentration and High Temperature

The formation of intra-aggregate pores is affected by soil microbial activities (Park et al., 2005). Responses of microbial activities to climate changes are not straightforward. With sufficient water and nutrients, greater temperatures and CO_2 concentrations would increase the quantity and diversity of microbial community (Ebersberger et al. 2003; Janus et al, 2005; Klironomos et al., 2005; Lipson et al., 2005). The greater microbial community would create more intra-aggregate pores in soil (Park et al., 2005). Soil fauna contributes to inter-aggregate pore formation as well by the stimulation of nutrient processes. Characterization of pore morphology would help to understand effects of climate changes on soil because there are different mechanisms of pore formations.

3.1.3 Pore Morphology and Hydraulic Properties

1) Pore Morphological Analyses

Soil pore size and shape influence soil water transport/biological processes, therefore quantification of these properties is important to understand these processes (Leij et al., 2006). Soil pores occur in a wide range of sizes and shapes in nature (Pagliai and Vignozzi, 2002). Pore size distribution is determined by water retention

measurements or mercury intrusion porosimetry (Pagliai et al., 1995; Strudley et al. 2008). The equivalent radius of the largest pore that is filled, with water/mercury, is a function of the soil water/mercury pressure through the capillary action. These experimental methods are fully developed and are considered good characterizations of soil pore size distributions. However, they cannot provide accurate description of pore sizes, because there can be changes of soil conditions (expansion or shrinkage of the sample) during the measurements (Pires et al., 2005). Recent development of image analyses, especially three dimensional image analyses, makes possible the quantification of pore volumes directly (Peth et al., 2008; Sluetel et al., 2008; Udawatta and Anderson, 2008). Pore sizes or volumes, from three dimensional images are a better measure of real pores than pore geometry measurements from two dimensional images, since soil pores are three dimensional systems in soil (Barstardie et al., 2003). Studying the computer tomography provides the images that pore volumes can be driven. Slutel et al. (2008) quantified pore volumes with a resolution of 1.7 μm in diameter, while Barstardie et al. (2003) analyzed pores created by earthworms with diameter of up to 10 cm.

Another characterization of pore geometry is pore shape, which is related to irregularity or roughness of a pore (Droogers et al., 1998). Pore shapes are normally categorized as rounded, irregular and elongated. Elongated pores are often associated with the packing of aggregates or sand grains and therefore, are usually well connected (Posadas et al., 2003). In contrast, round pores are generally created by arrangements of particles or by compaction. These pores have lower connectivity than elongated pores (Fox et al., 2004; Lima et al., 2006). Irregular pores are intermediate between elongated and rounded pores.

Pore shapes affect soil water transport because round pores are less effective in transmitting water than irregular and elongated pores (Fox et al., 2004). Therefore, understanding pore shape is critical to estimate accurate hydraulic properties (Assouline and Or, 2008). To date, pore shapes were quantified from two dimensional soil images (Posadas et al., 2003; Fox et al., 2004), which may not be an accurate representation of real pore shapes (Glab, 2007). There has been no actual measurement of pore shape from three dimensional soil images.

3.1.2 *Hydraulic Properties*

The characterization of water movement through soil is important to determine soil quality for agricultural/ environmental management of soil (Strudley et al., 2008). Characterizations of hydraulic properties reflect pore structural characteristics in a soil system (Hayashi et al., 2006). The hydraulic behavior of soils is affected by pore structure and it becomes complicated by the duality of the pore system of large inter-aggregate pores and the much finer intra-aggregate pores.

1)   Water Retention Characteristic Curves

Water retention characteristic curves (WRC) refer to the relation between the matric potential of soil water and volumetric water content (Gimenez et al., 1997). Soil texture and soil structure affect WRC (Wittmuss and Mazurak, 1958; Tamboli et al., 1964; Amemiya, 1965). For example, comparing soils with small and large aggregates, the former tend to have smaller water retention values at matric potentials from 0 to 1 kPa, greater water retention values at lower matric potentials than the latter (Tamboli et al., 1964; Chang, 1968).

Since three dimensional images can provide distributions of pore volumes, water retention values can be computed inversely from pore size distributions and matric potentials from corresponding pore sizes (Vogel and Roth, 2001). Peth et al. (2008) calculated WRC from aggregate images and found computed WRC captured different pore systems that resulted by different treatments.

Water retention models are developed to describe WRC. One of the most widely used models is the van Genutchen (1980) model, which fits experimental data relatively well (Dexter, 2004). However, this model describes pore structure as a unimodal system while a soil pore system is commonly a dual system. Therefore, hydraulic parameters or functions from unimodal models can be inaccurate. Gerke and van Genuchten (1993) developed dual-porosity models which describe the porous medium as two systems, representing the macro (inter)- and micro (intra-aggregate)-porous systems. Durner (1994) and Seki (2007) used bi-modal hydraulic functions to describe the properties of the inter- and intra-aggregate pore regions. Dual-porosity models and bi-modal hydraulic functions have been widely used in modeling soil WRCs (Jarvis, 2008; Simunek and van Genutchen, 2008).

1) Hydraulic Conductivity

Hydraulic conductivity is determined by the ability of the soil fluid to flow through the soil matrix system under a specified hydraulic gradient (Radcliffe and Rasmussen, 2002). The hydraulic conductivity is especially related to inter-aggregate pore conditions (Balland et al., 2008). Under conditions close to saturation, the large inter-aggregate pores form the primary pathways for rapid infiltration.

Hydraulic conductivity can also be estimated from three dimensional soil images. Hydraulic conductivity can be calculated with soil water contents and matric potentials (Green and Corey, 1971; Mualem, 1976; Wosten and Van Genuchten, 1988). The van Genutchen - Mualem model (van Genutchen, 1980) is one of most widely used models to estimate hydraulic conductivity. However, if the soil has a dual pore system, this unimodal model of conductivity is not accurate and some studies questioned its validity (Durner, 1994; Mohanty et al., 1997; Vogel and Roth, 2004). Bimodal hydraulic conductivity curves can be characterized with two or more distinct curves of conductivity across potentials that describe inter- and intra-aggregate pore system separately (Durner, 1994).

Hypotheses of this chapter were that changes of atmospheric CO_2 concentration and temperature would induce changes of pore formation, and that the change of pore structure would be observed from pore geometry and measured and computed hydraulic properties.

The objectives of this study were

1. Characterization soil pore morphology, from three dimensional images, based on a pore network model from local porosity distributions at cell size 8^3 voxels,

2. Combine measured hydraulic properties from experiments with calculated hydraulic properties from images to describe accurate pore structure and

3. Compare hydraulic properties (water retention and hydraulic conductivity) between bulk soils from different atmospheric CO_2 concentrations and temperatures.

3.2 Materials and Methods

3.2.1 Soils

All soil samples were taken from the sites in Baltimore, MD as explained in Chapter 2. In this study, one aggregate and one bulk soil sample from the urban (with highest atmospheric CO_2 concentration and temperature) and the rural (with lowest atmospheric CO_2 concentration and temperature) sites were used for morphological analysis. The representative sample from each site was selected to have Emax and Lo values close to the average values of each site (Chapter 2).

3.2.2 Image Acquisition and Image Analyses

The same image processes from previous chapters were used and the image resolution was 22 μm for the bulk soils and 6 μm for the aggregates. Image size for the bulk soil was 10648 mm^3 and the aggregate was 10.76 mm^3. The binarization procedure was explained in Chapter 2.

A pore network model was applied for local porosity distributions at the cell size of 8^3 voxels (0.176 mm for the bulk soil and 0.048 mm for the aggregate) since this cell size was the minimum size possible for computation.

    1)   Local Porosity Distribution

First, the local porosity distribution for a cell size of 8^3 voxels (L^3) was calculated. The three dimensional images were divided by L^3 and porosity of each cell was recorded. The local porosity ($\phi(L^3)$) was obtained as:

$$\phi(L^3) = \frac{VP(L^3)}{V(L^3)} \tag{1}$$

where $V(L^3)$) is total number of voxels from a cell and $VP(L^3)$ is a number of pore voxels from a cell. This calculation was repeated to cover all cells in an image.

    2)   Pore Identification From Local Porosity

A Fortran code was written to identify pores from local porosity distribution (Appendix C). The local porosity distribution displayed porosities ranging from 0 to 1 from each cell (Fig. 3.1). These local porosities were assigned to solid (0) voxel or pore (1) voxel from each cell. Cells with porosities of less than 0.5 were considered solid cells and assigned a value of 0, while others were considered pore cells with a value of 1. For example, if a cell had porosity of 0.52, that cell was assigned a value of 1. Hu and Stroeven (2005) considered cells with more than 0.45 in porosity as percolated pore cells from three dimensional porous images.

This study adopted 26-connectivity to define connected cells (Lee et al., 1994). This algorithm considered all possible connections such as face, edge and point connections to a center or a given cell (Fig. 3.2). The code followed connected pore cells until a loop or a connection was closed. The 26-connectivity method required more time and computer capability than the traditional 6-connectivity technique which considered only face connections to a given cell. However, Lee et al. (1994) found that the 26-connectivity method was more sensitive and accurate to define connectivity and geometry of three dimensional objects. To discriminate noises from real pores and separate individual pores more clearly from neighboring pores, pore cells with less than 2 connected pore cells were not considered as pore cells.

This process provided locations and identifications of each pore in an image. After finishing pore identification, total porosity for each image was calculated by dividing total number of pore cells divided by the number of cells.

3)   Burning and Medial-Axis Skeletonization

Medial-axis skeletonization was applied to extract representative pore geometry and pore networks (Lindquist and Venkatarangan, 1999). This algorithm was derived by finding continuous axes located in the middle of a pore to provide simple and compact geometric information (see Fig. 1.3). The first step of medial-axis skeletonization is burning pore cells. Lindquist and Venkatarangan (1999) explained that burning is analogous to fire spreading. If each pore is set in fire simultaneously all around its boundary, it will burn toward the center of the pore. As fire moves inside, pore pixels or voxels, in contact with the fire, are assigned burn numbers that increase towards the center of a pore.. Greater burn numbers imply larger pores, since it takes longer to reach the center of the pore.

In this study, boundary pore cells (i.e., connected to solid cells) were assigned the burn number 1. The next layer of connected pore cells were assigned burn number 2. This was repeated with unit increment of a burn number until all pore cells were assigned burn numbers (Fig. 3.3.a).

Medial-axis (MA) represents the skeleton of a pore, constructed by connecting the center voxels of a pore. Lindquist et al. (1996) selected MA voxels based on burning directions. If burning entered two different directions into one voxel, that voxel became a MA. However, this study did not follow that approach because it was computationally very demanding. Instead, MA cells were selected based on burn numbers and location of pore cells according to the following criteria:

    a.   pore cells with maximum burn number (orange cells in Fig. 3.3.a)

    b.   greater burn number than all connected pore cells (local maximum, blue cells in Fig. 3.3.a)

    c.   pore cells with the same burn number at perpendicular positions (yellow

        cells in Fig. 3.3.a), and

    d.   pore cells with the same distance from different boundaries (green cells in

        Fig. 3.3.a).

After selecting MA cells from a pore, all MA cells were connected from a top

slice of the pore in the z direction to a MA cell at bottom (Fig. 3.3.a). The final result of

MA construction would be representative center cells connected from top to bottom of

each pore (Fig. 3.3.b).

    4)   Throat and Coordination Number Calculation

In geometrical terms, pores are modeled as a relatively large pore-body connected

by relatively small throats (Vogel and Roth, 2003). In this study, pore-body and throats

were calculated based on MA cells. First, nodes for each pore were selected if a MA cell

with the maximum burn number was connected with at least three different MA cells (Fig.

3.3.a, cells with black bold burn numbers). A pore-body volume can be calculated by

dilating a cube from a node with a maximum burn number (center node) (Lindquist and

Venkatarangan, 1999). An initial cube corresponding to a cell unit volume was placed on

a center node and the its volume was dilated until it touched a boundary of the pore or a

boundary of other pore-body volume. This cube volume became a pore-body volume

(dark blue line in Fig. 3.3.a). In case of more than one node with the same maximum

burn number this procedure was repeated from each node and added up for a total pore-

body volume. In case of multiple pore-bodies, volumes of channels connecting two pore-

bodies (i.e., throats) were calculated (Fig. 3.3.a). Similar to pore-body volume, throat

volume was calculated by placing a unit cell size cube in a node and the volume

increased until it touched boundary or pore body cells (purple line in Fig. 3.3.a). The

throat nodes were selected if a MA cell with a local maximum burn number was

connected with two MA cells (cells with red bold burn number in Fig. 3.3.a). In the pore

network model, coordination number implies connectivity and is expressed as number of

throats connected to a pore-body. In Fig. 3.3.a, a pore-body with one connected throat is

illustrated (coordination number equal to 1).

5)   Length and Tortuosity Calculation

Pore length and tortuosity were calculated for all pores. Pore length was

determined as the length from the MA cell at the top of a pore (closest to surface) to the

MA cell at a bottom of a pore (gray line in Fig. 3.3.a). Tortuosity was calculated a the

ratio between a shortest or straight distance from the top to the bottom of a pore (dashed

line in Fig. 3.3.a) an the actual pore length (gray line in Fig. 3.3.a).

6)   Pore Shape

The pore shape index S was calculated as (Marwan et al., 2007);

$$S = \frac{SA}{\sqrt[3]{36\,\pi V^2}} \tag{2}$$

where SA is the surface area (mm^2) and V is the volume of a pore. The SA values were

calculated from the radius and length of each pore by assuming that pores were of

cylindrical shape. Therefore, the SA were calculated as $2\pi\,(r^2+rl)$, where r is pore radius

and l is pore length. Pore radius (r) was calculated from pore volume (V) as $(V^{1/3})/2$. A

S value of 1 implies a spherical shape. As pores elongate and tend to a cylindrical shape,

the values of S increases.

4.2.3 Bulk Density

After scanning the bulk soil sample, the bulk density (ρ_b) was measured by the saran resin procedure (Sheldrich, 1984). The sample was prepared by coating the sample with a saran resin. This sample was weighed in air and then in water. The weights before and after dipping in saran and weight after immersed into water were used to calculate actual weight and volume of the sample (Brasher et al., 1966).

$$\rho_b = \frac{W}{V} \tag{3}$$

where ρ_b is the bulk density, W is weight of soil sample and V is volume of soil sample. W was calculated by ($W1$-$W2$/N-1) +$W1$-$W2$, where $W1$ is weight in air after N time dipping into saran and $W2$ is weight in air before dipping. Volume V was calculated as $W1$- $W3$-(W/1.3), where $W3$ is weight after immersed into water and 1.3 (g/cm^3) is the density of saran. Bulk density was measured in triplicates.

The saturated water contents (θ_s) from all samples were calculated from the bulk density results as;

$$\theta_s = 1 - \frac{\rho_b}{\rho_p} \tag{4}$$

where ρ_b is the bulk density and ρ_p is particle density assumed to be equal to 2.65 g/cm^3.

3.2.4 Water Retention and Hydraulic Conductivity

Water retention and infiltration rate were measured after measuring bulk density. Each sample was cut in discs of 3 cm in height and flat surfaces at both ends. One of the ends was placed on top of a ceramic plate contained in a cell designed to measure hydraulic conductivity and soil water retention in the range of the pressure heads between 0 and -10 kPa. Before the samples were placed in the pressure plate extractors, steady-state infiltration rate was measured for all bulk soil samples. The tension disc

infiltrometer used in this study was from Decagon Devices (Pullman, WA). Five pressure heads of – 0.2, - 0.3, - 0.4, -0.5, and – 0.6 kPa were applied and the steady-state infiltration rates were measured.

Soil water retention was measured at pressure potentials of -0.3, -0.6, -1, -1.5, -3, -6, and -10 kPa. After measuring water retention at -10 kPa, water retention at pressures of -30, -100, and -300 kPa were measured on the samples using pressure plate extractors.

Water retention was also computed from pore size distributions for the bulk soil images by assuming that pores hold water inside with capillary force and matric potential ψ_i was calculated with corresponding pore radii r_i, using Young – Laplace equation (Peth et al. 2008):

$$\psi_i = 2\sigma \cos(\varpi)r_i^{-1} \tag{5}$$

where σ is the interfacial tension between air and water (72.7×10-3 Nm^{-1}) and ϖ is the contact angle assumed to be 0. At each potential, pores whose radii are smaller than the radius corresponding to the potential are saturated. This water content value at each potential was divided by image volume. Since the measured water retention data were calculated by gravimetric water content, computed water retention data were divided by the average bulk density of each soil. If a pore had throats, the smallest throat radius was used in Eq. (4). The computed data were matched to the measured water retention. In the matching process, the highest matric potential from images was about -0.3 kPa. Therefore water contents at -0.3 kPa from images and average water content at -0.3 kPa from measurements were assumed as the same value of water retention. Water retention contents from images at greater matric potentials were added to the retention value at -0.3 kPa

Unsaturated hydraulic conductivity was calculated as according to Green and

Corey, (1971);

$$K(\theta) = \frac{K_s}{K_{sc}} \cdot \frac{30 \, r^2}{\rho_w \cdot g \cdot \eta} \cdot \frac{\varepsilon^{\tau}}{n^2} \sum [(2j + 1 + 2i)\psi_j^{-2}] \tag{6}$$

where $K(\theta)$ is the calculated conductivity for a specified water content or pressure (m/s),

θ is the water content (m^3/m^3), i denotes the last water content class, ρ_w is the density of

water (kg/m^3), g is the gravitational constant (m/s^2), γ is the viscosity of water ($kg/m \, s^{-1}$),

ε is the porosity (m^3/m^3) or water content at corresponding potential, τ is a tortuosity

parameter, n is the total number of pore classes, ψ_i is the pressure for the largest pore

with water filled by capillary force. The pressure ψ_i corresponding to θ_j was obtained

from water retention data. The τ value was calculated as (actual pore length/shortest

length)^2 from each pore. K_s / K_{sc} is the matching factor, where K_s is the measured

saturated conductivity and K_{sc} is calculated conductivity. The value of K_s was

0.11cm/min for the urban bulk soil and 0.06 cm/min for the rural bulk soil from

infiltration rate measurement at -0.1kPa. K_{sc} values were calculated from the largest

pore in the image of each sample and the urban bulk soil was 0.45 cm/min and the rural

soil was 0.32 cm/min. The greatest matric potential from the measured conductivity data

was -0.2 kPa and the computed conductivity at -0.2 kPa from an image was matched to

the one from the measured data at -0.2 kPa.

3.2.5 Statistical Analysis

All properties (except number of pores and coordination numbers) were

calculated exhibited lognormal distribution (Appendix B). Thus, the geometric mean (*E*)

and standard deviation (*StdDev*) were calculated as;

$$E = e^{\mu + \sigma^2/2} \tag{7}$$

and

$$StdDev = \sqrt{(e^{\sigma^2} - 1)e^{2\mu + \sigma^2}} \tag{8}$$

where μ and σ are the mean and standard deviation of the natural log transformed variables.

Water retention curves were fitted with the bimodal model of Durner (1994);

$$S_e = v_1 \left[\frac{1}{1 + (\chi_1 \psi)^{n_{11}}} \right]^{m_1} + (1 - v_1) \left[\frac{1}{1 + (\chi_2 \psi)^{n_{12}}} \right]^{m_2} \tag{9}$$

where S_e is the effective water content, Ψ is matric potential (kPa), and v_1, χ_1 (m^{-1}), χ_2 (m^{-1}), n_1, and n_2 are fitted parameters. The m parameters are determined by $m = (1-1/n)$. The fitting of water retention was done with the software "SWRC fit" developed by Seki (2007) (http://seki.webmasters.gr.jp/swrc/).

The hydraulic conductivity curves ($k(\psi)$) from image analyses and measurements were fitted with the bimodal model of Durner et al. (1999);

$$k(\psi) = \begin{cases} K_s (v_2 S_{e1})^\tau \dfrac{\left(v_2 \chi_3 \left[1 - (1 - S_{e1}^{1/m_{21}})^{m_{21}}\right]\right)^2}{(v_2 \chi_3)^2} & \psi < \psi_b \\ \\ K_s ((1 - v_2) S_{e2})^\tau \dfrac{\left(v_3 \chi_4 \left[1 - (1 - S_{e2}^{1/m_3})^{m}\right]\right)^2}{(v_3 \chi_4)^2} & \psi_b < \psi \le 0 \end{cases} \tag{10}$$

where $S_{ei} = \left[1 + (\alpha_i |\psi|)^{n_i}\right]^{m_i}$ is the partial saturation of the ith pore system and ψ_b is the matric potential at a breakpoint of different pore systems. The v_2, v_3, χ_1, χ_2, n_3, n_4 and $m_2 = (1-1/n)$ are fitted parameters. The parameter τ is related to tortuosity and average

tortuosity results from image analysis were applied to Eq. (9). The fitting was performed with a Fortran program.

Statistical differences among fitted parameters from water retention curves and hydraulic conductivity curves were determined by multivariate ANOVA. The t-test at 95% level was applied to find statistical differences in configuration entropies from all samples. All distributions of pore properties from the aggregate and bulk soil sample were converted to histograms to obtain frequencies and test differences between soil samples. The logarithm of pore-body volumes were grouped into 30 classes covering from 1×10^{-4} to 2000 mm^3. Throat volume data were converted into 20 classes ranging from 2×10^{-6} to 0.05 mm^3. Pore length data were converted into 20 classes ranging from 0.05 to 5 mm, while tortuosity data were grouped into 5 classes covering values from 1 to 5. The statistical tests were performed by three categories; two samples (aggregate and bulk soil), three image sizes and 12 cell sizes. The chi-square test was applied to test the equality of frequency distributions at 95% level using SPSS software (SPSS Inc.).

3.3 Results and Discussion

3.3.1 The Configuration Entropy and Local Porosities

Configuration entropies were computed as in Chapter 2 and there were statistical differences between pore structure in the bulk soil samples from the urban site and the one from the rural site On the other hand, there was no difference in the configuration entropy of aggregates images from the urban and the rural sites (Fig. 3.4). The urban bulk soil showed greater Emax 0.84 at Lo of 20 voxel cell size, while rural soil had Emax of 0.76 at 35 voxel cell size. Both aggregates from the urban and rural had Lo values equal to 21 voxel and Emax values of 0.76 and 0.74, respectively.

These results imply that aggregates had similar soil structure, although it is hard to be conclusive with only the results of the entropy. Local porosity was calculated at cell size of 8^3 voxels (Fig. 3.5). Pore morphological properties were calculated on these images.

3.3.2 Pore Morphological Properties

1) Porosity and Numbers of Pore and Throat

Porosity and numbers of pores and throats were obtained from all images (Table 3.1). There was only one value of porosity and number of pores and throats from each sample. Therefore, it was not possible to compare the results statistically. The bulk soil from urban site had greater porosity, but the porosities from two aggregates were almost identical. The numbers of pores and throats were obtained by counting individual pores at cell size of 8^3 voxels and the rural site had greater number of pores than urban, while the throat number was greater in urban bulk soil (Table 3.1). In aggregate samples, numbers of pores and throats were almost the same, while there were greater numbers of

pores in both aggregates than in bulk soils. Since image resolution for aggregates was much greater than for bulk soils, images of the aggregates captured more pores, increasing their number (Sleutel et al., 2008). Based on porosity and number of pores from bulk soil samples, soils at the urban site had less pores but higher porosity values than soil at the rural site.

2) Pore-body and Throat Volumes

Each pore is composed of pore-bodies and throat(s). The average pore-body volume from the urban bulk soil was significantly different than for the rural site (p =0.00), while there was no difference among aggregate samples (Table 3.1). Pores with the pore-body volume less than 0.05 mm^3 were 38% for the urban soil and 50% for the rural soil (Fig. 3.6). On the other hand, pore volume greater than 1 mm^3 was 10% in the urban soil and 3% in the rural soil. Pore volumes in the urban and rural sites ranged from 0.01 to 218 mm^3 and from 0.01 to 121 mm^3, respectively.

These results from bulk soils agreed with the results of the configuration entropy and the universal multifractals analyses in Chapter 2. The configuration entropy (Eq. 3 in Chapter 2) and structure function analysis (Eq. 5 in Chapter 2) from images indicated that urban soils had more pore clustering (smaller α parameter values) than rural soils that had more isolated pores (see Chapter 2). The H parameter from the structure function analysis revelead greater H value from urban soil (0.27) than for the rural soil (0.20), which implies a more heterogeneous distribution of pores in the former than in the latter. Based on spatial distribution analyses and pore-body size analysis, urban soil had larger size pores and wider distribution of pore sizes.

Throat volumes between the aggregate and bulk soil samples were statistical different, but there was differences between sites (Fig. 3.7). The coordination numbers in bulk soil samples were greater in urban soil than in rural soils, but the difference was not statistically significant. Udawatta et al. (2008) observed soil pore volume, throat area and coordination number differences under different managements (tree *vs*. grass buffer). They found that large size pores have larger throats, while soils with small pores had smaller throat and coordination numbers.

3) Pore Length and Tortuosity

The urban soil had greater pore length than the rural soil ($p=0.03$). On the other hand, average pore-length of both aggregates did not show any difference. In aggregate samples, more than 95% of pore lengths were smaller than 0.1 mm in both sites (Fig. 3.5). Pores shorter than 1 mm in bulk soils, represented 74% and 87% of soils in the urban and rural sites, respectively (Fig. 3.8). The proportion of pores longer than 10 mm was 3% in the urban soil and 0.8% in the rural soil.

There was no difference of tortuosity across sites. In bulk soils, tortuosity values of less than 2 were 72% for the urban bulk soil sample and 65% for the rural sample (Fig. 3.9). On the other hand, both aggregate pores had more than 90% of tortuosity values less than 2. As a result, pores that are more tortuous were found in the rural bulk soil, since tortuosity values greater than 5 were 1% in the rural while urban had none.

Perret et al. (1999) found that inter-aggregate pores have tortuosity values ranging from 1 to 2.5 and in this study, the urban soil had greater amount of pores with tortuosity values of less than 2. Smaller average pore sizes tend to have greater tortuosity and smaller saturated conductivity values (Hendrayanto et al. 2000; Vervoort

and Cattle, 2003). Therefore, soil at the rural site had greater tortuosity and smaller average pore sizes based on pore volume and tortuosity results.

4) Pore Shape

The values of the pore shape index S (Eq. 2) ranged between 1 and 5 (Fig. 3.10), with pores becoming more elongated as the value of S increases (Manwart, 2007). The S values of urban and rural bulk soil were significantly different (p=0.02), while the values between two aggregates were no different (p >0.05).

From the definition of S, values of 1 indicate that pore shapes are close to sphere shape (rounded pores). The aggregates and bulk soils had the greatest frequency at S value less than 1.5. The S values of less than 1.5 were more than 90% in aggregates and more than 50% in bulk soils. Greater S values were found more in urban (27%) than in rural (18%) bulk soil. Virto et al. (2003) investigated pore size relation to pore shape and concluded that larger pores had more elongated shape. This result confirmed the finding from pore length, tortuosity and shape that soil at the urban bulk site had more elongated pores.

Based on pore morphological properties, aggregate samples from the two sites were not different in all properties. Aggregate samples had more rounded and small pores than the bulk soils. Since aggregates contain intra-aggregate pores, they should have great amount of isolated and small size pores within pore systems. Pore properties from bulk soils had differences in average pore-body/ throat volumes and pore length. The bulk soil from the urban site had greater pore volumes and lengths than the corresponding soil from the rural site and slightly greater values of connectivity and

smaller tortuosity. Pore shape analysis confirmed that pores at the rural site had more rounded pores, while soil at the urban site had more elongated pores.

3.4.2 Bulk Density and Hydraulic Properties

Average bulk densities from three replicates of each site were not significantly different ($p > 0.05$) between the urban and the rural site (Table 3.2).

Computed water retention data and measured data from laboratory experiments were matched and fitted with Eq (5) (Fig. 3.11). There was no information for pores with radii of less than 0.1 mm from image analysis due to image resolution and unit cell size.

There were two distinct curves between the computed water retention curve from images and measured retention curve from experiments. This implies that the bulk soil samples had dual pore systems (Spohrer et al., 2006). Therefore, a bimodal model (Durner, 1994) fits the water retention curves reasonably well ($r^2 > 0.99$). The water retention curves from both soils had no difference of water retention at high matric potentials, but the retention data from both soils were statistically different at - 0.1 to - 10 kPa ($p=0.03$). Vogel (2000) compared water retention curves from a silty soil image to ones from a random simulated porous image. He found that water retention curves from two images had most differences in the range of potentials from -1 to -10 kPa and the random pore system with less connected pores had greater water retention values in that potential range. In our case, this would imply that soils from the urban site, which had smaller retention values at low potentials, had more connected pores than rural soil. The parameters χ_1 and χ_2 from Eq. (9) are scaling factors that indicate the positions of maximum pore size and n_1 and n_2 are related to the width of pore size distribution

(Abenny-Mickson, 1996). Pires et al. (2008) compared water retention parameters before and after applying a number of dry-wet cycles. They found that a greater number of dry-wet cycles increased pore size, porosity, and the value of α and n. The urban soil had greater values of α and n parameters, because of more inter-aggregate pores, but the difference in retention curves was not significant (Table 3.2).

Saturated water contents estimated with the Durner model (1994) were about 29% greater than measured saturated water contents from bulk density values. Previous studies stated that the saran resin bulk density measurement tends to overestimate bulk density because saran can penetrate into large pores with opening to the sample surface (Bashour and Sayegh, 2007).

Hydraulic conductivity distributions were computed from pore radii and water retention data with Eq. (6). Pores with throats and tortuosity values were applied to the calculation to define more accurate estimation of conductivity (Kutilek, 2004) (Fig. 3.12). Water in a pore with a throat is not released until matric potential is greater than the potential corresponding to throat diameter. In addition, under unsaturated conditions, water in a pore moves along the wall of a pore. Commonly the value of the tortuosity parameter in Eq. (6) is assumed equal to 0.5 based on average tortuostiy values from different texture soils (Mualem, 1976). However, Vervoot and Cattle (2003) argued that a constant tortuosity may not be correct and recommended to use individual tortuosity from each pore from image analysis of pore geometry.

Conductivity data from measurements and computed from images had two different fitting parameters. However, soils from the urban site had the breakpoint at -0.3 kPa, while the rural soil did not have a breakpoint in conductivity data. In other words,

the rural soil did not have bimodal distribution or dual pore system in conductivity data. The bulk soil from the urban site had significantly greater conductivity at matric potentials greater than -0.1 kPa (p=0.01). The results of bimodal fitting model suggested that dual porosity system developed in the urban soils and the differences of conductivity data between two soils were in inter-aggregate pore region. The estimated saturated hydraulic conductivities (k_s) from both samples were greater than measured conductivities by more than 10%. Ventrella et al. (2005) stated that estimated k_s values from Eq. (10) were much greater than the measured values. They stated that estimated values should be treated as a fitting parameter rather than the actual conductivity at saturation, because computed k_s values from conductivity models are not accurate estimation from pore geometry. Other fitted parameters, v_2, v_3, χ_1, χ_2, n_3, and n_4, did not have a similar trend or values in comparison to the parameters from the water retention model. These results may result from data of infiltration measurements. The results of infiltration measurements from two site soils were not significantly different.

3.4.3 Climate Effects on Morphological Properties of Soil Pores

The bulk soil from the urban site which was exposed to greater concentrations of CO_2, temperature, soil moisture and biomass showed greater pore-body volume and less tortuous pore system than soil from the rural site. Prior et al. (2004) measured saturated hydraulic conductivity in soil planted to soybean under elevated concentration of CO_2, and found increase in conductivity values. It can be speculated that conductivity results from this study and the results from Prior et al. (2004) were more affected by plant roots activity induced by elevated CO_2 concentration and temperature than other processes such as microbial activity. Prior et al. (2004) concluded that in enriched CO_2

concentration, there would be an increase in root biomass and quality of soil. These increases would decrease bulk density and increase hydraulic conductivity. Aggregates from the urban and the rural site did not show any difference in all pore properties. Although there was only one sample from each site, those two aggregates had almost the same characteristics in pore morphology. Increase of CO_2 concentration and temperature and changes in environmental variables did not affect pore structure at the aggregate level. One reason for this result could be that there were not enough time to induce changes at the aggregate level. Secondly, the differences in CO_2 concentration and temperature between the urban site and the rural site were not great compared to other studies, where CO_2 concentration levels were double that of the control condition (Niklaus et al. 2003; Rillig et al., 2002). Therefore, the impacts of climate changes were not powerful enough to change pore structure at the aggregate level.

To explain difference of pore structure in urban and rural bulk soil, the site ecological properties should be considered. Plant productivity was studied earlier and there was a positive correlation between plant productivity and atmospheric CO_2 concentration and temperature level (Ziska et al., 2004). Soil moisture and soil temperature data from each site were analyzed in Chapter 2. The conclusion was that soils from the urban site had similar soil moisture content and higher temperature than soils from the rural site. Increase in root growth creates more well-connected intra-aggregate pores and these conditions increased hydraulic conductivity (Ersahin et al., 2002). There was no report on root properties from these sites, but pore structure characteristics implied to that there may be more growth in roots from the urban soils.

3.5 Conclusions

Soil pore morphological properties have been analyzed from three dimensional images. To measure a large size sample, local porosity with an 8^3 voxel cell size was used to reduce the number of voxels to measure. This method was sensitive enough to characterize pore properties from aggregates and bulk soils of different atmospheric CO_2 concentration and temperature levels.

This study concluded that greater plant biomass, soil moisture, atmospheric CO_2 concentration and temperature may affect soil properties by increasing inter-aggregate pores and saturated hydraulic conductivity. At the aggregate level, there was no difference in pore geometry under different environmental and climate conditions while bulk soil samples exhibited differences in pore morphological properties. This result may be a hint that climate and environmental changes will affect inter-aggregate pore system in the first place. Roots had first impact on pore structure to change inter-aggregate pores, while intra-aggregate pores were not affected. More detailed measurements and long term analyses of soil properties are required to generalize changes of soil properties under climate changes.

Reference

Amemiya, M. 1965. The influence of aggregate size on soil moisture content capillary conductivity relations. *Soil Sci. Soc. Am. Proc.* 29:744-748.

Andraud, C., A. Beghdadi and J. Lafait. 1994. Entropic analysis of random morphologies. *Physica A*. 207: 208-212

Assouline, S. and D. Or. 2008. Air entry-based characteristic length for estimation of permeability of variably compacted earth materials. *Water Resour. Res*. 44(11): W11403.

Balland, V., J.A. P. Pollacco, and P.A. Arp. 2008. Modeling soil hydraulic properties for a wide range of soil conditions. *Ecol. Model.* 219(3-4): 301-316.

Bashour, I. I.and A. H. Sayegh. 2007. Methods of analysis for soils of arid and semi-arid regions. Rome, Italy: FAO, Viale delle Terme di Caracalla 00153.

Bastardie. F, Y. Capowiez , J.R. de Dreuzy and D. Cluzeau. 2003. X-ray tomographic and hydraulic characterization of burrowing by three earthworm species in repacked soil cores. *Appl. Soil Ecol.* 24(1): 3-16.

Chang, R.K. 1968. Component potentials and hysteresis in water retention by compacted clay soil aggregates. *Soil Sci.* 105:172-176.

Chun, H.C., D. Gimenez, and S.W. Yoon. 2008. Morphology, lacunarity and entropy of intra-aggregate pores: Aggregate size and soil management effects. *Geoderma*. 146(1-2); 83-93.

Couteaux, M.M. and T. Bolger. 2000. Interactions between atmospheric CO_2 enrichment and soil fauna. *Plant Soil.* 224: 123–134.

Dexter, A.R., 2004. Soil physical quality. Part III. Unsaturated hydraulic conductivity and general conclusions about S-theory. *Geoderma.* 120: 227–239.

Droogers, P., A. Stein, J. Bouma, and G. De Boer.1998. Parameters for describing soil macroporosity derived from staining patterns. *Geoderma* 83, 293–308.

Durner, W. 1994. Hydraulic conductivity estimation for soils with heterogeneous pore structure. *Water Resour Res*. 30:211–33.

Durner, W., E. Priesack, H.-J. Vogel., and T. Zurmühl. 1999. Determination of parameters for flexible hydraulic functions by inverse modeling. In: M. Th. van Genuchten, F. J. Leij and L. Wu (eds.) Proc. Int. Workshop, Characterization and Measurement of the Hydraulic Properties of Unsaturated Porous Media. p. 817-830. University of California, Riverside, CA.

Ebersberger, D., P.A. Niklaus, and E. Kandeler. 2003. Long term CO_2 enrichment stimulates N-mineralisation and enzyme activities in calcareous grassland. *Soil Bio. Biochem*. 35: 965–972.

Ersahin, S., R.I. Papendick, J.L. Smith, C.K. Keller, and V.S. Manoranjan. 2002. Macropore transport of bromide as influenced by soil structure differences. *Geoderma* 108:207–223.

Fox, D.M., R.B. Bryan, and C.A. Fox. 2004. Changes in pore characteristics with depth for structural crusts. *Geoderma*. 120(1-2):109120.

Gerke, H.H. and M.Th. van Genuchten. 1993. A dual-porosity model for simulating the preferential movement of water and solutes in structured porous media. *Water Resour*

Res 29:305–19.

Gimenez. D., E. Perfect, W.J. Rawls, and Y. Pachepsky. 1997. Fractal models for predicting soil hydraulic properties: a review. *Eng Geol.* 48 (3-4): 161-183.

Green, R. E. and J. C. Corey. 1971. Calculation of hydraulic conductivity: A further evaluation of some predictive methods. *Soil Sci. Soc. Am. Proc.* 32(561-565).

Hayashi, Y., K. Ken'ichirou, and T. Mizuyama. 2006. Changes in pore size distribution and hydraulic properties of forest soil resulting from structural development. *J. Hydrol.* 331: 85– 102.

Hollister, R.D., P.J. Webber, F.E. Nelson, and C.E. Tweedie. 2006. Soil thaw and temperature response to air warming varies by plant community: results from an open-top chamber experiment in northern Alaska. *Arct. Alp. Res.* 38:206–215.

Horn, R. and A.J.M. Smucker. 2005. Structure formation and its consequences for gas and water transport in unsaturated arable and forest soils. *Soil Tillage Res.* 82:5–14.

Jarvis, N.J. 2008. Near-saturated hydraulic properties of macroporous soils, *Vadose Zone J.* 7(2): 1256-1264.

King, J.S., K.S. Pregitzer, D.R. Zak, W.E. Holmes, and K. Schmidt. 2005. Fine root chemistry and decomposition in model communities of north-temperate tree species show little response to elevated atmospheric CO2 and varying soil resource availability. *Oecologia.* 146: 314–328.

Koca, D., B. Smith, and M.T. Ske. 2006. Modelling regional climate change effects on potential natural ecosystems in sweden. *Climatic Change.* 78: 381–406.

Kosugi, K., Y. Nakayama. 1997. A method for estimating unsaturated hydraulic properties of vertically heterogeneous soils from transient capillary pressure profiles. *Agr. Forest. Meteorol.* 84 (1-2): 37-50.

Kutilek, M. 2004. Soil hydraulic properties as related to soil structure. *Soil Till. Res.* 79: 175-184.

Lee, T.C., R.L. Kashyap, and C.N. Chu. 1994. Building skeleton models via 3-D medial surface axis thinning algorithms. CVGIP-Graph. Model Image Proc. 56(6): 462-478.

Leij, F.J., A. Sciortino,and A.W. Warrick. 2006. Infiltration in two parallel soil columns. *Water Resour Res.* 42 (12): W12408.

Leipprand, A. and D. Gerten. 2006. Global effects of doubled atmospheric CO_2 content on evapotranspiration, soil moisture and runoff under potential natural vegetation. *Hydrolog. Sci. J.* 51(1): 171-185.

Lima, H.V., A.P. Silva, M.C.Santos, M. Cooper, amd R.E. Romero. 2006. Micromorphology and image analysis of a hardsetting Ultisol (Argissolo) in the state of Ceara (Brazil). *Geoderma.* 132(3-4):416-426.

Lindquist, W.B., S.M. Lee, D.A. Coker , K.W. Jones, and P. Spanne. 1996. Medial axis analysis of void structure in three-dimensional tomographic images of porous media. *J. Geophys. Res.* 101(B4): 8297-8310.

Marwan, N., P. Saparin, and J. Kurturban. 2007. Measures of complexity for 3D image analysis of trabecular bone. *Eur. Phys. J-Spec. Top.* 143:109116.

Mohanty, B.P., R.S. Bowman, J.M.H. Hendrickx, and M.T. van Genuchten. 1997. New piecewise-continuous hydralic functions for modeling preferential flow in an intermittent-flood-irrigated field. *Water Resour. Res.* 33: 2049– 2063.

Morgan, J.A., D. E. Pataki, C. Körner, H. Clark, S.J. Del Grosso, J.M. Grünzweig, A. K. Knapp, A.R. Mosier, P.C.D. Newton, P.A. Niklaus, J.B. Nippert, R.S. Nowak, W.J. Parton, H.W. Polley, and M.R. Shaw. Water relations in grassland and desert ecosystems exposed to elevated atmospheric CO_2. 2004. *Oecologia.* 140: 11–25.

Mualem Y.A. 1976. A new model for predicting the hydraulic conductivity of unsaturated porous media. *Water Resour Res*. 12:513–22.

Niklaus, P.A., J. Alphei, D. Ebersberger, C. Kampichler, E. Kandeler, and D. Tscherko. 2003. Six years of in situ CO_2 enrichment evoke changes in soil structure and soil biota of nutrient-poor grassland. *Global Change Biol.* 9: 585–900.

Nimmo, J.R., W.N. Herkelrath, and A.M. L. Luna. 2007. Physically based estimation of soil water retention from textural data: General framework, new models, and streamlined existing models. *Vadose Zone J.* 6 (4): 766-773.

Ou, Z., L. Jia, H. Jin, A. Yediler, X. Jiang, A. Kettrup, and T. Sun. 1999. Formation of soil macropores and preferential migration of linear alkylbenzene sulfonate (LAS) in soils. *Chemosphere* 38: 1985–1996.

Pagliai, M., and M. De Nobili. 1993. Relationships between soil porosity, root development and soil enzyme activity in cultivated soils. *Geoderma* 56:243–256.

Pagliai, M., M.Raglione, T.Panini, M.Maletta,and M. Lamarca. 1995. The structure of two alluvial soils in Italy after ten years of conventional and minimum tillage. *Soil Till. Res*. 34 (4): 209–223.

Pagliai M. and Vignozzi N., 2002. The soil pore system as an indicator of soil quality. *Advances in Geoecology*, 35.

Park, E.J., and A.J.M. Smucker. 2005. Saturated hydraulic conductivity and porosity within macroaggregates modified by tillage. *Soil Sci. Soc. Am. J.*69:38–45.

Pendall, E., S. Bridgham, P.J. Hanson, B. Hungate, D.W. Kicklighter, D.W. Johnson , B.E. Law, Y.Q. Luo, J.P. Megonigal , M. Olsrud, M.G. Ryan, and S.Q. Wan . 2004. Below-ground process responses to elevated CO_2 and temperature: a discussion of observations, measurement methods, and models. *New Phytol.* 162:311–322.

Peth, S., R. Horn, F. Beckmann, T. Donath, J. Fischer, A.J.M. Smucker. 2008. Three-dimensional quantification of intra-aggregate pore-space features using synchrotron-radiation-based microtomography. *Soil Sci. Soc. Am. J.* 72(4): 897-907.

Pierce, F.J., M.C. Fortin, and M.J. Staton. 1994. Periodic plowing effects on soil properties in a no-till farming system. *Soil Sci. Soc. Am. J.* 58 (6): 1782–1787.

Pires, L.F., M. Cooper, F.A.M. Cássaro, K. Reichardt, O.O.S. Bacchi and N.M.P. Dias. 2008. Micromorphological analysis to characterize structure modifications of soil samples submitted to wetting and drying cycles. *Catena.* 72(2): 297–304.

Pires, L.F., J.R. Macedo, M.D. Souza, O.O.S. Bacchi, and.K. Reichardt. 2003. Gamma-ray computed tomography to investigate compaction on sewage-sludge-treated soil. *Appl. Radiat. Isot.* 59(1): 17–25.

Posadas, A.N.D., D. Gimenez, M. Bittelli, C. M. P. Vaz, and M. Flury. 2003. Multifractal characterization of soil particle-size distributions. *Soil Sci. Soc. Am. J.* 65(5): 1361-1367.

Prior, S.A., G.B. Runion, H.A. Torbort, and H.H. Rogers. 2004. Elevated atmospheric CO2 in agroecosystems: Soil physical properties. *Soil Sci.* 196 (6):434-439.

Radcliffe, D.E. and T.C. Ramussen. 2002. Soil water movement. In: Warrick, A.W. (ed). Soil Physics Companion. CRC Press, Boca Raton, FL.

Rillig, M.C., S.F. Wright, M.R. Shaw, and C. B. Field. 2002. Artificial climate warming positively affects arbuscular mycorrhizae but decreases soil aggregate water stability in an annual grassland. *Oikos*. 97: 52-58.

Seki, K. 2007. SWRC fit - a nonlinear fitting program with a water retention curve for soils having unimodal and bimodal pore structure. *Hydrol. Earth Syst. Sci. Discuss*. 4: 407-437.

Simunek, J. and M.Th. van Genuchten. 2008. Modeling nonequilibrium flow and transport processes using HYDRUS. *Vadose Zone J*. 7: 782-797.

Six, J., S.D. Frey, R.K. Thiet, and K.M.Batten. 2006. Bacterial and fungal contributions to carbon sequestration in agroecosystems. *Soil Sci Soc Am J*. 70:555–569.

Sleutel, S., V. Cnudde, B. Masschaele, J. Vlassenbroek, M. Dierick , L. Van Hoorebeke, P. Jacobs, and S. De Neve. 2008. Comparison of different nano- and micro-focus X-ray computed tomography set-ups for the visualization of the soil microstructure and soil organic matter. *Comput. Geosci.* 34(8): 931-938.

Spohrer, K., L. Herrmann, J.Ingwersen, and K. Stahr. 2006. Applicability of uni- and bimodal retention functions for water flow modelling in a tropical acrisol. *Vadose Zone J.* 5: 48–58.

Strudley, M. W., T.R. Green, and J.C. Ascough. 2008. Tillage effects on soil hydraulic properties in space and time: State of the science. *Soil Till. Res.* 99:4-48.

Tamboli, P.M., W.E. Larson, and M. Amemiya. 1964. Influence of aggregate size on moisture retention. *Iowa Acad. Sci.* 71:103-108.

Udawatta, R.P. and S.H. Anderson. 2008. CT-measured pore characteristics of surface and subsurface soils influenced by agroforestry and grass buffers. *Geoderma*. 145(3-4): 381-389.

van Genuchten, M.Th. (1980) A Closed-form Equation for Predicting the Hydraulic Conductivity of Unsaturated Soils, *Soil Sci. Soc. Am. J.*, 44(2): 892-898.

Ventrella, D., N. Losavio, A.V. Vonella, and F.J. Leij. 2005. Estimating hydraulic conductivity of a fine-textured soil using tension infiltrometry. *Geoderma.* 124(3-4): 267-277.

Vervoort, R.W.and S.R. Cattle. 2003. Linking hydraulic conductivity and tortuosity parameters to pore space geometry and pore size distribution. *J. Hydrol*. 272 (1–4): 36–49.

Vogel, H.J. 2000. A numerical experiment on pore size, pore connectivity, water retention, permeability, and solute transport using network models. *Europ. J. Soil Sci*. 51: 99-105.

Vogel, H.J. and K.I. Roth. 2001. Quantitative morphology and network representation of soil pore structure. *Adv. Water Resour*. 24(3-4):233–242.

Vogel, H.J. and K.I. Roth. 2004: Direct measurement of the soil water retention curve using X-ray absorption. *Hydrol. Earth Syst. Scienc*., 8: 2-7.

Volk, M., P.A. Niklaus, and C. Körner. 2000. Soil moisture effects determine CO2 responses of grassland species. *Oecologia*. 125:380-388.

Wittmuss, H.D., and A.P. Mazurak. 1958. Physical and chemical properties of aggregates

in a Brunizem soil. *Soil Sci. Soc. Am. Proc.* 22:1-5.

Wosten, J.H.M., and M.T. van Genuchten. 1988. Using texture and other soil properties to predict the unsaturated soil hydraulic functions. *Soil Sci. Soc. Am. J.* 52:1762–1770.

Zak, D.R., K.S. Pregitzer, J.S. King, and W.E. Holmes. 2000. Research review: Elevated atmospheric CO2, fine roots and the response of soil microorganisms: A review and hypothesis. *New Phytol.* 147 (1): 201-222.

Ziska, L.H., J.A. Bunce, and E.W. Goins. 2004. Characterization of an urban-rural CO2/temperature gradient and associated changes in initial plant productivity during secondary succession. *Oecologia.* 139 (3): 454-458.

Table 3. 1 Summary of pore morphological analyses from bulk soil and aggregate of the urban and the rural site. All properties are presented by average and standard deviation values, except porosity, number of pores and throats.

		Porosity	Number of pores	Average pore-body volume (mm³)	Number of throats	Average throat volume (mm³)	Coordination number	Pore length (mm)	Tortuosity
Bulk soil	Urban	0.25	789	0.85±0.16[a]	454	0.21±0.00	2.37±12.32	1.1±0.36[a]	1.03±0.17
	Rural	0.20	929	0.64±0.08[a]	245	0.19±0.00	1.16±10.49	0.78±0.17[a]	1.06±0.16
Aggregate	Urban	0.24	3000	0.16±0.00	348	0.07±0.00	0.26±0.94	0.57±0.01	1.03±0.05
	Rural	0.24	3009	0.15±0.00	334	0.08±0.00	0.26±0.87	0.57±0.01	1.03±0.06

The letter 'a' indicates statistical difference at 95% level between sites.

Table 3.2 Average bulk density from three bulk soil samples and fitted parameters from water retention (Eq. (5)) and hydraulic conductivity (Eq. (6)). θs and θr are estimated saturated water content and residual water content from Eq. (9), respectively. Numbers in parenthesis are standard error of fitting.

	Urban	Ls
Bulk density (g/cm^3)	1.47±0.06	1.52±0.05
Saturated water content (cm^3/cm^3)	0.44±0.02	0.42±0.02
Water retention fitting (Eq. (9))		
θ_s (cm^3/cm^3)	0.57	0.54
θ_r (cm^3/cm^3)	0.15	0.15
$w1$	0.29	0.28
α_1	2.67	1.04
n_1	4.99	4.73
α_2	0.01	0.01
n_2	7.75	2.83
Hydraulic conductivity fitting (Eq. (10))		
$w1$	0.01	0.41
α_1	0.17	0.09
n_1	1.01	1.04
α_2	0.02	-
n_2	1.01	-
Ψ_b (kPa)	-0.3	-
K_s (cm/min)	0.50	0.21

A   B   C

0.2	0.3	0.1	0	0
0.3	1	1	0.6	0.3
0.4	1	1	1	0.4
0.2	0.7	1	0.8	0.2
0	0.1	0.2	0.1	0

0	0	0	0	0
0	1	1	1	0
0	1	1	1	0
0	1	1	1	0
0	0	0	0	0

Figure 3.1 Diagram of binarization from local porosities. The orange object represents a pore in an image. A is a pore divided by cells. B shows values of local porosity for each cell. C is binarization results after conversion.
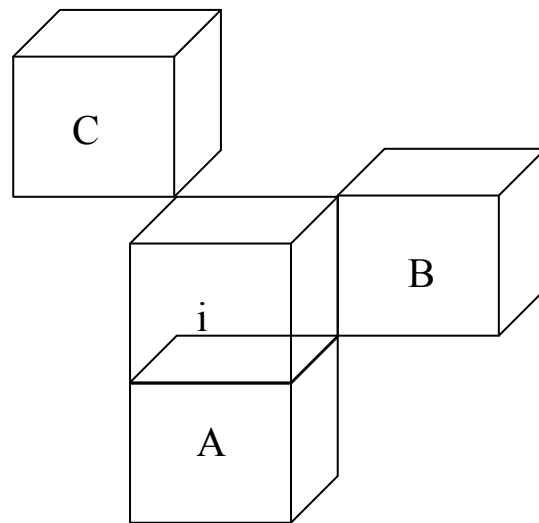
Figure 3.2 Different connection types in three dimensional cubes; i is the cube of interest, A is a cube with face connection, B is a cube with edge connection and C is a cube with a point connection to the i cube.
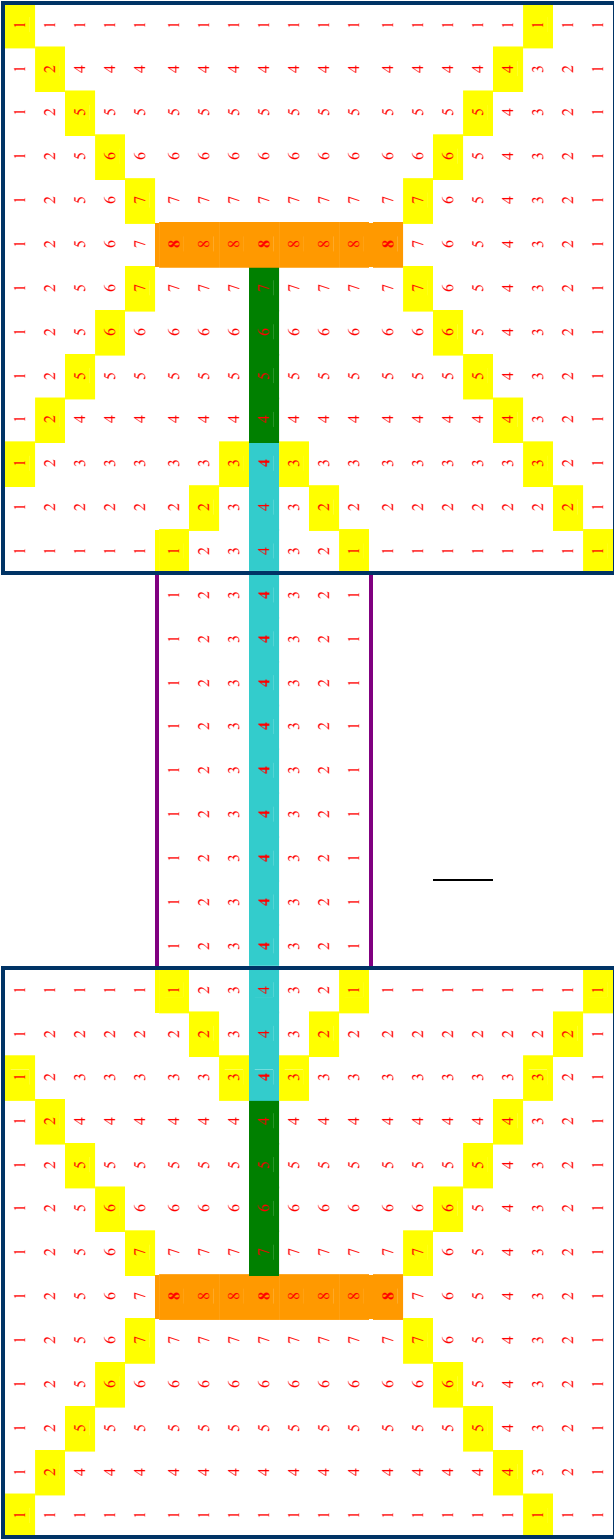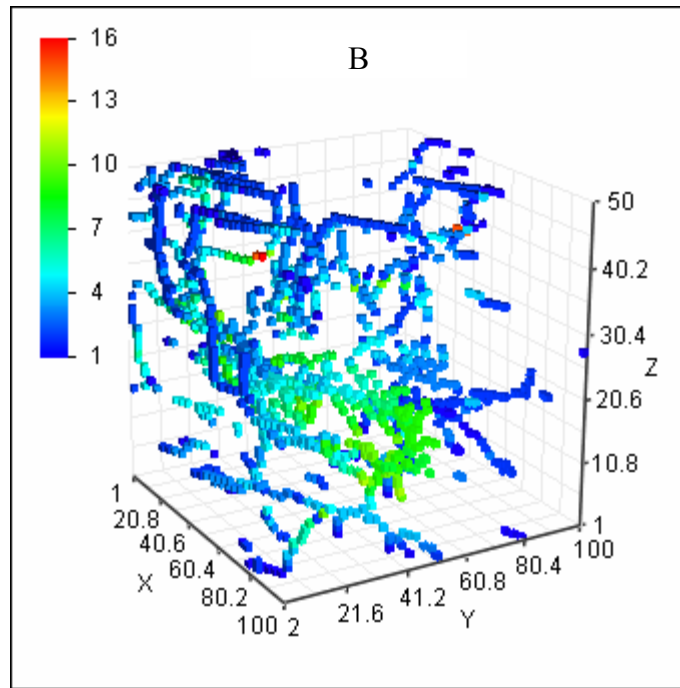
Figure 3.3 A: A simple pore diagram of burning numbers and MA constructions. The red solid lines is the boundary of the pore. Cells with black numbers are pore-body cells and red ones are throat cells. Numbers in each cell represent burning numbers. Colored cells represent MA cells; orange is maximum burn number, light blue is local maximum burn number, green color is distance from different boundaries, and yellow color –represents the same burn number at perpendicular positions. Black bold numbers are nodes for pore-body and red bold number are node for throat. The dark blue line represent the boundary of pore-body volume and the purple line represents the boundary of throat volume. The pink solid line is the length of the pore and the dashed line is the shortest path from top to bottom of the pore. B: An example of MA construction from the aggregate sample. The legend is local porosity values from each cell.
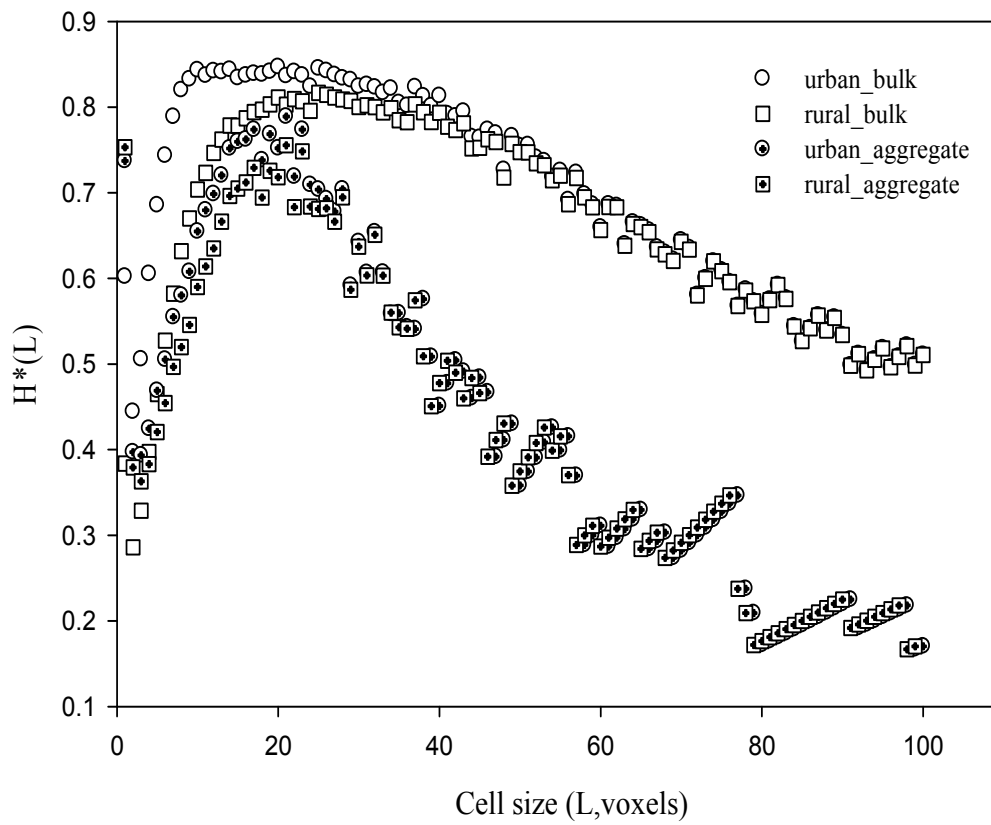
Figure 3.4 Results of configuration entropy from bulk soil and aggregate of the **urban** and the rural site.

A   B
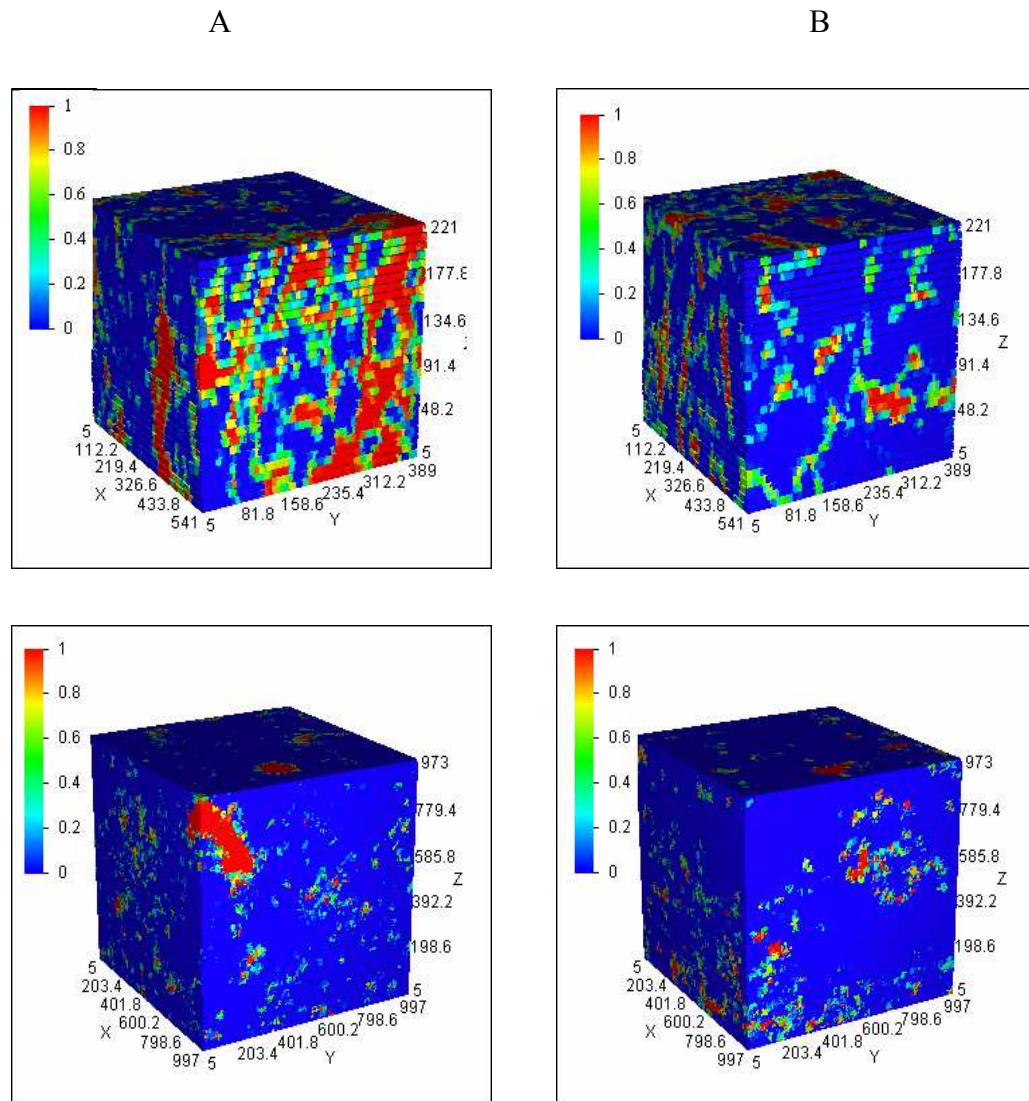
Figure 3.5 Local porosities from all samples at cell size of 83 voxels. A: soils from the urban site and B: soils from the rural site. Top images are aggregate samples and bottom images are bulk soil images. The legend represents local porosity values.
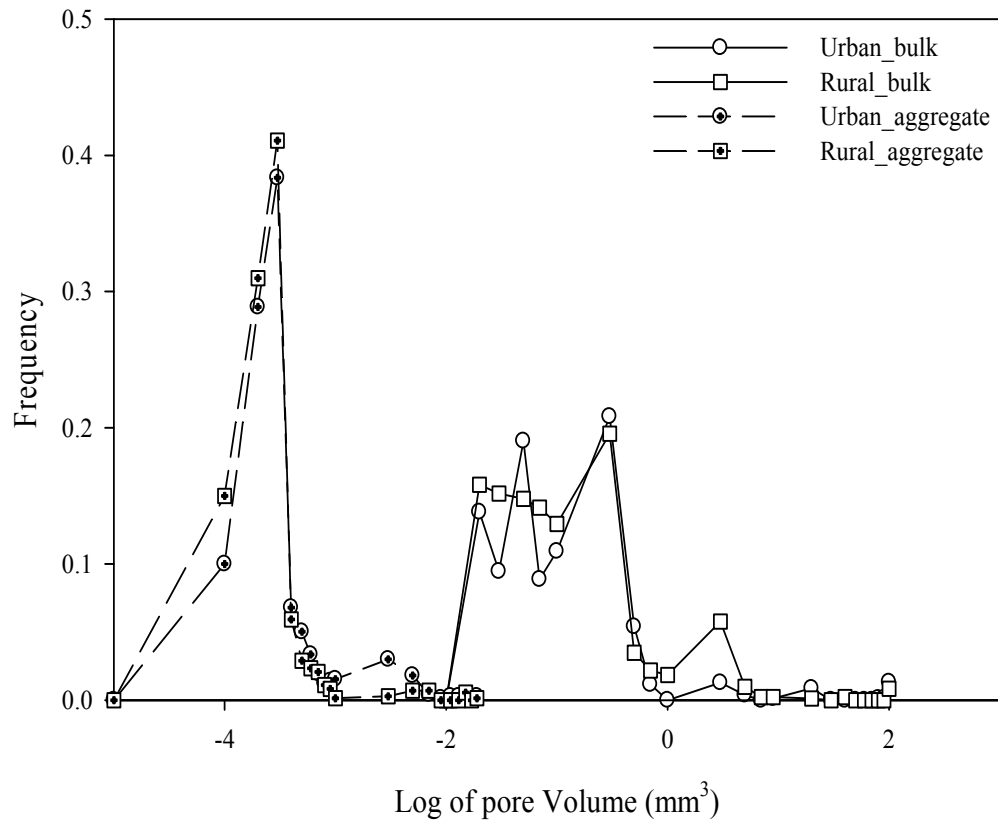
Figure 3.6 Frequency distributions of pore-body volumes in logarithm scale from bulk soils and aggregates of the urban and the rural site.
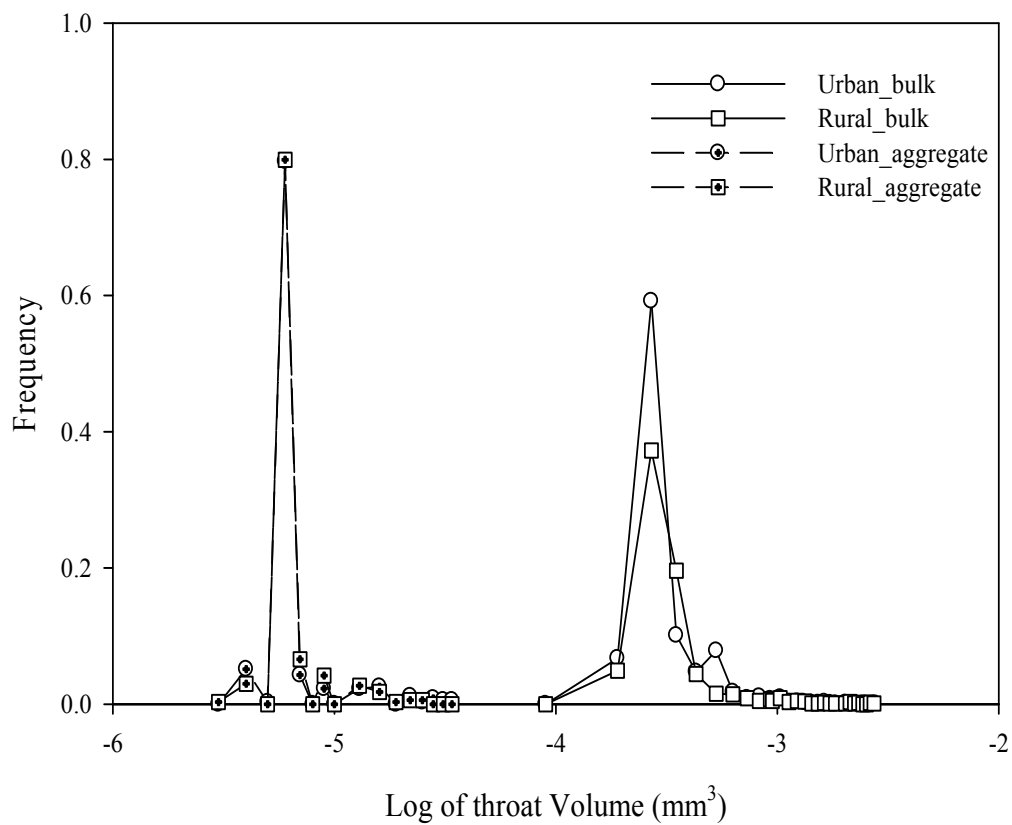
Figure 3.7 Frequency distributions of throat volumes in logarithm scale from bulk soils and aggregates of the urban and the rural site.
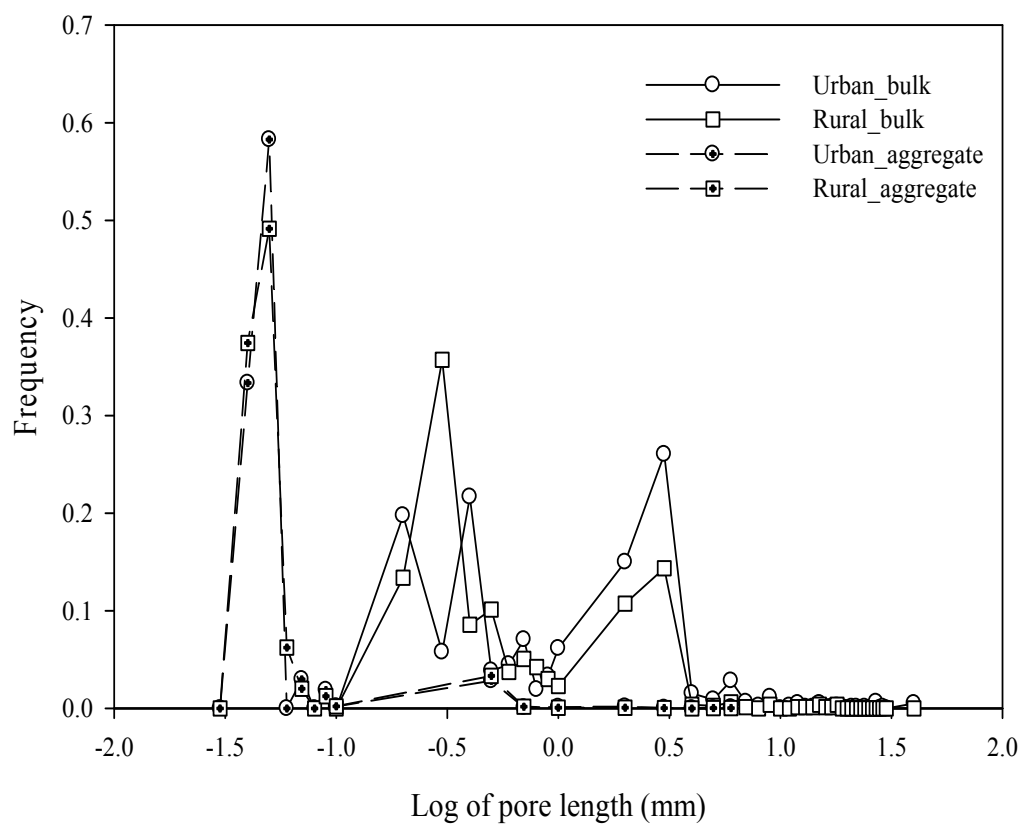
Figure 3.8 Frequency distributions of pore lengths in logarithm scale from bulk soils and aggregates of the urban and the rural site.
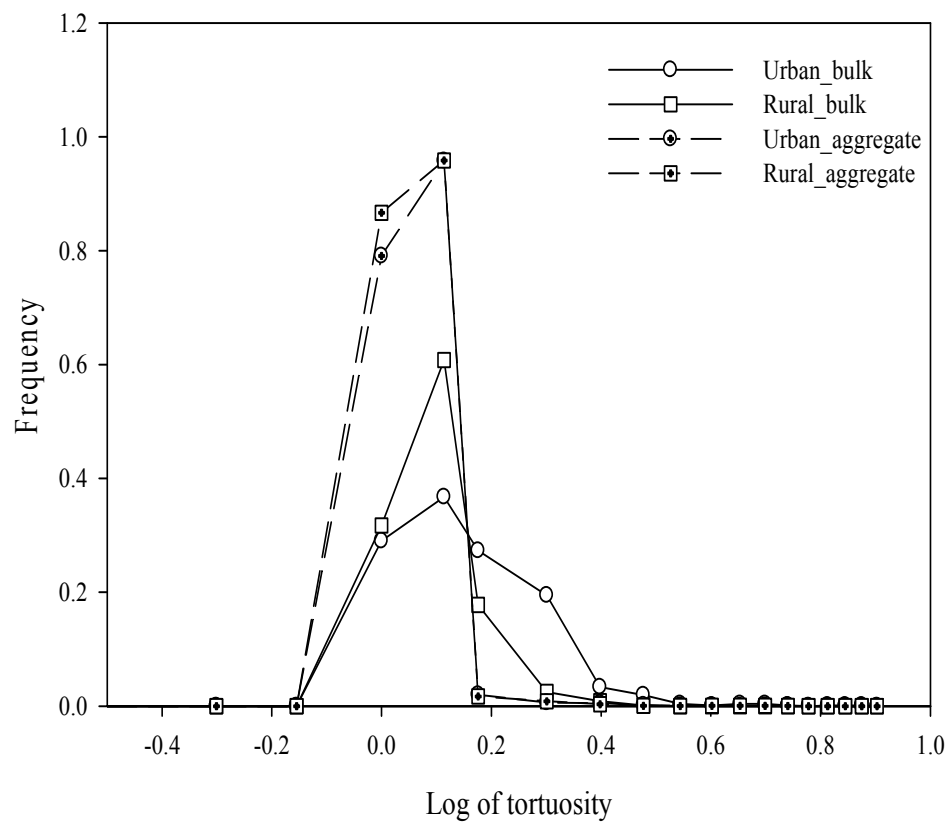
Figure 3.9 Frequency distributions of tortuosity in logarithm scale from bulk soils and aggregates of the urban and the rural site.
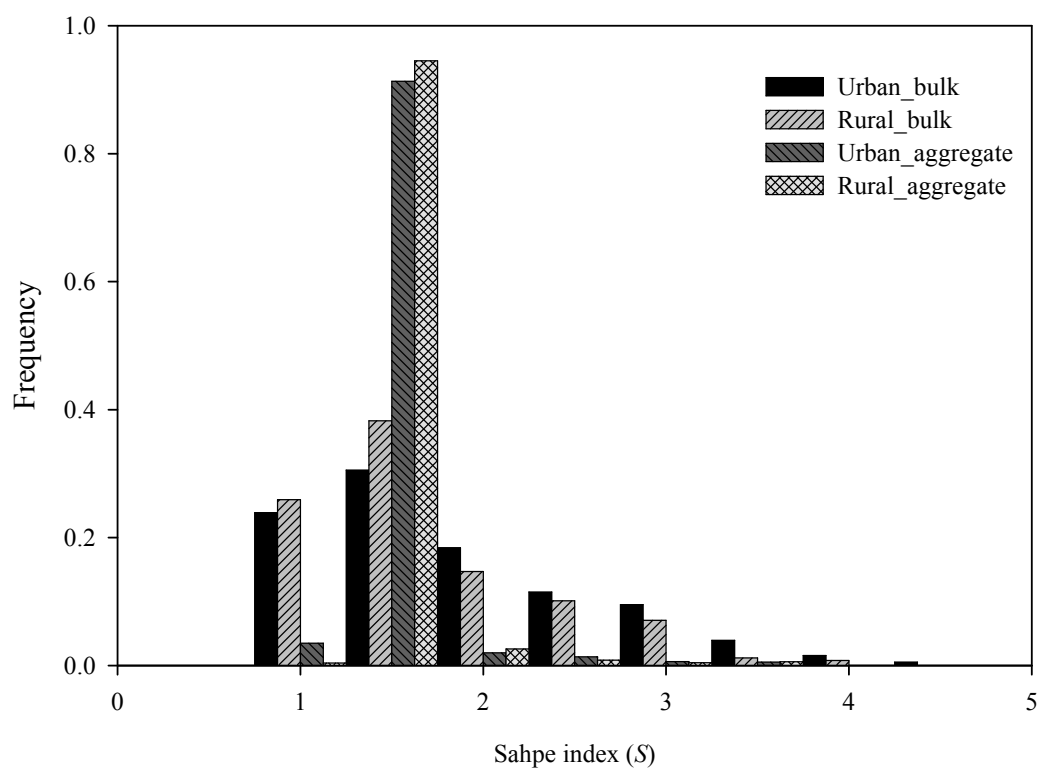
Figure 3.10 Histogram of pore shape index from bulk soils and aggregates of the urban and the rural site.
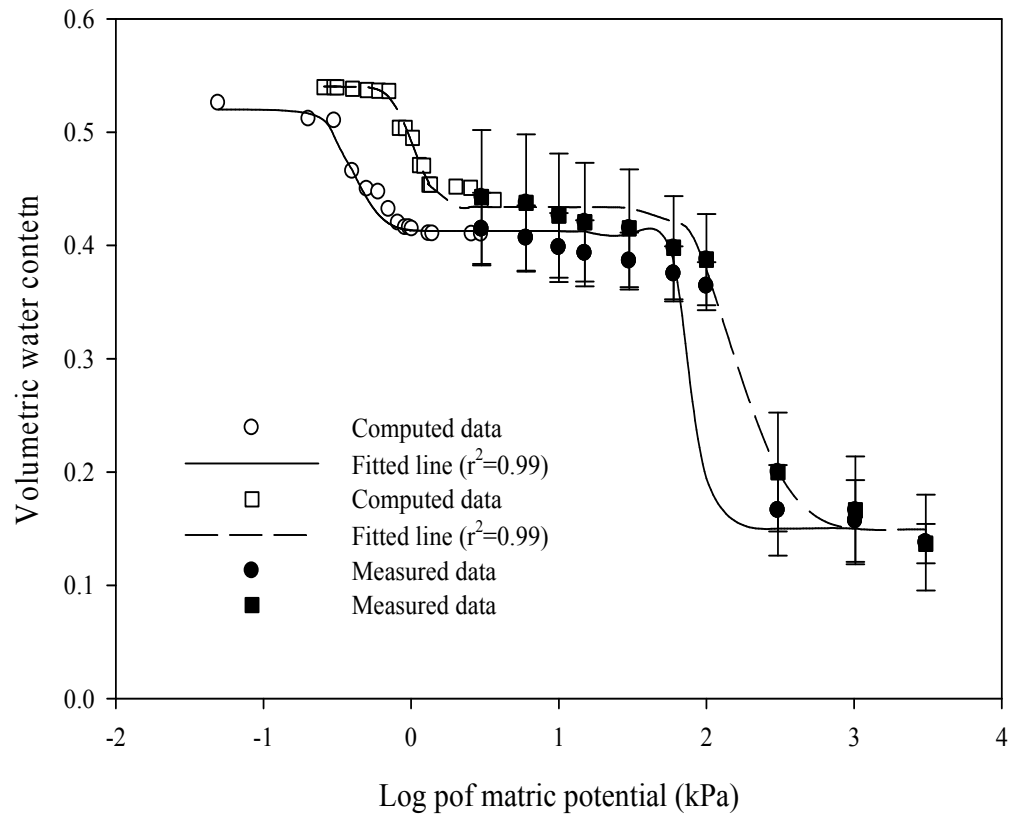
Figure 3.11 Computed and average water retention of measurements data from the bulk soils and fitted line by Eq.(9). Circle symbols represent data from the urban soil and square symbols do data from the rural soil. Solid line is fitted line for urban soil and dash line is for the rural soil.
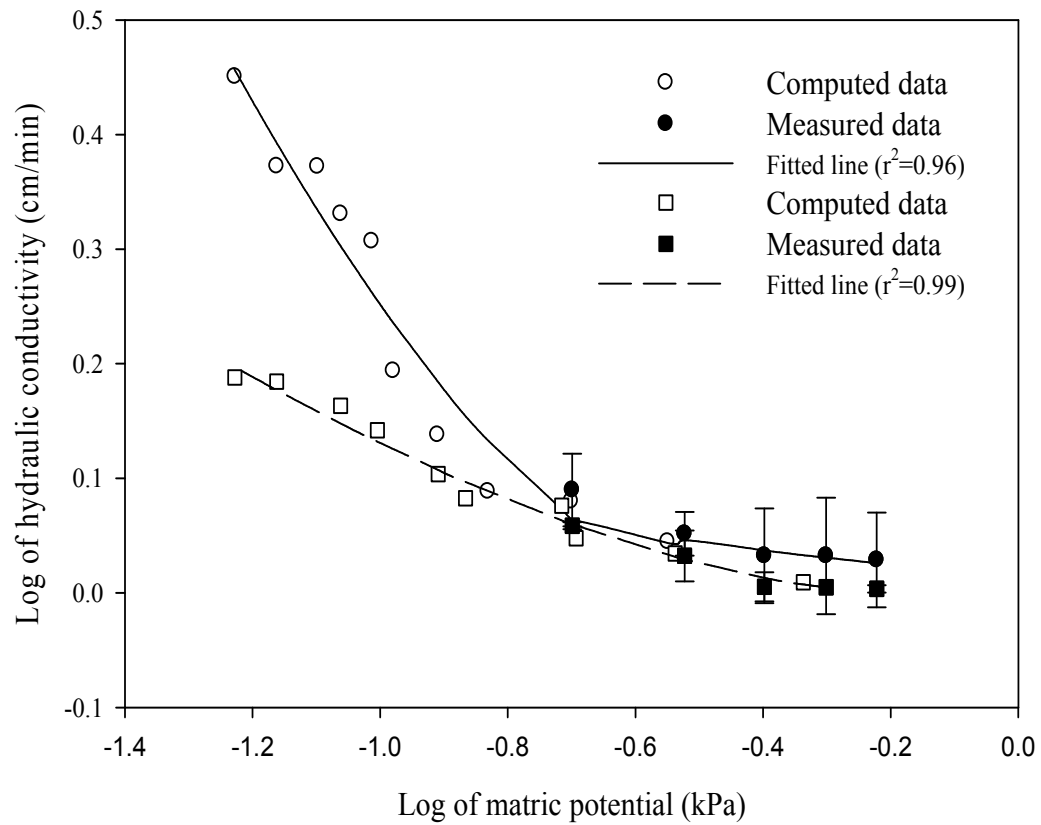
Figure 3.12 Computed and average hydraulic conductivity of measurements data from the bulk soils and fitted line by Eq.(10). Circle symbols represent data from the urban soil and square symbols do data from the rural soil. Solid line is fitted line for the urban soil and dash line is for the rural soil.

Chapter 4 : Scaling of Pore Morphological Properties in Aggregate and Bulk Soil Images

4.1 Introduction

In the field, soil properties are variable in space (spatial heterogeneity) and that variation is caused by complexity of soil systems and components, such as heterogeneous soil structure (Elkateb et al., 2003). This structural heterogeneity is the result of the bimodal distribution of pore sizes; intra- (pores within aggregates) and inter-aggregate pores (pores between aggregates) in a soil pore system (Young *et al.,* 2001). The effect of scale on soil properties need to be better understood in order to predict changes of soil properties and processes at different scales (Hopmans et al., 2002; Bartoli et al., 2005). Detailed information of scales are explained in Chapter 1.

4.1.1 Scale Effects on Soil Properties

Scale consists of three components; *extent*, *spacing* and *support* (Blőchl and Sivapalan, 1995). Extent is the total coverage of the measurements or area of interest; spacing is the distance between measured points and support is the sample size. The term scaling refers to using information from one scale to infer information at another scale. Scaling is a fundamental problem in soil science, especially because soil property changes with scales (Pachepsky et al., 2003). Porosity, bulk density or hydraulic conductivity has been measured to indirectly characterize changes of pore structure across sample sizes. Changes of porosities and densities across aggregate sizes follow a power law (Rieu and Sposito, 1991; Gimenez et al., 2002). As sample size increases, porosity increases and aggregate density decreases. This phenomenon is explained by the porosity exclusion principle, which states that lower order structures exclude pores of the next higher structure, which implies that smaller aggregates are denser and contain smaller pores than larger aggregates (Currie, 1966; Dexter, 1988).

Similar to the aggregate property, changes in variability of hydraulic

conductivity in the bulk soil decreases as sample length decreases (Gimenez et al.,

1997). Gimenez et al. (1999) discussed that at small sample sizes, conductivity data

showed simple scaling behavior, but as size increased, variance of conductivity

measurements increased and the data exhibited multi scaling.

Based on these studies, aggregates and bulk soils are two different structural

systems. Rodriguez-Iturbe et al. (1995) demonstrated that log of soil moisture and log

of porosity had linear relationships with the log of the observed areas (km scale).

Therefore, pore properties at the aggregate and the laboratory scale may be related.

Defining scale effects can be challenging, since projecting information from one scale

to another scale requires accurate measurements of soil properties at each scale. Image

analysis may be a powerful tool to investigate scaling effects on soil pore properties

because it measures directly pore structure and pore geometry (Al-Roush and Willson,

2005). Besides accurate measurements of pore geometry, image analysis facilitates the

measurements of pore properties such as pore sizes at various scales from one sample

image.

4.1.2 Scaling of Soil Structure from Images

1) Resolution

Image analyses are affected by magnification or resolutions (Liu et al., 2005).

Resolution affects spatial distributions of pore structure from two or three dimensional

soil images (Dathe et al., 2001) and pore structural parameters such as surface fractal

value and lacunarity from two dimensional images (Dathe and Thullner, 2005;

Pendleton et al., 2005). The surface fractal values or lacunarity values from soil images

varied with image resolution. On the other hand, Ogawa et al. (1999) observed no effect of image resolution on pore surface fractal. These contrasts may result from difference in changing image resolution techniques. Dathe and Baveye (2003) tested resolution effects with different magnification techniques and found no significant changes in pore surface fractal. There has been no clear trend in image resolution effects on pore structure from two dimensional images.

Pore morphological properties from three dimensional images are affected by image resolution (Al-Roush and Willsons, 2005; Lehmann et al., 2006; Jassogne et al., 2007). Pore sizes and porosities from low resolution are greater than those from high resolutions. Al-Roush and Willsons (2005) reported that the number of pores is proportional, and average pore size is inversely proportional, to image resolution. Lehmann et al. (2006) demonstrated that a resolution of 3.5 μm captures too many small pores, while low resolution of 60 μm overestimates the sizes of small pores and causes greater deviation from the known pore size distribution of simulated images. The studies described above confirm that image resolution affects pore morphology significantly, but neither of them showed a pattern of pore morphological changes across resolution due to a lack of enough resolution levels or measured pore properties.

2) Image Size

The effect of image size has been investigated with the concepts of representative element area (REA) or volume (REV) (VandenBygaart and Prots, 1999; Bartoli et al., 2005; Baveye et al., 2002). The REA or REV refers to the sample size at which the variation of the measured property is reduced to its minimal expression (Bear, 1974). Small images exhibit the greater fluctuation of measured values and this

fluctuation decreases as image size increases. In many cases, the REA has been determined based on variation of porosity with image sizes (VandenBygaart and Prots, 1999; Bartoli et al., 2005; Papadopoulos 2006). Baveye et al. (2002) tested the effect of image size on porosity and found that small images tend to have the greater fluctuations in porosity. Representative elementary area or volume is not an inherent property for every soil structure since every soil property tends to have different REV and occasionally there is a property with no REV (Bartoli et al. 2005). Therefore, it is important to understand pore property changes across image sizes.

Cislerova and Votrabova (2002) investigated the effect of image size on spatial analyses of solid-pore arrangements from three dimensional images. They analyzed autocorrelation and semivariogram of solid-pore arrangements in soil across three different image sizes, and found no variation in the autocorrelation and semivariogram functions with image size. The autocorrelation and semivariogram may not be sensitive enough to capture differences of pore structure across image sizes. Furthermore, they analyzed only spatial distributions of inter-aggregate pores.

So far, the effect of image size on pore morphological properties remains unknown. To understand image size effect on pore structure, it is necessary to perform more detailed measurements of pore properties across different image sizes.

3) Cell Unit

Series of cell sizes are applied to characterize spatial distributions of pore structure. Properties are measured within cell units (commonly box or cube shape) and calculations are repeated until they cover the entire image (Tarquis et al., 2003). These measured properties are plotted against cell sizes to find or quantify scaling effects on

pore properties. Unlike image resolution or size scaling, cell unit scaling is determined by series of cell sizes on the same resolution and image size. So far, cell unit scaling has been used to characterize the spatial distribution of pore cells or local porosities. Fractal, local porosity and entropy analyses are well known methods to characterize spatial distributions of pore cells or local porosities across series of cell sizes (Cislerova and Votrabova, 2002; Tarquis et al., 2003; Posadas et al., 2003). Detailed descriptions of these methods and applications on soil images are presented in Chapter 1.

Tania et al. (2007) stated that major research related to pore morphological analyses from CT images focused on inter-aggregate pore properties, such as, pores created by roots (Pierret et al, 1999), earthworm or earthworm burrows (Capowiez et al, 2003; Bastardie et al., 2003), and hydraulic processes through inter-aggregate pores (Monga et al., 2008). Investigations of large size pores require large size samples and image sizes. For instance, the sizes of images reported in the literature are less than $500\times500\times500$ voxels (except for simulated images) and large sample sizes had lower resolution than 1 cm. It is doubtful that low resolutions and small image sizes can fully characterize inter- and intra-aggregate pores in soil. Pierret et al. (2005) stated that low resolution such as 50 μm cannot recognize fine roots (< 50 μm in diameter) and image sizes of $70 \times 70 \times 1$ mm are too small to quantify full fine root length or pores creased by roots.

There is a need to improve pore network models for handling large size images. This study combines local porosity distributions at various cell sizes and medial- axis skeletonization to study pore geometry. This combination would provide less image data and time to compute morphological properties. Moreover, there has been no

investigation of the image resolution and size (or volume) scaling effects on pore morphological properties from aggregate and bulk soil images. Investigations of scaling effects on pore geometry within an aggregate and a bulk soil images would help to predict changes in pore geometry at different scales.

The hypotheses of this study were

1)   Aggregate and bulk soil have different pore structures, and

2)   Pore morphological properties across different image resolutions and sizes can be scaled.

The objectives of this study were to

1)   Develop a pore network model to quantify pore geometry from local porosity, and

2)   Assess effects of image resolution and cell size on pore geometry by applying the local porosity distribution at 12 cell sizes and three different image volumes.

4.2 Materials and Methods

4.2.1 Soils

Detailed information of sampling sites and soil sample descriptions can be found in Chapter 2. In Chapter 2 and 3, the bulk soils and the aggregate samples were analyzed with the configuration entropy. Most samples had Lo values of less than 30 voxels and small standard deviations across replicates. This result meant that cell size at Lo contains most heterogeneous and characteristic pore structure from the samples and there was no great difference among replicates. Therefore, in this study, one bulk soil sample and one aggregate sample from the rural site were selected for the morphological analysis.

4.2.2 Image Acquisition

Image acquisition and CT information were explained in Chapter 2 and 3.

4.2.3 Image Processing

1)   Thresholding and Image Sizes

Detailed information of CT and scanning processes can be found in Chapter 2. The bulk soil and aggregate images were reduced again from the center of each image into one half and one fourth of the $1000 \times 1000 \times 1000$ voxel volume: $500 \times 500 \times 500$ voxels (1331 mm^3) and $250 \times 250 \times 250$ voxels (166.38 mm^3) from the bulk soil and $270 \times 198 \times 115$ voxels (1.33 mm^3) and $135 \times 99 \times 58$ voxels (0.17 mm^3) for the aggregate (Fig. 4.1.). After thresholding, initial porosity of each sample was calculated by number of pore voxels divided by the total number of voxels in an image.

2)   Local Porosity Calculations at Different Cell Sizes

Local porosity distributions at series of cell sizes were used to mimic changing image resolutions. Image resolution refers to a number of pixels in a row and a column of the image; for example, 1 by 1 resolution means one pixel in a row and a column (Fig. 4.2). As pixel numbers in a row and a column increase, image quality improves. In this study, soil images had a constant voxel resolution. From each image, the resolution was changed by applying series of cell sizes. If a two dimensional image has 4 by 4 pixel resolution and each pixel has value of 0 or 1, this image has cell size of 1 by 1 pixel (Fig.4.2.A). In resolution term, this image has 4 by 4 image resolution. If the cell size increases to 2 by 2 pixels, a new pixel value of a cell is estimated by probability of four pixel values from cell size of 1 pixel. This calculation is repeated to cover the entire image and the resolution is 2 by 2 (Fig.4.2.B). If the cell size increases

to 4 by 4, there is one pixel in the image with resolution of 1 by 1 and the new pixel

value is estimated by probability of four pixels from cell size of 2 by 2 pixels (Fig.

4.2.C). This process created a series of image resolutions from one image. As cell size

increases, image resolution is degraded. In this study, 12 cell sizes were applied to

three image volumes for the aggregate and bulk soil image (Table 4.1).

3) Image Analysis Processing and Calculation of Pore Geometry

After obtaining local porosity values at different cell sizes from three volumes,

the rest of image processes and calculations were same as explained in Chapter 3. After

following the procedure, number of pores/throats, volumes of pore-body/throat, pore

length, tortuosity and coordination numbers were obtained.

Pore numbers from reduced image volumes were normalized to compare pore

numbers from the initial volume which were 10648 mm^3 for the bulk soil image and

10.76 mm^3 for the aggregate image. The proportion of the initial image size to a

reduced image size was multiplied by the pore numbers of the reduced image size.

4) Statistical Analyses

The average and standard deviation for each property (pore-body/ throat

volumes, lengths and tortuosity) was calculated as explained in Chapter 3. After log

conversion of the values, each property was converted to a histogram distribution.

Pore-body and throat volumes were grouped in to 30 and 20 classes based on their

respective ranges of volumes, which were 1×10^{-4} to 2000 mm^3 for pore volume and 2

$\times 10^{-6}$ to 0.05 mm^3 for throat volume Pore length data were converted into 20 classes

histogram ranging from 0.05 to 5 mm. The tortuosity data were grouped into 5 classes

covering 1 to 5. All properties at the cell volume of 512 voxels were compared between

the two samples (aggregate and bulk soil) and among three image volumes. Chi-square test at 95% level was performed to test homogeneity in pore property distributions in SPSS (Statistical Package for the Social Sciences, SPSS Inc).

The number of pores and volumes of pore-body and throat from each sample yielded linear relationships in log-log plots of these properties against cell sizes. Fractal dimensions (D) were estimated as the slopes of linear regressions of these relationships. Fractal dimensions from pore numbers were obtained from the number-size relationship (Gimenez et al., 1997).

$$N_f(L) = KL^{-D} \tag{1}$$

where $N_f(L)$ is number of pores at cell size, L. K is a number of initiators of unit length.

The D values for pore-body and throat volumes were calculated as:

$$N(L^3) \propto L^{3-D} \tag{2}$$

where $N(L^3)$ is a volume value at cell size of L.

The F-test was applied to compare linear regression of pore numbers and volumes of pore-bodies and throats at the 95% significant level (Neter $et\ al.$, 1990):

$$F = \frac{SSR(X_2, X_1 X_2 | X_1)}{NA} \div \frac{SSE(X_1, X_2, X_1 X_2)}{M - (2 \times NA)} \tag{3}$$

where M represents the combined sample size for X_1 and X_2, NA is the number of parameters in a model. $SSR(X_2, X_1 X_2 | X_1)$ is the sum of errors of the X_1 and X_2 models, and $SSE(X_1, X_2, X_1 X_2)$ is the sum of errors of the combined model of X_1 and X_2.

4.3 Results and Discussions

4.3.1 Total Porosity and Local Porosity Distribution

Local porosity at all 12 cell sizes (Table 4.1) were calculated for three different image volumes of the aggregate and the bulk soil (Fig. 4.5). As cell size increased, pore shapes were transformed into blocky shapes compare to the pore shapes from smaller cell sizes (Fig. 4.5). The degree of deformation was related to the ratio between image size and cell size. The cell size of 32 voxels was relatively large size cell to aggregate image size, since pores appear blocky at that cell size (Fig. 4.5).

Total porosities from the bulk soil and the aggregate images increased with cell size (Table 4.1 and Table 4.2). The initial porosity of each image was calculated from the original image and the porosity was 0.16 for the bulk soil and 0.21 for the aggregate, increasing in the bulk soil and in the aggregate up to 24% at cell size of 2.80 mm and 22% at cell size of 0.77 mm. Lehmann et al. (2006) found that a resolution of 3.5 μm overestimated small size pores and resulted in greater porosity than porosity from an image with a resolution of 11.5 μm. Similarly, larger cell sizes from this study had greater porosity than porosities in smaller cell sizes. This increment was caused by the conversion of local porosity values. If a cell had porosity of 0.50, the cell would be assigned a value of 1 as explained in page 62 and this would increase porosity more by 0.50 (=1-0.50). Another reason for the increase in porosity is more pore merging of pores with an increase in cell size. Isolated pore cells (less than two connected pore cells) would be merged into other pores and added to the total porosity while those cells were ignored at smaller cell sizes. As a result,

pores were merged and transformed into large blocky shapes at a large cell size (Fig. 4.5).

4.3.2 Numbers of Pores and Throats

Normalized number of pores had a linear relationship across image volumes and cell sizes in a log-log plot (Fig. 4.6.A). Sleutel et al. (2008) compared porosity and pore sizes from three dimensional soil images with two resolutions (2.5 μm and 1.74 μm). They found that there were greater pore numbers at a resolution of 2.5 μm because at this resolution a greater amount of fine pores (< 5 μm in diameter) were captured. Similarly, pore numbers were greater at smaller cell sizes and decreased with an increase in cell size. However, Al-Raoush and Willson (2005) found lower numbers of pores at a resolution of 23 μm than at a resolution of 11.3 μm, but this result may have been the consequence of using different image sizes at different resolutions and not normalized the results as in this study. The D values of the bulk soil and the aggregate were 2.79 and 2.12, respectively; and statistically different according to an *F*-test analysis (p=0.03). The greater slope value from the bulk soil may imply that the pores in the bulk soil merged into each other more rapidly as cell size increased.

In a log-log scale, the normalized number of throats decreased linearly with cell size (Fig. 4.6.B). As cell size increased, throat areas merged into pore -body volumes and the number of throats decreased. The D value of the throat numbers across cell sizes was significantly greater in the aggregate (2.47) than in the bulk soil (1.97) (p=0.00), which was the opposite result to the D value from the pore number results (Table 4.4). The maximum throat number for the aggregate was 4,680 at cell size of 0.01 mm from the smallest image volume. The change rate of throat number from 4,680 to 334 (Table XX)

of the aggregate was 1.90 and the one from 40,128 to 1235 of the bulk soil was 2.51.

Similar to pore numbers, changes of image volume affected more throat numbers in the

bulk soil than in the aggregate. However, the rate of throat number changes from 0.18 to

2.82 mm from the initial bulk soil volume was 1.92 and the one from 0.05 to 0.77 mm of

the initial aggregate volume was 2.69.

As discussed by Bartoli et al., (2005), soil structure is a discrete hierarchical

structure with a clear disparity in pore structures between different hierarchical levels.

The difference in D values and trends of pore and throat numbers between the aggregate

and the bulk soil sample may have resulted from different hierarchical levels of the two

samples.

4.3.3 *Pore-Body Volume*

Pore -body and throat volume followed lognormal distributions (Table 4.2 and

Table 4.3). Thus, the geometric mean and geometric standard deviations were used to

characterize the distributions (Chapter 3

The bulk soil had wider range of volumes and greater amount of large size pores

than the aggregate (Fig. 4.7). Average pore-body volumes were overall greater in the

bulk soil than the aggregate. There were relatively greater standard variations at cell

sizes of 0.70 to 2.82 mm from the bulk soil and 0.77 mm from the aggregate sample

(Table 4.2 and Table 4.3). These greater standard deviations were caused by increases in

pore volumes from merging pores. This change induced a wider range of pore -body

volumes among fewer pores, therefore variations of pore -body volume increased. This

may suggest that there is a limitation in pore-volume scaling by changing cell sizes since

too large cell size displayed too many significantly different values compared to values

from smaller cell sizes; for example, there was one pore at the cell size 2.82 mm from the bulk soil. The volume from this cell size was ignored in Fig. 4.7.

In a log-log scale, the average pore -body volumes increased linearly with cell size with no difference in volume changes across cell sizes, except volumes at a cell size of 2.816 mm for the bulk soil and 0.126 mm for the aggregate ($p > 0.05$) (Fig. 4.7.A). The small increment of average pore-body volume was induced by increase of minimum pore-body sizes corresponding to cell size increase.

Average pore–body volumes across cell sizes were fitted with linear regression and the slope of fitted lines were 1.15 for the bulk soil and 0.71 for the aggregate. The D values, calculated with Eq. (2), for the bulk soil and the aggregate were 1.85 and 2.29, respectively (Table 4.4) and statistical different ($p=0.00$). These results mean that small pores in the aggregate did not merge to other pores as much as the bulk soil did, since the slope value of the aggregate was much lower. There has been no fractal dimension information for pore volume across cell sizes. Perfect (1999) found that coarse textured soils with larger pores had lower D values in water retention scaling across pressures. Our results suggested that lower D value from the bulk soil implies more large size pores or inter-aggregate pores than the aggregate.

Average throat volumes from the aggregate and the bulk soil increased with cell sizes (Fig. 4.7.B). Similar to average pore-body volumes, this increment was caused by minimum throat volume increase corresponding to increase of cell size. The increment of throat volumes was not significant until cell sizes greater than 0.704 mm from the bulk initial volume. The D values were calculated with Eq. (2) similar to D value calculation for the pore–body volume. According to an F- test, the aggregate had statistically greater

(p=0.00) D value (2.775) than the bulk soil (2.820). Bartoli et al. (1999) reported that soils with less connected pores and smaller porosity had smaller throat sizes and greater fractal dimension. Based on this finding, the aggregate had relatively greater throat sizes than the bulk soil did. These results were reflected by the average ratio of pore-body volume to throat volume across cell sizes. The average ratio of the bulk soil was 5.50± 3.06, while the ratio from aggregate was 1.77 ± 0.40. The changes in throat numbers and sizes from the aggregate were relatively greater across cell sizes than those from the bulk soil. As cell size increased, the number of throats from the aggregate decreased greatly, while throat sizes increased. Aggregate throats did not merge into pore–body volumes, but merged into other throats with increases in cell sizes.

Al-Raoush and Willson (2005) analyzed pore-body and throats properties in CT imaging of sand with two resolutions (11.5 and 23 μm). They found that average pore-body volume increased as the image resolution was reduced. The throat number decreased at a lower resolution, while the average throat sizes increased. The pore-body and throat volume results from the aggregate and the bulk soil agreed with the results from Al-Raoush and Willson (2005).

Greater coordination number (i.e., is number of throats from each pore) indicate greater connectivity. In terms of scaling, there was no trend in the coordination number from the bulk soil and aggregate. Overall, aggregate coordination numbers were smaller than in bulk soil. It is a reasonable result since bulk soil would have more connected pores from inter-aggregate pores. Udawatta and Anderson (2008) reported that soils with more inter-aggregate pores had greater values of coordination number. In aggregate and bulk soil respectively, the coordination number tended to increase or at least not decrease

with cell size, but not significantly (p >0.05). However, the coordination number

dropped as cell size increased further than 0.704 mm for the bulk soil and 0.126 mm for

the aggregate. Probably for cell sizes greater than 0.704 mm for the bulk soil and 0.126

mm for the aggregate, throats merged into pore -bodies without creating new throats,

therefore the coordination number decreased.

4.3.4 Length and Tortuosity

Average pore lengths from bulk soil increased with cell size but not significantly

(p>0.05). Pore l lengths at cell size of 0.176 mm from the reduced image volumes were

different than pore length at cell size of 0.176 mm from the image volume of 1000 by

1000 by 1000 voxels (Table 4.2 and Table 4.3). Results of pore length in the aggregate

exhibited a similar trend as in the bulk soil , but the degree of changes was smaller and

did not have significant differences until cell size of 0.192 mm. The length results from

both samples did not have any pattern or relationships between pore length and cell sizes

/ image volumes (Fig. 4.8).

Average tortuosity values were not different across cell sizes in the bulk soil and

aggregate (Table 4.2 and Table 4.3). Tortuosity values were expected to decrease with

cell size, because pores became straighter as cell size increase. However, average length

increased or did not decrease significantly as cell size increase. Therefore, tortuosity

values did not decrease and this resulted in no scaling effect or changes on tortuosity

across cell and image sizes (Fig. 4.9).

There has been no study about pore length or tortuosity changes with image

resolution. Investigations of pore surface fractal dimensions at different resolution

images were related to pore lengths and tortuosity (Gimenez et al., 1997; Dathe and

Baveye, 2003). However there was no clear scaling effect pore surface fractal dimensions with resolution.

4.4 Conclusion

In this study, the morphological properties of pores were calculated from three dimensional soil images. Scaling effects on pore morphology were studied using: 1) aggregate and bulk (column) samples, 2) different image volumes, and 3) series of cell sizes. The pore systems in the aggregate and bulk samples were different by having distinct values and trends of measured properties across cell sizes and image volumes at the aggregate and laboratory scale, which supports a discrete hierarchical structure in pore systems.

The most accurate method to capture pore properties in three dimensional images is analyzing images at a voxel unit, but there are limitations in computer capacity and time. Instead, the use of pore network model applied to local porosity at a series of cell sizes reduces time and computer capacity. From this study, it can be concluded that pore numbers and average pore volume (pore-body and throats) can be scaled across resolutions and image volumes at the aggregate and laboratory scale, while pore length, tortuosity and coordination number cannot be scaled.

It can be challenging to find changes of soil properties from different sample sizes or image resolutions, because changing physical sample sizes or magnification levels from optical equipments, such as CT can be difficult and time consuming. Using local porosity with different cell sizes can be a useful method to investigate scaling effects of sample sizes and resolutions on soil, since it is relatively easier to achieve in change image sizes and resolutions.

References

Al-Raoush, R.I. and C. S. Willson. 2005. Extraction of physically realistic pore network properties from three-dimensional synchrotron X-ray microtomography images of unconsolidated porous media systems. *J. Hydrol*. 300(1-4): 44-64.

Baveye, P., H. Rogasik, O. Wendroth , I. Onasch, and J.W. Crawford. 2002. Effect of sampling volume on the measurement of soil physical properties: simulation with x-ray tomography data. *Meas. Sci. Technol.* 13(5): 775-784.

Bear, J. 1974. Dynamics of fluids in porous media. Dover Publications, Inc., New York.

Bl¨oschl, G. And M. Sivapalan. 1995. Scale issues in hydrological modeling: a review. *Hydrol. Process*. 9:251–90.

Cislerova, M. and J. Votrabova. 2002. CT derived porosity distribution and flow domains. *J. Hydrol*. 267(3-4): 186-200.

Currie, J. A. 1966. The volume and porosity of soil crumbs. J. Soil Sci. 17(1):24-35.

Dathe, A., S. Eins, J. Niemeyer, and G. Gerold. 2001. The surface fractal dimension of the soil–pore interface as measured by image analysis. *Geoderma*, 103: 203–229.

Dathe, A. and P. Baveye. 2003. Dependence of the surface fractal dimension of soil pores on image resolution and magnification. *Eur. J. Soil Sci*. 54: 453–466.

Dathe, A. and M. Thullner. 2005. The relationship between fractal properties of solid matrix and pore space in porous media. *Geoderma*. 129(3-4): 279-291.

Dexter, A. R. 1988. Advances in characterization of soil structure. *Soil Till. Res.* 11: 199-238.

Elkateb, T., R. Chalaturnyk, and P.K. Robertson. 2003. An overview of soil heterogeneity: quantification and implications on geotechnical field problems. *Can. Geotech. J.* 40: 1–15.

Gibson, J.R., H. Lin, and M. A. Bruns. 2006. A comparison of fractal analytical methods on 2-and 3-dimensional computed tomographic scans of soil aggregates. *Geoderma*. 134(3-4): 335-348.

Gimenez, D., R.R. Allmaras, E.A. Nater, and D.R. Huggins . 1997. Fractal dimensions for volume and surface of interaggregate pores - Scale effects. *Geoderma*. 77(1): 19-38.

Gimenez. D., E. Perfect, W.J. Rawls, and Y. Pachepsky. 1997. Fractal models for predicting soil hydraulic properties: a review. *Eng Geol.* 48 (3-4): 161-183.

Gimenez, D., W.J. Rawls, and J. G. Lauren. 1999. Scaling properties of saturated hydraulic conductivity in soil. *Geoderma*. 88: 205–220.

Hopmans, J. W., D.R. Nielsen, and K. L. Bristow. 2002. How useful are small-scale soil hydraulic property measurements for large-scale vadose zone modeling? In D. Smiles et al. (*ed.*) Heat and mass transfer in the natural environment. The Philip Volume. Geophysical Monogr. Ser. 129. p. 247–258. AGU, Washington, DC.

Jassogne, L., A. McNeill, and D. Chittleborough. 2007. 3D-visualization and analysis of macro- and meso-porosity of the upper horizons of a sodic, texture-contrast soil. *Eur. J. Soil Sci.* 58(3): 589-598.

Lehmann, P., P. Wyss, A. Flisch, E. Lehmann, P. Vontobel, M. Krafczyk, A. Kaestner, F. Beckmann, A. Gygi, and H. Fluhler. 2006. Tomographical imaging and mathematical description of porous media used for the prediction of fluid distribution. *Vadose Zone J.* 5(1): 80-97.

Liu, Z.B., B.Shi, H.I.Inyang, and Y. Cai. 2005. Magnification effects on the interpretation of SEM images of expansive solds. *Eng. Geol*. 78(1-2): 89-94.

Neter, J., W. Wasserman, and M. H. Kutner. 1990. Applied Linear Statistical Models, 3rd edition. Richard D. Irwin, Inc., Burr Ridge, Illinois.

Ogawa, S., P. Baveye, C.W. Boast, J.Y. Parlange, and T. Steenhuis. 1999. Surface fractal characteristics of preferential flow patterns in field soils: evaluation and effect of image processing. . *Geoderma.* 88(3-4): 109-136.

Pachepsky, Y., D.E. Radcliffe, and H.M. Selim. 2003. Scaling Methods in Soil Physics. CRC Press, Boca Raton, FL.

Papadopoulos, A., N.R.A. Bird, S.J. Mooney, and A.P. Whitmore. 2008. Fractal analysis of pore roughness in images of soil using the slit island method. *Vadose Zone J*. 7(2): 456-460.

Pendleton, D.E., A. Dathe, and P. Baveye. 2005. Influence of image resolution and evaluation algorithm on estimates of the lacunarity of porous media. *Phys. Rev. E.* 72(4).

Perfect, E. 1999. Estimating soil mass fractal dimensions from water retention curves. *Geoderma*. 88(3-4): 221-231.

Posadas, A. N. D., D. Gimenez, M. Bittelli, C. M. P. Vaz, and M. Flury. 2003. Multifractal characterization of soil particle-size distributions. *Soil Sci. Soc. Am. J.* 65(5): 1361-1367

Rodriguez-Iturbe, I., G.K. Vogel, R. Rigon, D. Entekhabi, F. Castelli, and A. Rinaldo. 1995. On the spatial organization of soil moisture fields. *Geophys. Res. Lett*. 22(20): 2757–2760.

Sleutel, S., V. Cnudde, B. Masschaele, J. Vlassenbroek, M. Dierick , L. Van Hoorebeke, P. Jacobs, and S. De Neve. 2008. Comparison of different nano- and micro-focus X-ray computed tomography set-ups for the visualization of the soil microstructure and soil organic matter. *Comput. Geosci*. 34(8): 931-938.

Udawatta, R.P and S.H. Anderson. 2008. CT-measured pore characteristics of surface and subsurface soils influenced by agroforestry and grass buffers. *Geoderma*. 145(3-4): 381-389.

VandenBygaart, A. J. and R. Protz. 1999. The representative elementary area REA in studies of quantitative soil micromorphology. *Geoderma*. 89: 333–346

Vogel, H.J. and K. Roth. 2003. Moving through scales of flow and transport in soil. *J. Hydroal*. 272(1-4): 95-106.

Young, I.M., J.W. Crawford, and C. Rappoldt. 2001. New methods and models for characterizing structural heterogeneity of soil. *Soil Till. Res*. 61:33-45.

Ziska, L.H., J.A. Bunce, and E.W. Goins. 2004. Characterization of an urban-ls CO2/temperature gradient and associated changes in initial plant productivity during secondary succession. *Oecologia*. 139(3): 454-458.

Table 4.1 Summary of cell unit sizes and three image sizes for each soil sample.

	Bulk soil		Aggregate
Image size (mm^3)	Cell unit size (mm)	Image size (mm^3)	Cell unit size (mm)
	0.04		0.01
166.38	0.09	0.17	0.02
	0.18		0.05
	0.07		0.04
1331		1.33	
	0.18		0.05
	0.18		0.05
	0.22		0.06
	0.35		0.10
10648	0.55	10.76	0.13
	0.70		0.19
	1.41		0.38
	2.82		0.77

Table 4.2 Summary of pore morphological properties from bulk soil. All properties are represented by average and standard deviation values, except for porosity, number of pores and throats.

Image size (mm^3)	Cell unit size (mm)	Porosity	Number of pores*	Average pore-body volume(mm^3)	Number of throats*	Average throat volume (mm^3)	Pore length(mm)	Tortuosity	Coordination number
166.38	0.04	0.04	64000	0.15±0.00	40128	0.02±0.00	0.29±0.000	1.02±0.01	0.20±3.12
	0.09	0.09	34880	0.26±0.00	6912	0.10±0.000	0.34±0.00	1.01±0.02	0.63±14.55
	0.18	0.14	2880	0.58±0.04 [a]	2048	0.18±0.00	0.40±0.00 [a]	1.01±0.04	0.89±2.62
1331	0.13	0.07	2672	0.33±0.00	2192	0.18±0.00	0.35±0.00	1.00±0.04	0.82±14.77
	0.18	0.08	1568	4.06±7.36	1752	0.19±0.00	0.37±0.00 [a]	1.00±0.05	1.12±14.86
	0.18	0.18	511	0.87±0.18	1235	0.19±0.00	1.04±0.27	1.17±0.22	1.25±8.45
	0.22	0.18	442	0.86±0.15	883	0.20±0.00	0.94±0.15	1.17±0.05	1.94±9.48
	0.33	0.18	126	1.02±0.59	675	0.22±0.00	1.07±0.38	1.16±0.20	3.62±12.60
10648	0.55	0.18	110	1.67±0.98	351	0.23±0.00	1.17±0.29	1.15±0.16	3.88±12.77
	0.70	0.19	69	2.16±4.29	86	0.24±0.00 [a]	1.21±0.68	1.15±0.15	8.58±20.12
	1.41	0.20	3	5.13±174.49	42	0.28±0.01 [a]	1.86±3.72	1.10±0.26	3.60±8.98
	2.82	0.20	1	2124.19	6	0.30±0.00 [a]	2.06	1	6

* indicates that the property values were normalized to the sample volume of 10648 mm^3.
The letter 'a' indicates statistical difference at 95% level among cell sizes. Properties at cell size of 0.18 mm from image volume of 166.38 and 1331 mm^3 were selected to compare to properties at 0.18 mm from 10648 mm^3.

Table 4.3 Summary of pore morphological properties from aggregate. All properties are represented by average and standard deviation values, except for porosity, number of pores and throats.

Image size (mm^3)	Cell unit size (mm)	Porosity	Number of pores*	Pore-body volume (mm^3)	Number of throats*	Throat volume (mm^3)	Pore length (mm)	Tortuosity	Coordination number
0.17	0.01	0.06	111936	0.072±0.00	4680	0.06±0.00	0.54±0.01	1.01±0.03	0.01±0.18
	0.02	0.11	17718	0.10±0.00	2544	0.06±0.00	0.63±0.01	1.01±0.03	0.03±0.53
	0.05	0.16	3420	0.18±0.00 [a]	896	0.0758±0.00	1.19±0.22 [a]	1.00±0.03	0.08±0.48
1.33	0.04	0.21	3250	0.11±0.00	2340	0.07±0.000	0.66±0.04	1.02±0.04	0.02±6.23
	0.05	0.42	1650	0.18±0.00 [a]	292	0.11±0.001	0.67±0.04	1.02±0.03	0.08±5.16
10.76	0.05	0.25	3009	0.15±0.00	334	0.08±0.00	0.55±0.01	1.02±0.05	0.26±0.94
	0.06	0.25	3000	0.16±0.00	128	0.08±0.01	0.56±0.01	1.02±0.03	0.23±1.26
	0.10	0.26	2049	0.16±0.00	72	0.099±0.00	0.56±0.01	1.02±0.02	0.30±8.86
	0.13	0.26	909	0.17±0.00	30	0.102±0.00	0.57±0.01	1.01±0.02	0.37±10.85
	0.19	0.26	416	0.38±0.00 [a]	8	0.106±0.002	0.71±0.01 [a]	1.004±.02	0.02±0.39
	0.38	0.27	63	0.62±0.02 [a]			0.90±0.02 [a]	1.00±0.30	
	0.77	0.27	5	1.27±0.64 [a]			0.80±0.03 [a]	1.00±0.00	

* indicates that the property values were normalized to the sample volume of 10.76 mm^3.

The letter 'a' indicates statistical difference at 95% level among cell sizes from image volume of 10.76 mm^3.

Properties at cell size of 0.05 mm from image volume of 0.17 and 1.33 mm^3 were selected to compare to properties at 0.05 mm from 10.76 mm^3.

Table 4.4 Fractal dimensions from selected pore properties. The fractal dimensions (D) were calculated with Eq. (1) for pore and throat numbers and with Eq. (2) for volumes of pore and throat. The numbers in parenthesis are standard error of the D value.

	Bulk soil	Aggregate
Number of pores	2.79 (0.17)	2.12 (0.16)
Pore-body volume	1.85 (0.16)	2.29 (0.05)
Number of throats	1.97 (0.09)	2.47 (0.27)
Throat volume	2.82 (0.01)	2.78 (0.05)
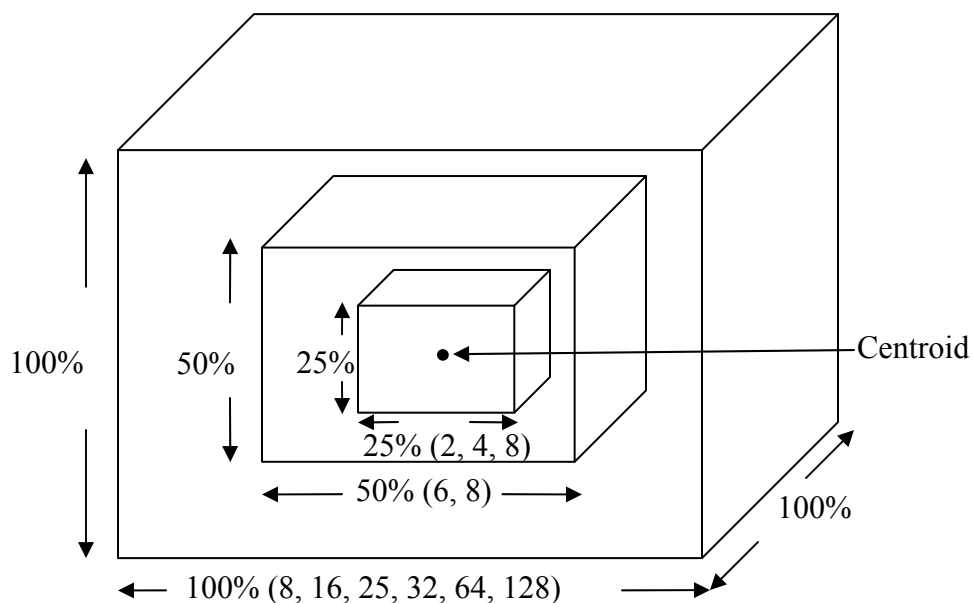
Figure 4.1 A Schematic illustration of sub-sampling for all samples; for the bulk soil, the volume size was 10648 mm^3 at 100% and the aggregate volume size was 10.76 mm^3 at 100%. Numbers within parentheses represent cell sizes (voxels) that applied to each volume.
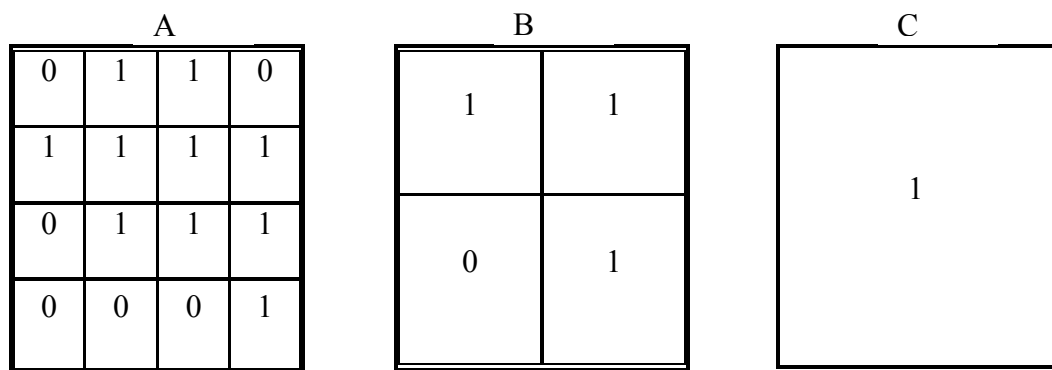
Figure 4.2 Image degradation by increasing cell sizes. A. Pixel values at cell size 1 by 1, B. Average pixel values at cell size 2 by 2 and C. Average pixel value at cell size 4 by 4. 0 and 1 represent pore and solid pixel.

A

B

L = 8

L = 16

L = 32
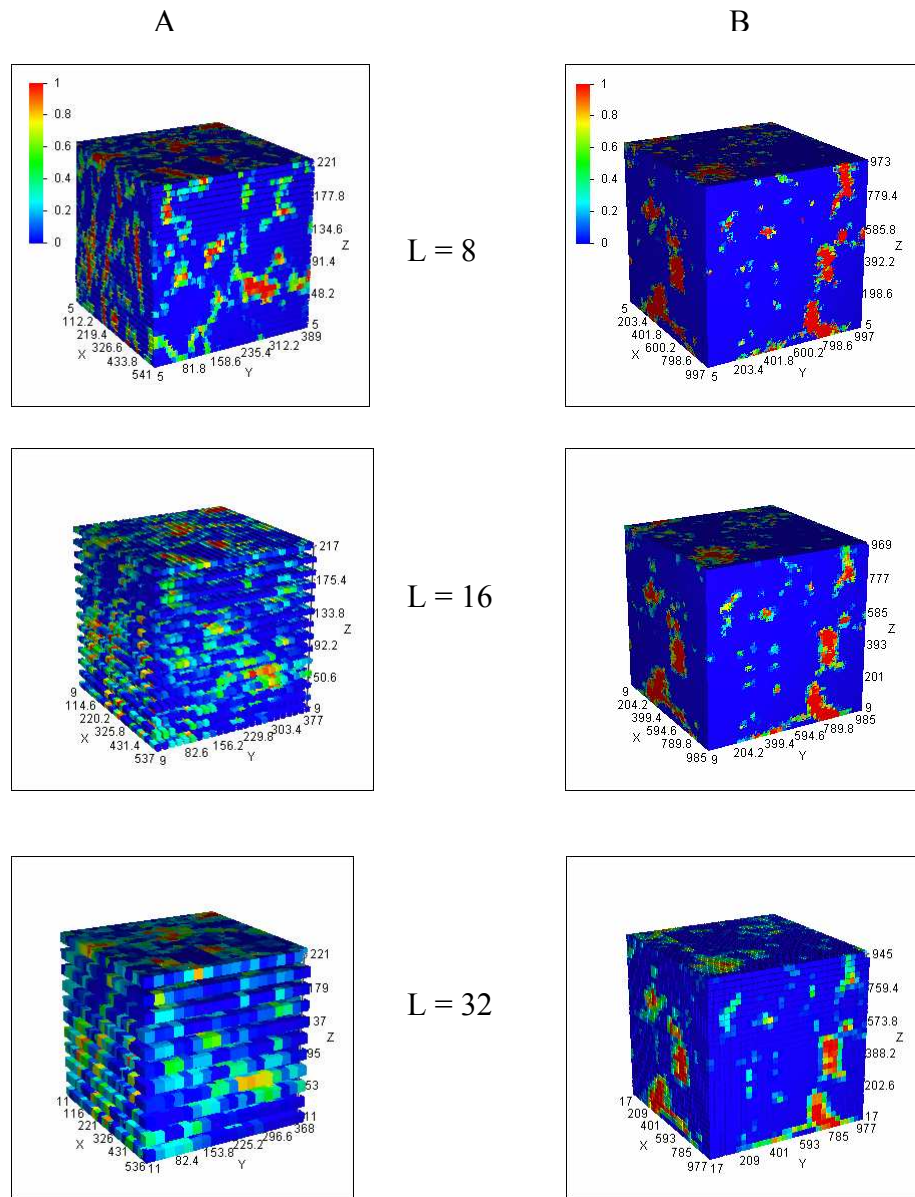
Figure 4.3 Selected soil images of local porosity distributions at difference cube size, L; A. Aggregate images and B. Bulk soil images.
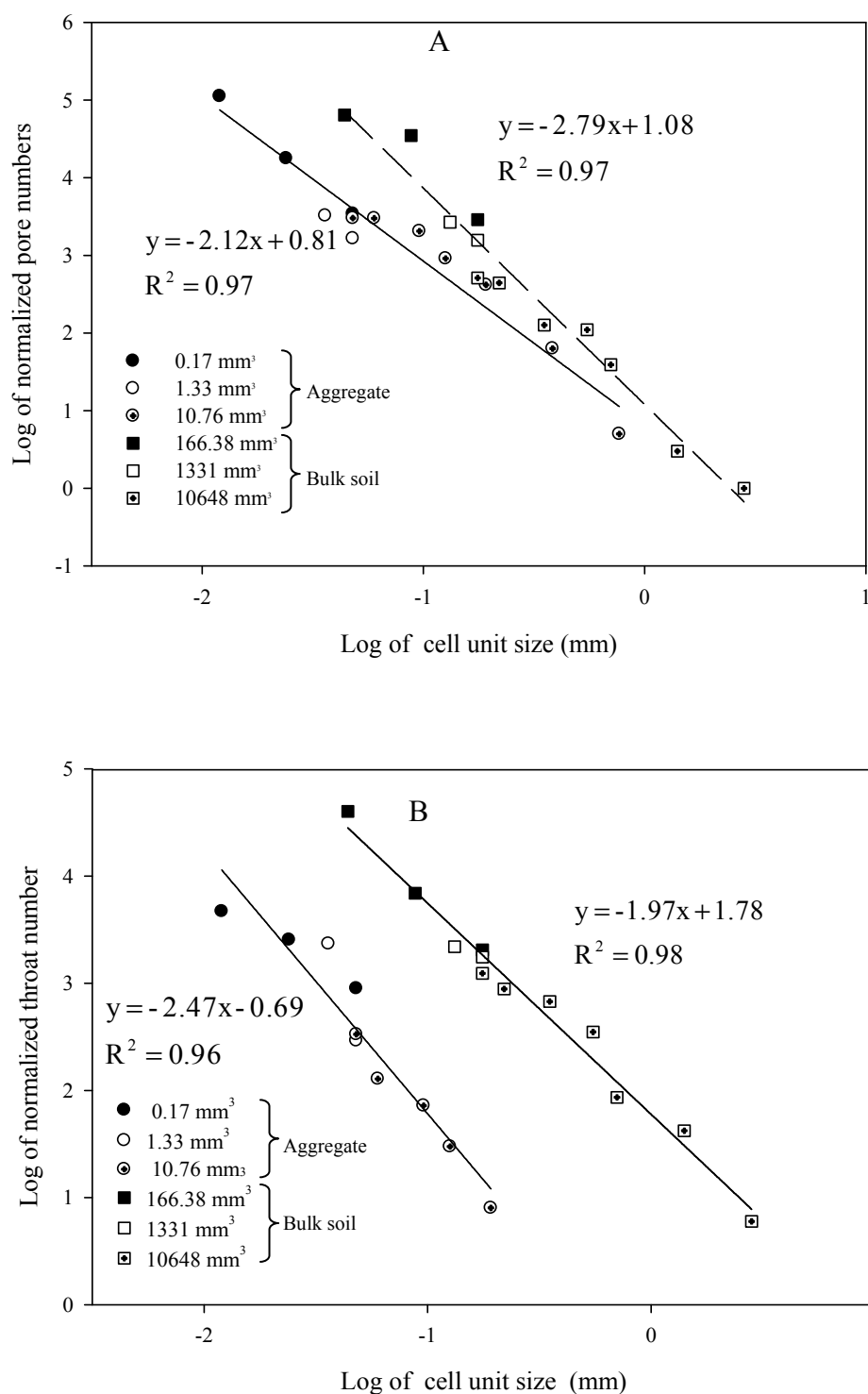
Figure 4. 4 A: : Number of pores from aggregate and bulk soil across cell unit sizes from all image volumes. B: Number of throat distributions from aggregate and bulk soil across cell sizes. The solid lines are linear regressions for the aggregate and the dash lines are linear regressions for the bulk soil. The legend refers to the image volumes.
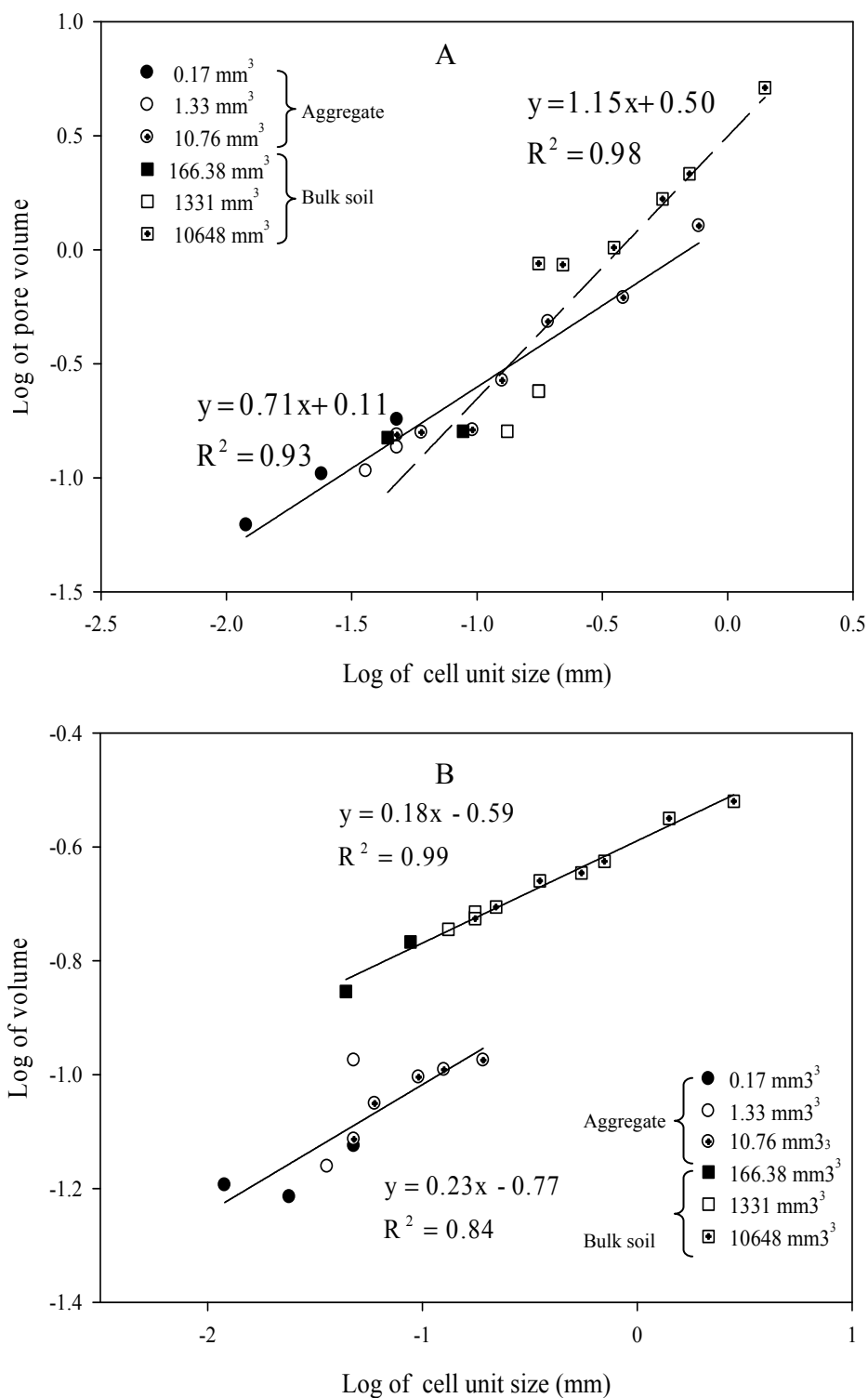
Figure 4.5 A: Average pore-body volumes across cell unit sizes from all image volumes. B: Average throat volumes across cell sizes from all image volumes. The solid lines are linear regressions for the aggregate and the long dash lines are linear regressions for the bulk soil. The legend refers to the image volumes.
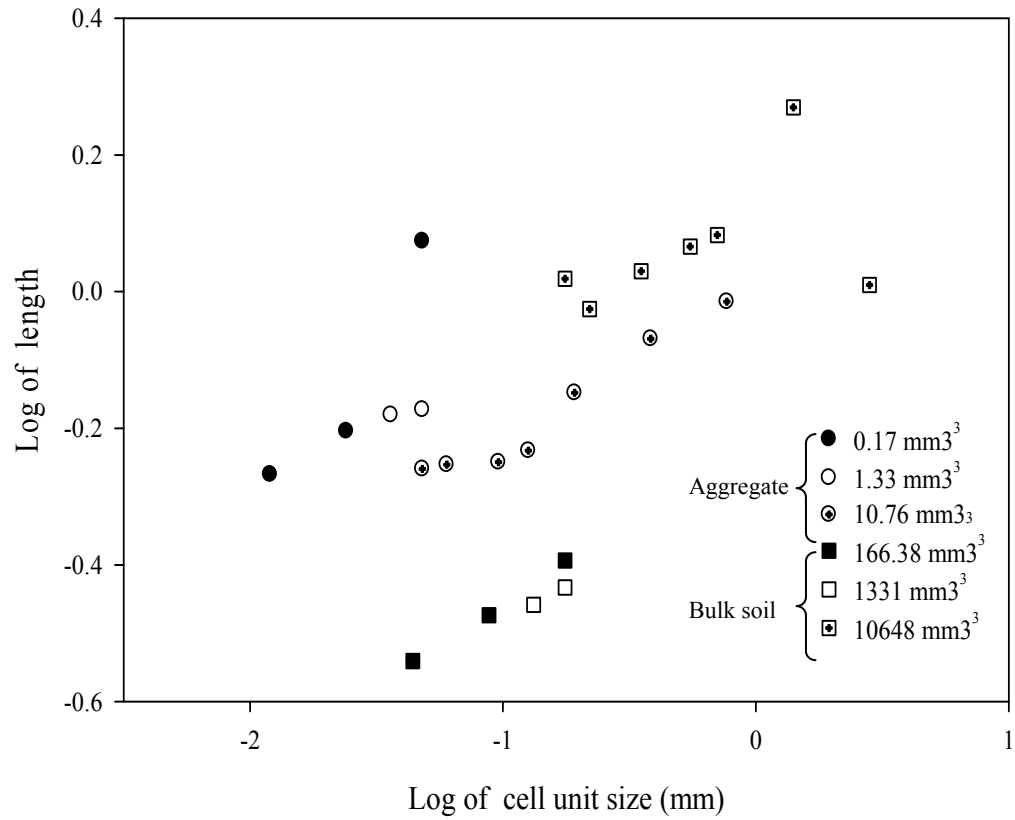
Figure 4. 6 Average pore length across cell unit sizes from all image volumes. The legend refers to image volumes.
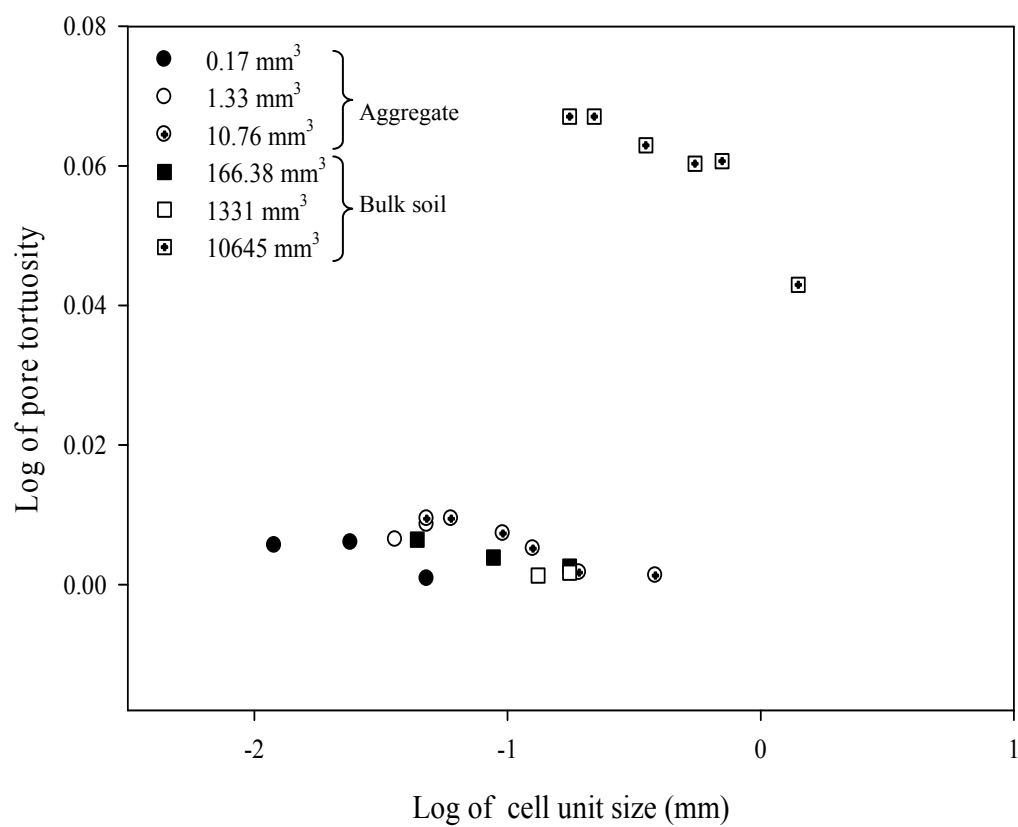
Figure 4. 7 Average values of tortuosity across cell size from all image volumes. The legend refers to image volumes.

Chapter 5 : Conclusions and Future Research

Image analysis of three dimensional images of soils is useful to quantify pore properties and characterize pore structure from soils with different scales. This study applied the pore network model, medial-axis transformation, with local porosity calculation to pore morphological analyses. This method characterized large data sets of soil images with less time and computer capacity. However, there was a limitation of applying local porosity at various cell sizes. As cell size increased, requirements of time and computer capacity were reduced, while small size pores were ignored and pore shapes were deformed greatly. Therefore it is important to choose the proper cell sizes based on a particular research interest. For investigations involving inter-aggregate pores, relatively large cell sizes would be fine and for intra-aggregate pores, small size cell sizes would be more appropriate. The pore network model with cell units can provide detailed pore geometry information, especially intra-aggregate pores, with less time than pore geometry calculation without local porosities.

The modified pore network successfully characterized aggregate pore structure and bulk soil pore structure and the morphological analyses showed a dual pore system in soil pore structure by comparing aggregate and bulk soil pore properties. This method also characterized scaling behaviors of pore geometry across different sample sizes at the aggregate and the laboratory scale and resolutions. However, pore length and tortuosity were not scalable across image sizes and resolutions.

Characterization of pore structures from soils with gradients of atmospheric concentration of CO_2 and temperature showed mixed results; changes in inter-aggregate pore system and no impacts on intra-aggregate pore system. Greater CO_2 concentration

and higher temperature with sufficient soil moisture developed more inter-aggregate pores in soil from both spatial analyses and morphological analyses. Image analyses of aggregates revealed no dissimilarity among any pore morphological properties from different CO_2 and temperature conditions. In addition, hydraulic properties from images and measurement supported pore structural difference at inter-aggregate pore level.

The modified pore network suggested that prediction of hydraulic properties from three dimensional images can be supplementary to laboratory measurements, especially, inter-aggregate pore properties. Combination of hydraulic data from an image and measurement had complete information of inter-aggregate pores and intra-aggregate pores since pores from images were limited by image resolutions and cell sizes and pores from measurement gave inaccuarate values for large size pores.

This pore network model with local porosity distribution can be applied to simulation of soil structure. Especially, this model is useful to predict hydraulic properties and inter-aggregate pore properties since the model can preserve large size pore properties as cell size of one voxel does and provides quantitative information of pore geometry and related properties. Simulation of pore structure using the modified pore network model would reveal more detailed information of soil properties as climate changes and predict changes of pore properties as atmospheric CO_2 concentration and temperature increases in the future.

Appendix A

Thresholding effects

In chapter 2 and chapter 4, soil images were binarized by 3DMA software, while images in chapter 3 were done by Java codes written by T. Elliot and Dr. Heck at the University of Guelph. The threshholding algorithm was theoretically same from the both programs as explained in chapter 2. However, 3DMA was more sensitive to noise and deleted more noise from images. We tested noise effect on spatial analysis of pores, since the images binarized by Java code were applied to spatial distribution analyses of pore structure. Fig. A.1 presents results from two different thresholding program from same soil image. There was a couple of noise lines showed up in the image binarized by Java code program (Fig. A.1.a). Three images were selected from each site and binarized from two programs respectively. The binary images were calculated for the configuration entropy. Emax and Lo (explained in chapter 3) paramters from the entropy calculation had almost same values from both programs. Lo values were identical from the two programs, while there were small deviations in Emax values between two programs. Based on these results, thresholding program by Java code did not affect entropy results significantly compare to entropy values from images binarized by 3DMA program.
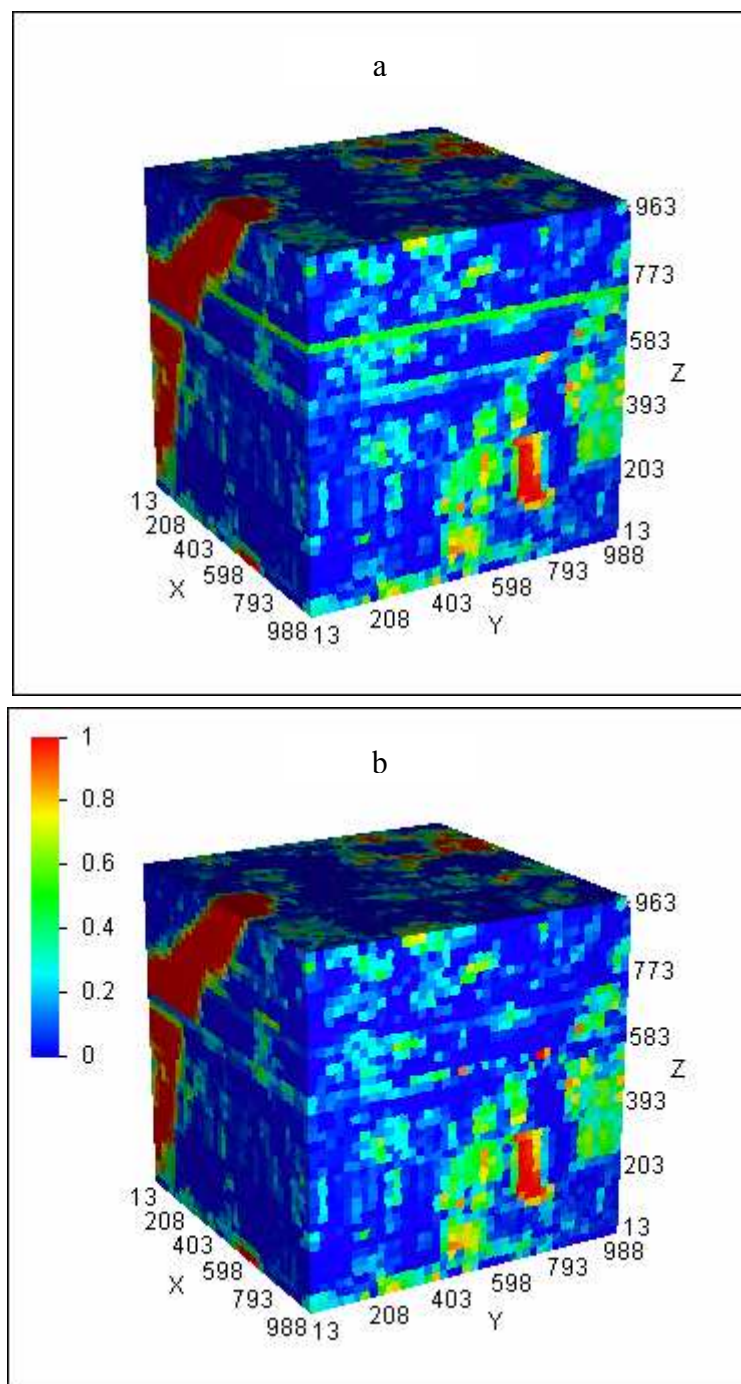
Figure A. 1 Example images from two thresholding programs. Soil image was one sample from urban site and cell unit size was 32 voxels. a presents local porosity

distribution result using thresholding from Java code program and b presents local porosity distribution result using thresholding from 3DMA.

a

b
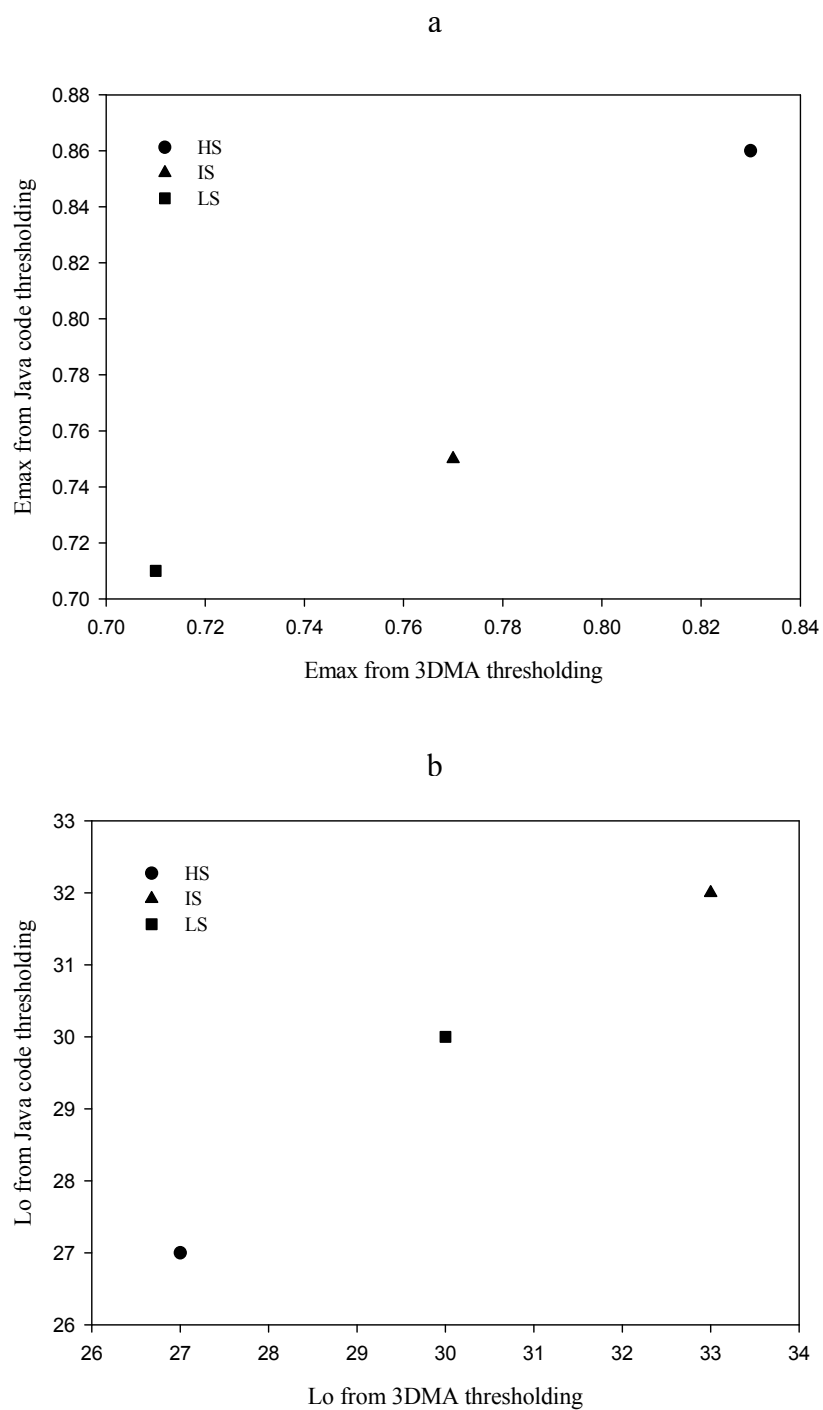
Figure A.2 Configuration entropy results from three images with two thresholding programs. A.Emax values from three sites and b. Lo values from three sites**.**

Appendix B

Example distributions of pore properties

A

B
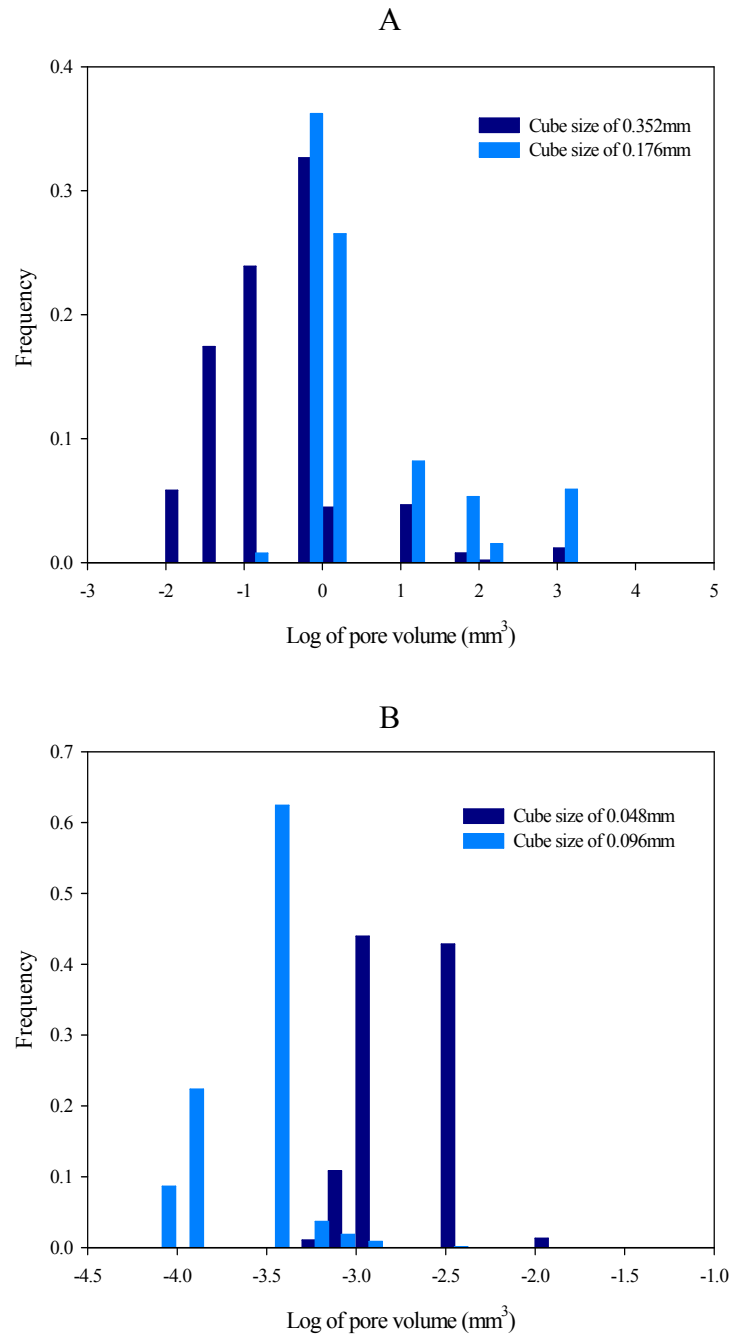
Figure B. 1 Frequency distributions of pore-body volume in logarithm scale; A. Distributions from bulk soil (image size of 10648 mm^3) and B. Distributions from aggregate (image size of 10.76 mm^3).

A
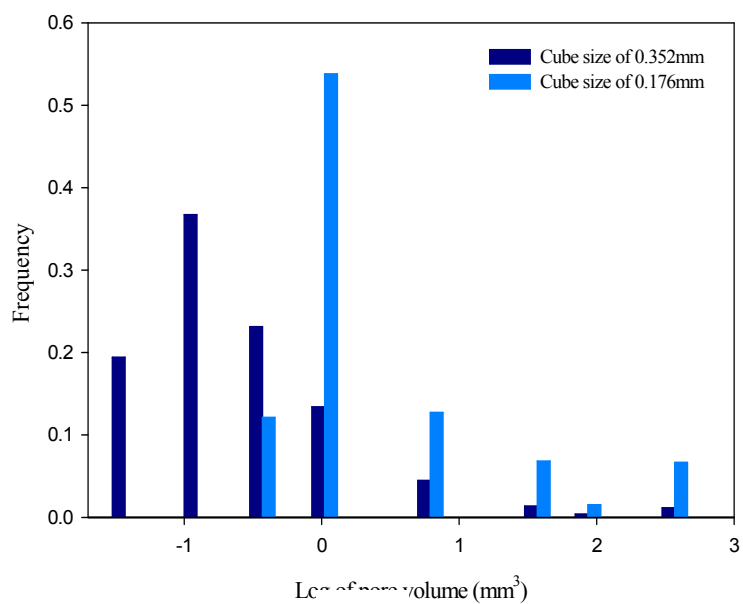
B
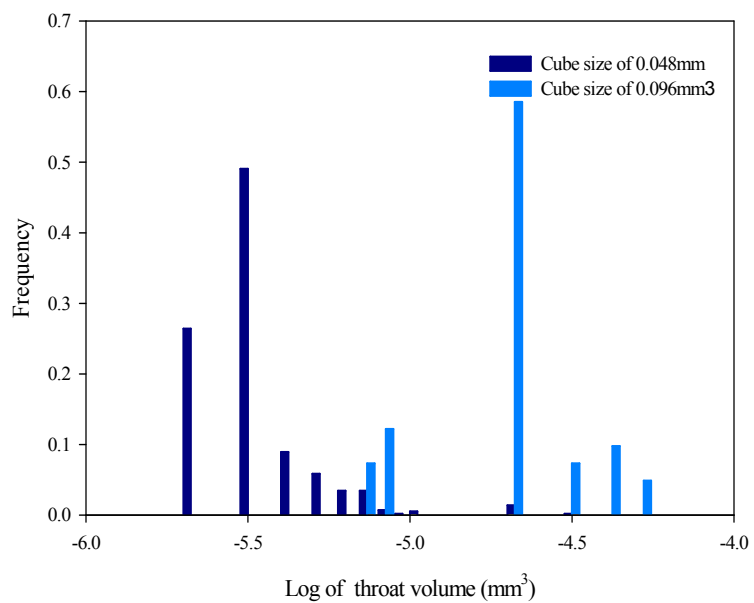
Figure B. 2 Frequency distributions of throat-body volume in logarithm scale; A. Bulk soil (image size of 10648 mm^3) and B. Aggregate (image size of 10.76 mm^3).

A

B
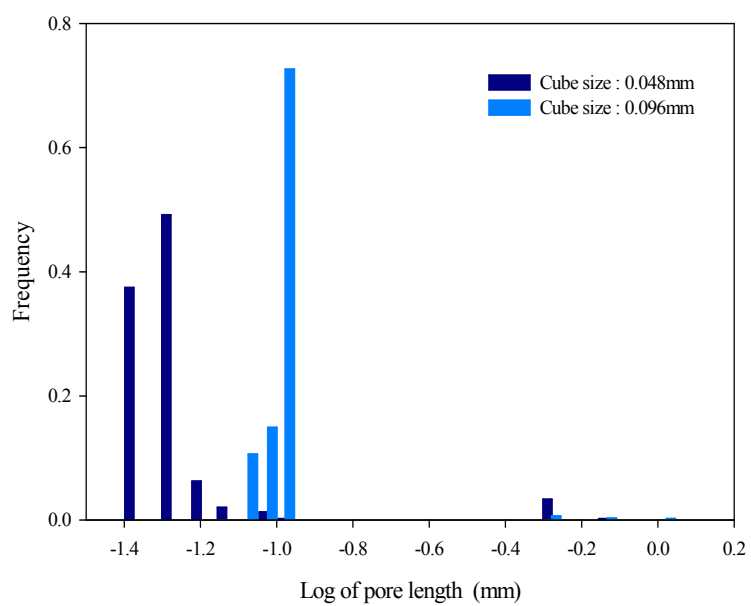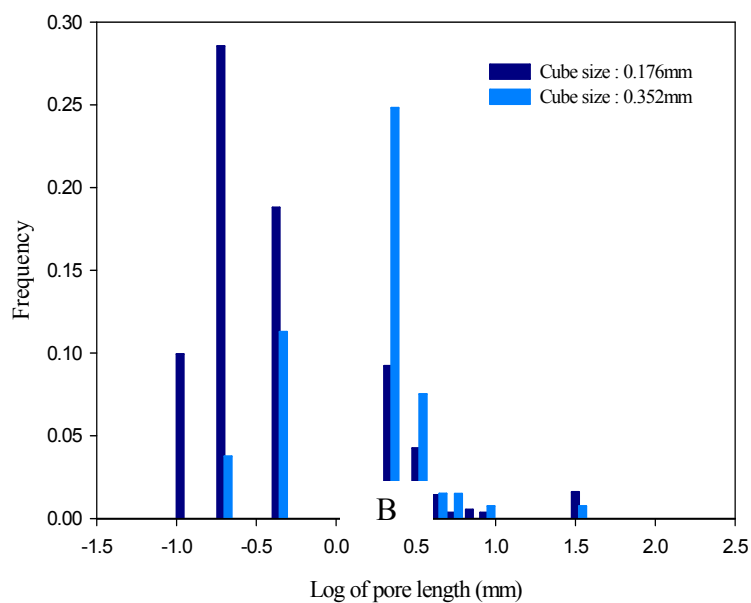
Figure B. 3 Frequency distributions of pore length in logarithm scale; A. Bulk soil (image size of 10648 mm^3) and B.   Aggregate (image size of 10.76 mm^3).

A

L   **B**   ıousity
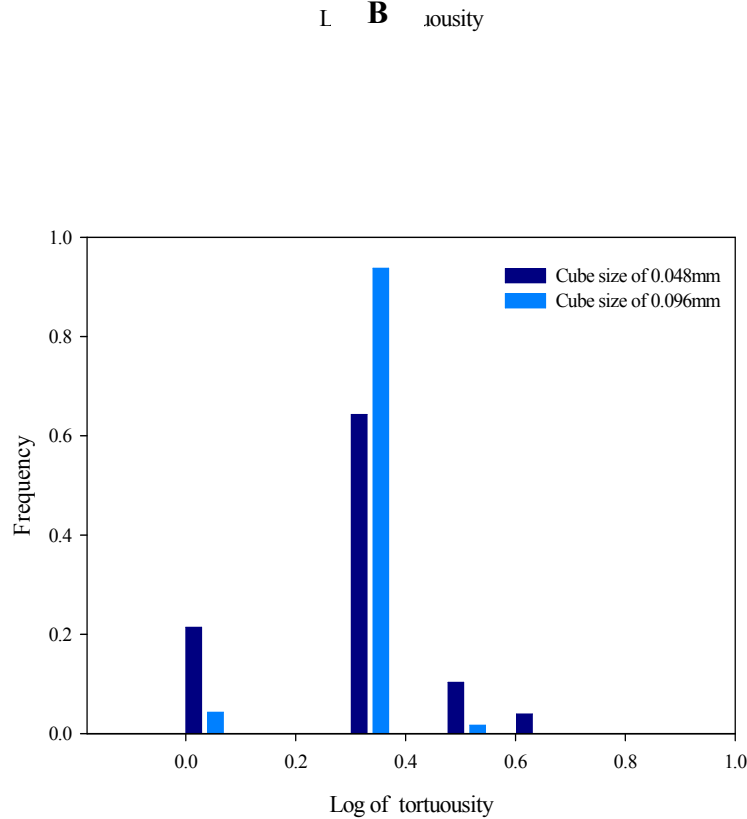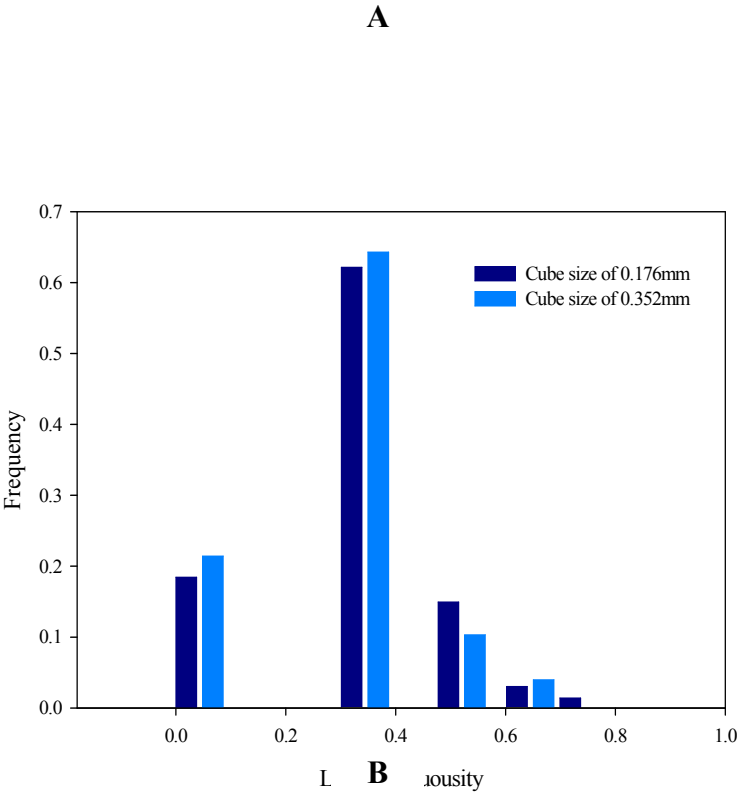
Figure B. 4 Frequency distributions of tortousity in logarithm scale; A. Bulk soil (image size of 10648 mm^3) and B. Aggregate (image size of 10.76 mm^3).

Appendix C

Fortran codes for local porosity and pore network model

1) Local porosity calculation

```fortran
dimension
ab(1000),ll(300,300),ll2(300,300),g(5000000),e(500,1000),lp(10000000),
x(10000000),y(10000000),zz(10000000)
dimension z1(1000,1000,200)
character*80 inpfil(5000),outfil1(5000), outfil2(5000),outfil3(5000)
real lp,ntp
integer x,y,zz,q2,bo,bo2,a,aa,b,bb,c,cc,q,sx,sy,sz,z1,zz1,ii,jj
OPEN(4,FILE='p1sc4_25.i')
   open(100,file='tt.out')
    open(101,file='tt2.out')
    read(4,*)nfile3
      do 1 nf3=1,nfile3


       READ(4,'(A)')  outfil1(nf3)
       write(*,*)outfil1(nf3)

      1 continue
      READ(4,*) nfile
      write(*,*)nfile
       DO 2 nf=1,nfile

    READ(4,'(A)') inpfil(nf)

     2  CONTINUE
     !Read data of each 2d image file!
       !cordinates of the starting point is a,b,and c!
     nn=0
       ww=1000
      qq=1000
      bo=25
      bo2=bo-1
      a=1
      b=1
      c=1
      q2=0
      aa=a+bo2
      bb=b+bo2
      cc=c+bo2

     zz1=0
    46 do 6 nf=c,nfile
 OPEN(5, FILE=inpfil(nf))
! write(*,*)inpfil(nf)

 zz1=zz1+1
 read(5,*)((z1(ii,jj,zz1),ii=1,ww),jj=1,qq)
```

```
  if(zz1.eq.bo) then
goto 16

  endif

 6 continue
16 ntp=0
   q2=q2+1
   q=0
! write(*,*)'zz1=',zz1
  do 20 sz=1,zz1
   do 21 sy=b,bb
   do 22 sx=a,aa
   ntp=ntp+1
   if(z1(sx,sy,sz).eq.255) then
 q=q+1

  endif
22 continue
21 continue
20 continue
  lp(q2)=q/ntp
 x(q2)=a+int(bo/2)
 y(q2)=b+int(bo/2)
 zz(q2)=c+int(bo/2)
 q=0
 a=a+bo
 aa=aa+bo
 if(aa.gt.ww) then
 goto 27
 else
 goto 16
 endif
27 a=1
   aa=a+bo2

 b=b+bo
 bb=bb+bo

 if(bb.gt.qq) then
 goto 29
 else
 goto 16
 endif
29 a=1
   aa=a+bo2
   b=1
   bb=b+bo2
 c=c+bo
 zz1=0
 cc=cc+bo

 !write(*,*)'cc=',cc
 if(cc.gt.nfile) then
 goto 30
```

```fortran
else
goto 46
endif
30  open(212,file=outfil1(1))
q2=q2-1
write(212,*)bo
do 40 qq2=1,q2

write(212,41) x(qq2),y(qq2),zz(qq2),lp(qq2)
41 format(i5,i5,i5,f10.6)
40 continue
close(212)
116 stop
end
```

2) Finding individual pores from local porosities

```fortran
dimension
x(10000000),y(10000000),z(10000000),lp(100000000),bx(1000,100000),by(1
000,100000),bz(1000,100000),fii(3000)
character*80 inpfil(5),outfil1(5), outfil2(5),outfil3(5)
integer q2,q,x,y,z,ii2,ii,bx,by,bz,fii
real lp
OPEN(4,FILE='p1sc4_25.i')
open(100,file='bx_p1sc4_25_25_0.1_0.2.out')
open(102,file='fii_p1sc4_25_25_0.1_0.2.out')
open(103,file='tt3.out')
read(4,*)nfile3

      do 1 nf3=1,nfile3


      READ(4,'(A)')  outfil1(nf3)

       write(*,*)outfil1(nf3)
     1 continue
    nf3=1
    open(5,FILE=outfil1(nf3))
    read (5,*)bo
    !write(*,*)q2
    q=1

    5 read(5,*,end=6)x(q),y(q),z(q),lp(q)
   ! write(103,*)x(q),y(q),z(q),lp(q)
    q=q+1
    goto 5
   6 i=q-1
   write(*,*)'q=',i
   a=1
   2 do i2=a,i
   if(lp(i2).gt.0.1) then
 !write(103,*)lp(i2),x(i2),y(i2),z(i2)
   goto 10
```

```fortran
      endif
      enddo
      goto 101
      !connected pore cube!
      !check if this cube was already assigned burnd cube!
   10 ci=i2

   do k2=1,k
   do ii2=1,100000

if(x(ci).eq.bx(k2,ii2).and.y(ci).eq.by(k2,ii2).and.z(ci).eq.bz(k2,ii2)
) then
 a=ci+200
 goto 2
 endif
 enddo
 enddo

 ii=1
 k=k+1
 ii3=1
 bx(k,ii3)=x(ci)
 by(k,ii3)=y(ci)
 bz(k,ii3)=z(ci)

write(103,*)'1',bx(k,ii3),by(k,ii3),bz(k,ii3)
15 x1=bx(k,ii3)-bo
 if(x1.lt.1) then
 x1=bx(k,ii3)
 endif
 x2=bx(k,ii3)+bo
 if(x2.gt.1000) then
 x2=bx(k,ii3)
 endif
 y1=by(k,ii3)-bo
 if(y1.lt.1) then
 y1=by(k,ii3)
 endif
 y2=by(k,ii3)+bo
 if(y2.gt.1000) then
 y2=by(k,ii3)
 endif
 z1=bz(k,ii3)-bo
 if(z1.lt.1) then
 z1=bz(k,ii3)
 endif
 z2=bz(k,ii3)+bo
 if(z2.gt.980) then
 z2=bz(k,ii3)
 endif
 !write(103,*)'x1=',x1,'x2=',x2,'y1=',y1,'y2=',y2,'z1=',z1,'z2=',z2
! write(103,*)bx(k,ii3),by(k,ii3),bz(k,ii3)
 do iz=z1,z2,bo
 do iy=y1,y2,bo
 do 12 ix=x1,x2,bo
```

```
 !write(103,*)'ix=',ix,'iy=',iy,'iz=',iz
 do 4 i2=1,i
 if(ix.eq.bx(k,ii3).and.iy.eq.by(k,ii3).and.iz.eq.bz(k,ii3))then
 goto 12
 endif
 if(x(i2).eq.ix.and.y(i2).eq.iy.and.z(i2).eq.iz.and.LP(i2).gt.0.2)
then
 goto 3
 else
 goto 4
 endif
 3 do k2=1,k
 do ii2=1,100000
 if(ix.eq.bx(k2,ii2).and.iy.eq.by(k2,ii2).and.iz.eq.bz(k2,ii2))then
 goto 12
 endif
 enddo
 enddo
 ii=ii+1
 if(ii.gt.100000) then
 ii=ii-1
 goto 201
 endif
 bx(k,ii)=ix
 by(k,ii)=iy
 bz(k,ii)=iz
 !write(103,*)'ii=',ii
 4 continue
 12 continue
 enddo
 enddo
 201 ii3=ii3+1
 !write(103,*)'ii3=',ii3,'ii=',ii
 if(ii3.lt.ii) then
 goto 15
 endif
 fii(k)=ii
 write(103,*)'k=',k,fii(k)
 if(ii.le.0) then
 do iii=1,fii(k)
  bx(k,iii)=0
 by(k,iii)=0
 bz(k,iii)=0
 enddo
 k=k-1
 endif
 a=ci+50
 if(a.lt.i.and. k.lt.1000) then
 goto 2
 endif
101  write(102,*)k
 do k2=1,k
 write(102,*)fii(k2)
 enddo
 do k2=1,k
```

```
 do ii2=1,fii(k2)
 !write(103,*)'k2=',k2,'ii2=',ii2,bx(k2,ii2),by(k2,ii2),bz(k2,ii2)
 write(100,200)bx(k2,ii2),by(k2,ii2),bz(k2,ii2)
 200 format(i5,i5,i5)
 enddo
 enddo
   stop
    end
```

3) Burning

```
dimension
x(10000000),y(10000000),z(10000000),lp(10000000),bx(1000,100000),by(10
00,100000),bz(1000,100000),fii(5000)
dimension bn(1000,100000),fjj(3000)
character*80 outfil1(5),outfil12(5)
integer q2,q,x,y,z,bn,bx,by,bz,fii,nj,i,ii,i2,ii2,ii3,k
real lp
!OPEN(1,FILE='prbinary4.i')
!read(1,*)nfile3


    open(103,FILE='test3.out')
    open(2,FILE='p3_500_8.out')
     read (2,*)bo
     q=1

   5 read(2,*,end=6)x(q),y(q),z(q),lp(q)
    ! write(100,*)x(q),y(q),z(q),lp(q)
    q=q+1
    goto 5
   6 i=q-1
    open(3,FILE='fii_p3_500_8_0.001_0.01.out')

    read(3,*)k
  fk=k

    write(*,*)'fk=',k
    do k2=1,k
read(3,*)fii(k2)
!write(103,*)k2,'fii=',fii(k2)
 enddo
 7 open(4,FILE='bx_p3_500_8_0.01_0.01.out')
 do k2=1,k
 do ii2=1,fii(k2)
 read(4,200)bx(k2,ii2),by(k2,ii2),bz(k2,ii2)
 200 format(i5,i5,i5)
! write(103,*)bx(k2,ii2),by(k2,ii2),bz(k2,ii2)
 enddo
 enddo
 do k2=1,k
 do ii2=1,fii(k2)
 bn(k2,ii2)=0
```

```fortran
      enddo
      enddo
      k2=1
       if(fii(k2).le.0) then

      goto 116
      endif
      13 ii2=1
      no=0
      12 x1=bx(k2,ii2)-bo
      if (x1.lt.1) then
      bn(k2,ii2)=1
      no=no+1
!write(103,*)'ii2=',ii2,no
      goto 11
      endif
      x2= bx(k2,ii2)+bo
      if (x2.gt.300) then
      bn(k2,ii2)=1
      no=no+1
!write(103,*)'ii2=',ii2,no
      goto 11
      endif
      y1=by(k2,ii2)-bo
      if (y1.lt.1) then
      bn(k2,ii2)=1
      no=no+1
       !write(103,*)'ii2=',ii2,no
      goto 11
      endif
      y2= by(k2,ii2)+bo
      if (y2.gt.300) then
      bn(k2,ii2)=1
      no=no+1
       !write(103,*)'ii2=',ii2,no
      goto 11
      endif
      z1=bz(k2,ii2)-bo
      if (z1.lt.1) then
      bn(k2,ii2)=1
      no=no+1
       !write(103,*)'ii2=',ii2,no
      goto 11
      endif
      z2= bz(k2,ii2)+bo
      if (z2.gt.300) then
      bn(k2,ii2)=1
      no=no+1
       !write(103,*)'ii2=',ii2,no
      goto 11
      endif
      nnj=0
!write(103,*)'k2=',k2,'ii2=',ii2
      do iz=z1,z2,bo
      do iy=y1,y2,bo
```

```
 do 111 ix=x1,x2,bo
 do 1113 iii2=1,fii(k2)

 if(bx(k2,iii2).eq.ix.and.by(k2,iii2).eq.iy.and.bz(k2,iii2).eq.iz)
then
 nnj=nnj+1
 goto 1112
 else
 goto 1113
 endif
1112 if(nnj.ge.6) then
goto 1114
else
goto 111
endif
 1113 continue
 goto 112
 111 continue
 enddo
 enddo
 1114  nnj=0
 goto 11
 112 bn(k2,ii2)=1
 no=no+1
 !write(103,*)'iii2=',iii2,'ix=',ix,'bx=',bx(k2,iii2),iy,by(k2,iii2),i
z,bz(k2,iii2)
!write(103,*)'k2=',k2,'ii2=',ii2,'no=',no
 !write(103,*)'bx=',bx(k2,ii2),'by=',by(k2,ii2),'bz=',bz(k2,ii2),'bn='
,bn(k2,ii2)
 11 ii2=ii2+1
 if(ii2.le.fii(k2)) then
 goto 12
 endif
 k2=k2+1
 write(103,*)'k=',k2
 if(k2.le.k) then
 goto 13
 endif
 !Finish boundary burning (bn=1)!
 k2=1
 ! write(103,*)'k2=',k2

 16 j=1

 15 ii2=1
 22 if(ii2.gt.fii(k2)) then
goto 222
 endif
 !write(103,*)'ii2=',ii2,bn(k2,ii2)
 if(bn(k2,ii2).ne.0.00) then
 ii2=ii2+1
 goto 22
 endif
 !write(103,*)'ii2=',ii2,bn(k2,ii2)
 nj=0
```

```fortran
 x1=bx(k2,ii2)-bo
 if (x1.lt.1) then
 x1=bx(k2,ii2)
 endif
 x2=bx(k2,ii2)+bo
 if (x2.gt.300) then
 x2=bx(k2,ii2)
 endif
 y1=by(k2,ii2)-bo
 if (y1.lt.1) then
 y1=by(k2,ii2)
 endif
 y2=by(k2,ii2)+bo
 if (y2.gt.300) then
 y2=by(k2,ii2)
 endif
 z1=bz(k2,ii2)-bo
 if (z1.lt.1) then
 z1=bz(k2,ii2)
 endif
 z2=bz(k2,ii2)+bo
 if (z2.gt.300) then
 z2=bz(k2,ii2)
 endif

!write(103,*)'bx=',bx(k2,ii2),'by=',by(k2,ii2),'bz=',bz(k2,ii2)
 do iz=z1,z2,bo
 do iy=y1,y2,bo
 do 23 ix=x1,x2,bo
 do ii3=1,fii(k2)
!write(103,*)'ix=',ix,'iy=',iy,'iz=',iz,bn(k2,ii3)

if(ix.eq.bx(k2,ii3).and.iy.eq.by(k2,ii3).and.iz.eq.bz(k2,ii3).and.bn(k
2,ii3).eq.j) then
 bn(k2,ii2)=j+1
 j2=j+1
!write(103,*)'j=',j,'k2=',k2,'ii2=',ii2,bn(k2,ii2)
 nj=nj+1
 goto 222
 endif
 enddo
 23 continue
 enddo
 enddo
222 ii2=ii2+1
 if(ii2.le.fii(k2)) then          !fii(k2)!
 goto 22
 endif
!write(1001,*)'ii2=',ii2
!open(1001,file='tt4.out')
 do ii2=1,fii(k2)          !fii(k2)
!write(1001,*)'k2',k2,'ii2=',ii2,'bn=',bn(k2,ii2)
 if (bn(k2,ii2).eq.0) then

 goto 20
```

```
 endif
 enddo
goto 14
 20 j=j+1
 !write(103,*)'j=',j
 goto 15
 14  fjj(k2)=j+1
 write(103,*)'k=',k2,'j=',j,'j2=',j2
 116 k2=k2+1
  write(103,*)'k=',k2,'j=',j,'j2=',j2
 if(k2.le.k) then
 goto 16
 endif

 open(100,FILE='burn_p3_500_8_0.001_0.01.out')
 do k2=1,k
 do ii2=1,fii(k2)
 write(100,201)bx(k2,ii2),by(k2,ii2),bz(k2,ii2),bn(k2,ii2)
 201 format(i5,i5,i5,i5)
 enddo
 enddo
 close(100)
 open(101,FILE='maxburn_p3_500_8_0.001_0.01.out')
 write(101,*)bo
 do k2=1,k
 write(101,*)fjj(k2)
 enddo
 close(101)


 stop
       end
```

4) Constructing Medial-Axis

```
dimension
bx(1000,70000),by(1000,70000),bz(1000,70000),fii(5000),nc(5000),di(500
0),fw(5000)
dimension mx(1000,40000),my(1000,40000),mz(1000,40000),mb(1000,40000)
dimension bn(1000,70000),fjj(5000)
character*80 outfil1(5),outfil2(5)
integer q2,q,x,y,z,bn,bx,by,bz,fii,nj,i,ii,i2,ii2,ii3
real lp

    open(5000,file='te.out')
    open(1004,FILE='fii_p3_500_8_0.001_0.01.out')
   read(1004,*)k
  fk=k
write(*,*)'fk=',fk
   do k2=1,fk
read(1004,*)fii(k2)
 enddo
 open(1005,FILE='maxburn_p3_500_8_0.001_0.01.out')
```

```
  read(1005,*)bo
       do k2=1,fk
read(1005,*)fjj(k2)
!write(5000,*)'k2=',k2,fjj(k2)
 enddo
      open(1001,FILE='burn_p3_500_8_0.001_0.01.out')
 do k2=1,fk
 do ii2=1,fii(k2)
read(1001,201)bx(k2,ii2),by(k2,ii2),bz(k2,ii2),bn(k2,ii2)
 201 format(i5,i5,i5,i5)
!write(5000,*)bx(k2,ii2),by(k2,ii2),bz(k2,ii2),bn(k2,ii2)
 enddo
 enddo
 !Maximum burn are all MA!
 k2=1
 10 w=1
 write(5000,*)'k2=',k2,fjj(k2)
 do ii=1,fii(k2)
 if(bn(k2,ii).eq.0) then
 goto 117
 endif
 if(bn(k2,ii).eq.fjj(k2)) then
 write(5000,*)k2,ii,'bn=',bn(k2,ii),fjj(k2)
 mx(k2,w)=bx(k2,ii)
 my(k2,w)=by(k2,ii)
 mz(k2,w)=bz(k2,ii)
 mb(k2,w)=bn(k2,ii)
write(5000,*)'1','k2=',k2,'w=',w,'mx=',mx(k2,w),'my=',my(k2,w),'mz=',m
z(k2,w),'bn=',bn(k2,ii)
 w2=w
 w=w+1

 endif
 enddo
 !Start from one of the max. burn!
 w3=1
 9 jj=1
 x1=mx(k2,w3)-bo
 if (x1.lt.1) then
 x1=mx(k2,w3)
 endif
 x2=mx(k2,w3)+bo
 if (x2.gt.300) then
 x2=mx(k2,w3)
 endif
 y1=my(k2,w3)-bo
 if (y1.lt.1) then
 y1=my(k2,w3)
 endif
 y2=my(k2,w3)+bo
 if (y2.gt.300) then
 y2=my(k2,w3)
 endif
 z1=mz(k2,w3)-bo
 if (z1.lt.1) then
```

```
z1=mz(k2,w3)
endif
z2=mz(k2,w3)+bo
if (z2.gt.300) then
z2=mz(k2,w3)
endif
do iz=z1,z2,bo
do iy=y1,y2,bo
do 1 ix=x1,x2,bo
do ii=1,fii(k2)
if(ix.eq.mx(k2,w3).and.iy.eq.my(k2,w3).and.iz.eq.mz(k2,w3)) then
goto 1
endif
do k3=1,fk
do w4=1,w2
if(ix.eq.mx(k3,w4).and.iy.eq.my(k3,w4).and.iz.eq.mz(k3,w4))then
goto 1
endif
enddo
enddo
if(bx(k2,ii).eq.ix.and.by(k2,ii).eq.iy.and.bz(k2,ii).eq.iz) then
nc(jj)=ii
jj=jj+1
endif
enddo
1 continue
enddo
enddo
!Surrounded by smaller burn=MA!

if(jj.eq.0) then
goto 3
endif
jj2=1
8  ii2=jj2        !nc(jj2)

x3=bx(k2,ii2)-bo
if (x3.lt.1) then
x3=bx(k2,ii2)
endif
x4=bx(k2,ii2)+bo
if (x2.gt.300) then
x4=bx(k2,ii2)
endif
y3=by(k2,ii2)-bo
if (y1.lt.1) then
y3=by(k2,ii2)
endif
y4=by(k2,ii2)+bo
if (y2.gt.300) then
y4=by(k2,ii2)
endif
z3=bz(k2,ii2)-bo
if (z1.lt.1) then
z3=bz(k2,ii2)
```

```fortran
      endif
      z4=bz(k2,ii2)+bo
      if (z2.gt.300) then
      z4=bz(k2,ii2)
      endif

      do iz=z3,z4,bo
      do iy=y3,y4,bo
      do 2 ix=x3,x4,bo
      do ii3=1,fii(k2)

      if(ix.eq.bx(k2,ii3).and.iy.eq.by(k2,ii3).and.iz.eq.bz(k2,ii3).and.bn(k
     2,ii3).gt.bn(k2,ii2)) then
      goto 7
      endif
      enddo
    2 continue
      enddo
      enddo
      goto 4
      !if there are same burn cubes in right angles=MA!
    3 goto 4
      d=1
      do iz=z3,z4,bo
      do iy=y3,y4,bo
      do 5 ix=x3,x4,bo
      do ii4=1,fii(k2)
      if(ix.eq.bx(k2,ii2).and.iy.eq.by(k2,ii2).and.iz.eq.bz(k2,ii2)) then
      goto 5
      endif

      if(bx(k2,ii4).eq.ix.and.by(k2,ii4).eq.iy.and.bz(k2,ii4).eq.iz.and.bn(k
     2,ii4).eq.bn(k2,ii2)) then
      di(d)=ii4
      d=d+1
      endif
      enddo
    5 continue
      enddo
      enddo
      d2=1
      d=d-1
    6 ii5=di(d2)
      do d3=1,d
      ii6=di(d3)
      dxx=(bx(k2,ii5)-bx(k2,ii6))**2
      dyy=(by(k2,ii5)-by(k2,ii6))**2
      dzz=(bz(k2,ii5)-bz(k2,ii6))**2
      fdi=dxx+dyy+dzz
      bo3=2*(bo*bo)
      if(fdi.eq.bo3) then
      goto 4
      endif
      enddo
      d2=d2+1
```

```fortran
      if(d2.le.d) then
      goto 6
      endif
      goto 7
    4 do k3=1,fk
      do w4=1,20000

      if(mx(k3,w4).eq.bx(k2,ii2).and.my(k3,w4).eq.by(k2,ii2).and.mz(k3,w4).e
     q.bz(k2,ii2)) then
      goto 7
      endif
      enddo
      enddo
      mx(k2,w)=bx(k2,ii2)
      my(k2,w)=by(k2,ii2)
      mz(k2,w)=bz(k2,ii2)
      mb(k2,w)=bn(k2,ii2)
      write(5000,*)'2','k2=',k2,'w=',w,'mx=',mx(k2,w),'my=',my(k2,w),'mz=',m
     z(k2,w),'bn=',bn(k2,ii2)
      w=w+1
      w2=w
      write(5000,*)'w=',w
      if (w.gt.100000) then
      goto 117
      endif
    7 jj2=jj2+2
      write(5000,*)'jj2=',jj2,'fii=',fii(k2)
      if(jj2.lt.fii(k2)) then        !jj
      goto 8
      endif
      !117 !w3=w3+1
      !if(w3.lt.w) then
      !goto 9
    ! endif
  117 fw(k2)=w-1
      k2=k2+1
      write(5000,*)'k2=',k2
      if(k2.le.fk) then
      goto 10
      endif
      open(1010,file='w_p3_500_8_0.001_0.01.out')
      do k3=1,fk
      write(1010,*)fw(k3)
      enddo
      close(1010)
      open(1003,FILE='ma_p3_500_8_0.001_0.01.out')
      do k3=1,fk
      do w=1,fw(k3)
      write(1003,300)mx(k3,w),my(k3,w),mz(k3,w),mb(k3,w)
  300 format(i5,i5,i5,i5)
      enddo
      enddo
      close(1003)
      stop
            end
```

5) Calculation of pore length

```fortran
dimension
bx(1000,70000),by(1000,70000),bz(1000,70000),fii(5000),nc(5000),di(100
0),fw(5000)
dimension
mx(1000,40000),my(1000,40000),mz(1000,40000),mb(1000,40000),TL(2000)
dimension
bn(1000,70000),fjj(1000),lx(5000),ly(5000),lz(5000),sl(5000),tor(5000)
character*80 outfil1(5000)
integer q2,q,x,y,z,bn,bx,by,bz,fii,nj,i,ii,i2,ii2,ii3
real lp,tl,tor,sl
open(2000,file='length_p3_8.out')
open(2001,file='length_p3_500_8.out')


      open(1004,FILE='fii_p3_500_8_0.001_0.01.out')
    read(1004,*)fk
 write(*,*)'fk=',fk
    do k2=1,fk
read(1004,*)fii(k2)
 enddo
 open(1005,FILE='maxburn_p3_500_8_0.001_0.01.out')
 read(1005,*)bo
      do k2=1,fk
read(1005,*)fjj(k2)
 enddo
      open(1001,FILE='burn_p3_500_8_0.001_0.01.out')
 do k2=1,fk
 do ii2=1,fii(k2)
read(1001,201)bx(k2,ii2),by(k2,ii2),bz(k2,ii2),bn(k2,ii2)
 201 format(i5,i5,i5,i5)
 enddo
 enddo
 open(1006,FILE='w_p3_500_8_0.001_0.01.out')
  do k3=1,fk
  read(1006,*)fw(k3)
  enddo
  close(1006)
 open(1003,FILE='ma_p3_500_8_0.001_0.01.out')
 do k3=1,fk
 do w=1,fw(k3)
 read(1003,300)mx(k3,w),my(k3,w),mz(k3,w),mb(k3,w)
 300 format(i5,i5,i5,i5)
 enddo
 enddo
 close(1003)
 !calculate the length first!
 k=1

 10 TL(k)=0
 write(2000,*)'k=',k
```

```fortran
      if(fw(k).le.1) then
      f=1
      lx(f)=mx(k,1)
      ly(f)=my(k,1)
      lz(f)=mz(k,1)
      write(2000,*)'f=',f,lx(f),ly(f),lz(f)
      tl(k)=bo
      tor(k)=1
      k=k+1

      goto 210
      endif
      maxz=1
      do w=1,fw(k)
      if(mz(k,w).gt.maxz) then
      maxz=mz(k,w)
      endif
      enddo
      maxy=1
      do w=1,fw(k)
      if(mz(k,w).eq.maxz.and.my(k,w).gt.maxy) then
      maxy=my(k,w)
      endif
      enddo
      maxx=1
      do w=1,fw(k)
      if(mz(k,w).eq.maxz.and.my(k,w).eq.maxy.and.mx(k,w).gt.maxx) then
      maxx=mx(k,w)
      mj=w
      endif
      enddo
      endx=mx(k,mj)
      endy=my(k,mj)
      endz=mz(k,mj)
      write(2000,*)'endx=', endx,'endy=', endy,'endz=', endz
      f=1
      f2=1
      minz=endz
      do w=1,fw(k)
      if(mz(k,w).le.minz) then
minz=mz(k,w)
 !write(2000,*)'minz=',minz
      endif
      enddo

       110 minx=300
      do w=1,fw(k)
      !write(2000,*)minz,'mz=',mz(k,w),'my(k,w)=',my(k,w)
      if(mz(k,w).eq.minz.and.mx(k,w).le.minx) then
      minx=mx(k,w)
      ! write(2000,*)minz,'miny=',miny
      endif
      enddo
miny=300
      do w=1,fw(k)
```

```fortran
! write(2000,*)minz,'mz=',mz(k,w),
miny,'my(k,w)=',my(k,w),'mx=',mx(k,w)
 if(mz(k,w).eq.minz.and.mx(k,w).eq.minx.and.my(k,w).le.miny) then
 miny=my(k,w)
 minj=w
!write(2000,*)'miny=',miny,'minx=',minx,'minj=',minj
 goto 111
 endif
 enddo
 111 lx(f)=mx(k,minj)
 ly(f)=my(k,minj)
 lz(f)=mz(k,minj)
 f2=f
 write(2000,*)'f=',f,lx(f),ly(f),lz(f)
 if(f.eq.1) then
 goto 5
 endif

  !write(2000,*)'f=',f,'lx(f)=',lx(f),'ly(f)=',ly(f),'lz(f)=',lz(f)
 f2=f-1
 sublx=(lx(f2)-lx(f))**2
 subly=(ly(f2)-ly(f))**2
 sublz=(lz(f2)-lz(f))**2
 subl=sqrt(sublx+subly+sublz)
 tl(k)=tl(k)+subl
  !write(2000,*)'k=',k,'tl=',tl(k)

 if(lz(f).eq.endz) then
 goto 3
 else
 f2=f
 goto 5
 endif

 5 x1=lx(f2)-(bo)
 if(x1.lt.1) then
 x1=lx(f2)
 endif
 x2=lx(f2)+(bo)
 if(x2.gt.300) then
 x2=lx(f2)
 endif
 y1=ly(f2)-(bo)
 if(y1.lt.1) then
 y1=ly(f2)
 endif
 y2=ly(f2)+(bo)
 if(y2.gt.300) then
 y2=lx(f2)
 endif
 z1=lz(f2)+bo
 if(z1.gt.300) then
 z1=lz(f2)
 endif
 z2=lz(f2)+bo
```

```fortran
      if(z2.gt.300) then
      z2=lz(f2)
      endif

      n2=0
      do 1 ix=x2,x1,-bo
      do iy=y2,y1,-bo
      do iz=z2,z1,-bo

      do w=1,fw(k)
      do f3=1,f
      if(ix.eq.lx(f3).and.iy.eq.ly(f3).and.iz.eq.lz(f3)) then
      goto 1
      endif
      enddo

      if(ix.eq.mx(k,w).and.iy.eq.my(k,w).and.iz.eq.mz(k,w)) then
      !write(2000,*)'ix=',ix,'iy=',iy,'iz=',iz,'mx=',mx(k,w),'my=',my(k,w),
     'mz=',mz(k,w)
      w2=w
      n2=n2+5

      goto 2
      endif
        enddo
      enddo
      enddo
       1 continue
       !write(2000,*)'n2=',n2,minz,'bo=',bo
       if(n2.eq.0) then
       f=f+1
       lz(f)=lz(f2)+bo

       lx(f)=lx(f2)
       ly(f)=ly(f2)
      if(lx(f).gt.250.or.ly(f).gt.250) then
      goto 3
      endif
       write(2000,*)'f=',f,lx(f2),ly(f2),lz(f)
       endif

       !write(2000,*)'min=',minz

       goto 200
      2 f=f+1
      lx(f)=mx(k,w2)
      ly(f)=my(k,w2)
      lz(f)=mz(k,w2)
      if(lx(f).le.1.or.ly(f).le.1.or.lz(f).le.1) then
      goto 3
      endif

       write(2000,*)'f=',f,lx(f),ly(f),lz(f)
      200 f2=f-1
      sublx=(lx(f2)-lx(f))**2
```

```
  subly=(ly(f2)-ly(f))**2
  sublz=(lz(f2)-lz(f))**2
  subl=sqrt(sublx+subly+sublz)
  tl(k)=tl(k)+subl
   !write(2000,*)'k=',k,'tl=',tl(k)
  if(lz(f).ge.endz) then
  goto 3
  else
  f2=f
  goto 5
  endif
  !Calculate tortuousity!
  3 lx(f)=endx
  ly(f)=endy
  lz(f)=endz
  !write(2000,*)'f=',f,lx(f),ly(f),lz(f)
  slx=(lx(1)-lx(f))**2
  sly=(ly(1)-ly(f))**2
  slz=(lz(1)-lz(f))**2
  sl(k)=sqrt(slx+sly+slz)
  tor(k)=tl(k)/sl(k)
   k=k+1

210 write(2000,*)'k=',k
if(k.le.fk) then
 goto 10
 endif
 do k2=1,fk
 write(2001,301)tl(k2),tor(k2)
 301 format(f10.2,f10.5)
 enddo
 stop
 end
```

6) Calculation of pore volume

```
dimension lp(10000000),x(10000000),y(10000000),z(10000000)
dimension
fii(1000),fw(1000),mbb(630),thb(10000),cc(1000),bx(600,70000),by(600,7
0000),bz(600,70000)
dimension
mx(600,40000),my(600,40000),mz(600,40000),mb(600,40000),cx(100000),cy(
100000),cz(100000)
dimension bn(1000,70000),fjj(1000),nn(50000),
vsv(5000),bbk(5000),tv(5000)
dimension
tvol(5000),thvol(630,5000),scx(1000,10000),scy(1000,10000),scz(1000,10
000)
integer q2,q,x,y,z,bn,bx,by,bz,fii,nj,i,ii,i2,ii2,ii3,ff,nn
real lp
open(2555,file='tt7.out')
open(2556,file='tt8.out')
open(2557,file='tt9.out')
```

```fortran
open(2001,file='volume_p3_500_8_0.001_0.01.out')
open(2002,file='thvolume_p3_500_8_0.001_0.01.out')
open(2222,FILE='p3_500_8.out')
open(3555,FILE='maxburn_p3_250_8.out')
      read (2222,*)bo
      q=1

 2225 read(2222,*,end=2226)x(q),y(q),z(q),lp(q)
    ! write(100,*)x(q),y(q),z(q),lp(q)
    q=q+1
    goto 2225
  2226 i=q-1
    write(*,*)i
    open(1004,FILE='fii_p3_500_8_0.001_0.01.out')
   read(1004,*)k
  fk=k

   do k2=1,fk
read(1004,*)fii(k2)
 enddo
 open(1005,FILE='maxburn_p3_500_8_0.001_0.01.out')
 read(1005,*)bo
 write(*,*)'bo=',bo
      do k2=1,fk
read(1005,*)fjj(k2)
 enddo
  open(1006,FILE='w_p3_500_8_0.001_0.01.out')
  do k3=1,fk
  read(1006,*)fw(k3)
 !write(*,*)fw(k3)
  enddo

 open(1003,FILE='ma_p3_500_8_0.001_0.01.out')
 do k3=1,fk
 do w=1,fw(k3)
 read(1003,300)mx(k3,w),my(k3,w),mz(k3,w),mb(k3,w)
  300 format(i5,i5,i5,i5)
 enddo
 enddo
 close(1003)
open(1001,FILE='burn_p3_500_8_0.001_0.01.out')
 do k2=1,fk
 do ii2=1,fii(k2)
 read(1001,201)bx(k2,ii2),by(k2,ii2),bz(k2,ii2),bn(k2,ii2)
 201 format(i5,i5,i5,i5)
 enddo
 enddo
 k=1
 write(2555,*)'k=',k,fii(k)
! do ii2=1,fii(k)
!write(2555,*)bx(k,ii2),by(k,ii2),bn(k,ii2)
!enddo
!write(2556,*)'k=',k,fii(k)
 !do ii2=1,fw(k)
!write(2556,*)mx(k,ii2),my(k,ii2),mb(k,ii2)
```

```
!enddo
!k=k+1
!if(k.le.fk) then
!goto 1
!endif
1 if(fw(k).le.10) then
 ncc=1
 vsv(ncc)=fw(k)*bo
 tv(k)= vsv(ncc)
 goto 1115
 endif
ff=0
  w=1
 2 cn=0
  x1=mx(k,w)-bo
 if (x1.lt.1) then
 x1=mx(k,w)
 endif
 x2=mx(k,w)+bo
 if (x2.gt.300) then
 x2=mx(k,w)
 endif
 y1=my(k,w)-bo
 if (y1.lt.1) then
 y1=my(k,w)
 endif
 y2=my(k,w)+bo
 if (y2.gt.300) then
 y2=my(k,w)
 endif
 z1=mz(k,w)-bo
 if (z1.lt.1) then
 z1=mz(k,w)
 endif
 z2=mz(k,w)+bo
 if (z2.gt.300) then
 z2=mz(k,w)
 endif
 !write(2556,*)'x1=',x1,'y1=',y1,'z1=',z1
 do iz=z1,z2,bo
 do iy=y1,y2,bo
 do 3 ix=x1,x2,bo
 do w2=1,fw(k)
 if(ix.eq.mx(k,w).and.iy.eq.my(k,w).and.iz.eq.mz(k,w)) then
 goto 3
 endif
 if(ix.eq.mx(k,w2).and.iy.eq.my(k,w2).and.iz.eq.mz(k,w2)) then
cn=cn+1
!write(2555,*)'k=',k,'cn=',cn
 endif
 enddo
 3 continue
 enddo
 enddo
 if(cn.ge.3) then
```

```
 ff=ff+1
 nn(ff)=w
 !write(2555,*)'k=',k,'ff=',ff, nn(ff)
 endif
 w=w+1
 if(w.lt.fw(k)) then
 goto 2
 endif
 write(2557,*)'k=',k,'ff=',ff
 if(ff.eq.0) then
 tvol(k)=fii(k)
 tvv=0
 nt=0
 !write(2001,*)'k=',k,'tvol(k)=',tvol(k)
 goto 113
 endif
 !
!
 !write(2557,*)mx(k,w),my(k,w)
 !enddo

!Find nodes with the maximum burn #!
maxj=0
do ff2=1,ff
w= nn(ff2)
if(mb(k,w).gt.maxj) then
maxj=mb(k,w)
endif
enddo
write(2555,*)'k=',k,maxj
nbb=0
do ff2=1,ff
w=nn(ff2)
if(mb(k,w).eq.maxj) then
 nbb=nbb+1
 mbb(nbb)=w
write(3555,*)'nbb=',nbb,mbb(nbb),mx(k,w),my(k,w),mz(k,w)
 endif
 enddo
 !place body square first!
 is=bo*(fjj(k))
 6 nbb2=1
 ncc=1          !# of sqaure!


 5 w4=mbb(nbb2)
 write(2555,*)'w4=',w4
  bk=1
 cx(ncc)=mx(k,w4)
 cy(ncc)=my(k,w4)
 cz(ncc)=mz(k,w4)
  write(2555,*)'is=',is
400 x3=cx(ncc)-bo
 !write(2555,*)'x3=',x3
 if(x3.lt.1) then
```

```
goto 4
endif
x4=cx(ncc)+is
!write(2555,*)'x4=',x4
if(x4.gt.300) then
goto 4
endif
y3=cy(ncc)-is
 !write(2555,*)'y3=',y3
if(y3.lt.1) then
goto 4
endif
y4=cy(ncc)+is
!write(2555,*)'y4=',y4
if(y4.gt.300) then
goto 4
endif
 z3=cz(ncc)-is
 !write(2555,*)'y3=',y3
if(z3.lt.1) then
goto 4
endif
z4=cz(ncc)+is
!write(2555,*)'y4=',y4
if(z4.gt.300) then
goto 4
endif
do iz=z3,z4,bo
do iy=y3,y4,bo
do ix=x3,x4,bo
do i2=1,i
if(ix.eq.x(i2).and.iy.eq.y(i2).and.iz.eq.z(i2).and.lp(i2).le.0.0)
then
 goto 4
 endif
 enddo
 enddo
 enddo
 enddo
 do iz=z3,z4,bo
 do iy=y3,y4,bo
 do ix=x3,x4,bo
 do ncc2=1,ncc
 do bk2=1,10000
 !write(2555,*)'ncc2=',ncc2

if(ix.eq.scx(ncc2,bk2).and.iy.eq.scy(ncc2,bk2).and.iz.eq.scz(ncc2,bk2)
) then
 goto 4
 endif
 enddo
 enddo
 enddo
 enddo
 enddo
```

```fortran
 do iz=z3,z4,bo
 do iy=y3,y4,bo
 do ix=x3,x4,bo
 scx(ncc,bk)=ix
 scy(ncc,bk)=iy
 scz(ncc,bk)=iz
!write(2555,*)'ncc=',ncc,'bk=',bk,scx(ncc,bk),scy(ncc,bk),scz(ncc,bk)
 bk=bk+1
 if(bk.gt.10000) then
 goto 401
 endif
 enddo
 enddo
 enddo
 xx=abs(x3-x4)+1
 yy=abs(y3-y4)+1
 zz=abs(z3-z4)+1
 vsv(ncc)=xx*yy*zz
 bbk(ncc)=bk
 write(2555,*)'ncc=',ncc,'xx=',xx,'yy=',yy,'zz=',zz,vsv(ncc)

ncc=ncc+1

goto 401
 !write(2555,*)'ncc=',ncc
 !if(ncc.ge.1000)then
 !goto 500
 !endif
 4 is=is-bo
 if(is.gt.bo) then
 goto 400
 endif
 401 nbb2=nbb2+1
 if(nbb2.le.nbb) then
 goto 5
 endif

 !Add b-b volume!
 500 do ncc2=1,ncc
 tvol(k)=tvol(k)+(vsv(ncc2))
 enddo
  write(2002,*)'k=',k
 write(2002,*)tvol(k)
 !Statr calculation with throats!
 nkk=0
 minb=1
 if(maxj.le.minb) then
 goto 113
 endif
 bk=1
 7 do ff2=1,ff
 w3=nn(ff2)
 if(mb(k,w3).eq.minb) then
 nkk=nkk+1
 thb(nkk)=w3
```

```fortran
      write(2556,*)'nkk=',nkk,thb(nkk)
      endif
      enddo
      if(nkk.eq.0) then
      minb=minb+1
      goto 7
      endif
      !min node=1...nkk!
      nt=0
      nkk2=1
  12  w5=thb(nkk2)
      l1=bo
      do ncc2=1,ncc
      do bk2=1,10000

      if(mx(k,w5).eq.scx(ncc2,bk2).and.my(k,w5).eq.scy(ncc2,bk2).and.mz(k,w5
     ).eq.scz(ncc2,bk2)) then
      nkk2=nkk2+1
      if(nkk2.gt.nkk) then
      goto 13
      else
      goto 12
      endif
      endif
      enddo
      enddo
      !x axis first!
      write(2556,*)'nkk2=',nkk2
      xx1=mx(k,w5)-l1
      write(2556,*)'1=','xx1=',xx1
  25  do i2=1,i

      if(xx1.eq.x(i2).and.my(k,w5).eq.y(i2).and.mz(k,w5).eq.z(i2).and.lp(i2)
     .ne.0) then
      goto 23
      endif
      enddo

      goto 24              !go to the opposite direction!
  23  do ncc2=1,ncc
      do bk2=1,10000

      if(xx1.eq.scx(ncc2,bk2).and.my(k,w5).eq.scy(ncc2,bk2).and.mz(k,w5).eq.
     scz(ncc2,bk2))then
      goto 24
      endif
      enddo
      enddo
      if(bk.gt.10000) then
      goto 164
      endif

      scx(ncc,bk)=xx1
      scy(ncc,bk)=my(k,w5)
      scz(ncc,bk)=mz(k,w5)
```

```fortran
 write(2556,*)'ncc=',ncc,'bk=',bk,scx(ncc,bk),scy(ncc,bk),scz(ncc,bk)
 bk=bk+1
 if(bk.gt.10000) then
 goto 164
 endif
 xx1=xx1-l1
 if(xx1.le.1) then
 goto 24
 else
 goto 25
 endif
 24 xx1=xx1+l1
 !write(2556,*)'xx1=',xx1
 xx2=xx1
35 do i2=1,i

if(xx2.eq.x(i2).and.my(k,w5).eq.y(i2).and.mz(k,w5).eq.z(i2).and.lp(i2)
.ne.0) then
 goto 33
 endif
 enddo

 goto 34            !go to the opposite direction!
 33 do ncc2=1,ncc
 do bk2=1,10000

if(xx2.eq.scx(ncc2,bk2).and.my(k,w5).eq.scy(ncc2,bk2).and.mz(k,w5).eq.
scz(ncc2,bk2))then
 goto 34
 endif
 enddo
 enddo
 if(bk.gt.10000) then
 goto 164
 endif
 scx(ncc,bk)=xx2
 scy(ncc,bk)=my(k,w5)
 scz(ncc,bk)=mz(k,w5)
 !write(2556,*)'ncc=',ncc,'bk=',bk,scx(ncc,bk),scy(ncc,bk)
 bk=bk+1
 if(bk.gt.10000) then
 goto 164
 endif
 xx2=xx2+l1
 if(xx2.gt.300) then
 goto 34
 else
 goto 35
 endif
 34 xx2=xx2-l1
 tx=abs(xx2-xx1)
 write(2556,*)'tx=',tx
 !Y axis!
 yy1=my(k,w5)-l1
```

```fortran
  !write(2556,*)'1=','yy1=',yy1
 45 do i2=1,i

if(mx(k,w5).eq.x(i2).and.yy1.eq.y(i2).and.mz(k,w5).eq.z(i2).and.lp(i2)
.ne.0) then
 goto 43
 endif
 enddo

 goto 44            !go to the opposite direction!
 43 do ncc2=1,ncc
 do bk2=1,10000

if(mx(k,w5).eq.scx(ncc2,bk2).and.yy1.eq.scy(ncc2,bk2).and.mz(k,w5).eq.
scz(ncc2,bk2))then
 goto 44
 endif
 enddo
 enddo
 if(bk.gt.10000) then
 goto 164
 endif

 scx(ncc,bk)=mx(k,w5)
 scy(ncc,bk)=yy1
 scz(ncc,bk)=mz(k,w5)
 write(2556,*)'ncc=',ncc,'bk=',bk,scx(ncc,bk),scy(ncc,bk),scz(ncc,bk)
 bk=bk+1
 if(bk.gt.10000) then
 goto 164
 endif
 yy1=yy1-l1
 if(yy1.le.1) then
 goto 44
 else
 goto 45
 endif
 44 yy1=yy1+l1
! write(2556,*)'yy1=',yy1
 yy2=yy1
  !write(2556,*)'1=','yy2=',yy2
 55 do i2=1,i

if(mx(k,w5).eq.x(i2).and.yy2.eq.y(i2).and.mz(k,w5).eq.z(i2).and.lp(i2)
.ne.0) then
 goto 53
 endif
 enddo

 goto 54            !go to the opposite direction!
 53 do ncc2=1,ncc
 do bk2=1,10000

if(mx(k,w5).eq.scx(ncc2,bk2).and.yy2.eq.scy(ncc2,bk2).and.mz(k,w5).eq.
scz(ncc2,bk2))then
```

```fortran
      goto 54
      endif
      enddo
      enddo
      if(bk.gt.10000) then
      goto 164
      endif
      scx(ncc,bk)=mx(k,w5)
      scy(ncc,bk)=yy2
      scz(ncc,bk)=mz(k,w5)
! write(2556,*)'ncc=',ncc,'bk=',bk,scx(ncc,bk),scy(ncc,bk)
      bk=bk+1
      if(bk.gt.10000) then
      goto 164
      endif
      yy2=yy2+l1
      if(yy2.gt.300) then
      goto 54
      else
      goto 55
      endif
 54   yy2=yy2-l1
      ty=abs(yy2-yy1)
      write(2556,*)'ty=',ty
      !z axis!
zz1=mz(k,w5)-l1
        !write(2556,*)'1=','yy1=',yy1
65 do i2=1,i

      if(mx(k,w5).eq.x(i2).and.my(k,w5).eq.y(i2).and.zz1.eq.z(i2).and.lp(i2)
      .ne.0) then
      goto 63
      endif
      enddo

      goto 64           !go to the opposite direction!
 63   do ncc2=1,ncc
      do bk2=1,10000

      if(mx(k,w5).eq.scx(ncc2,bk2).and.my(k,w5).eq.scy(ncc2,bk2).and.zz1.eq.
      scz(ncc2,bk2))then
      goto 64
      endif
      enddo
      enddo
      if(bk.gt.10000) then
      goto 164
      endif
      scx(ncc,bk)=mx(k,w5)
      scy(ncc,bk)=my(k,w5)
      scz(ncc,bk)=zz1
      write(2556,*)'ncc=',ncc,'bk=',bk,scx(ncc,bk),scy(ncc,bk),scz(ncc,bk)
      bk=bk+1
      if(bk.gt.10000) then
      goto 164
```

```fortran
      endif
      zz1=zz1-l1
      if(zz1.le.1) then
      goto 64
      else
      goto 65
      endif
   64 zz1=zz1+l1
!     write(2556,*)'yy1=',yy1
      zz2=zz1
!       write(2556,*)'1=','yy2=',yy2
  165 do i2=1,i

      if(mx(k,w5).eq.x(i2).and.my(k,w5).eq.y(i2).and.zz2.eq.z(i2).and.lp(i2)
     .ne.0) then
      goto 163
      endif
      enddo

      goto 164          !go to the opposite direction!
  163 do ncc2=1,ncc
      do bk2=1,10000

      if(mx(k,w5).eq.scx(ncc2,bk2).and.my(k,w5).eq.scy(ncc2,bk2).and.zz2.eq.
     scz(ncc2,bk2))then
      goto 164
      endif
      enddo
      enddo
      if(bk.gt.10000) then
      goto 164
      endif
      scx(ncc,bk)=mx(k,w5)
      scy(ncc,bk)=my(k,w5)
      scz(ncc,bk)=zz2
!     write(2556,*)'ncc=',ncc,'bk=',bk,scx(ncc,bk),scy(ncc,bk)
      bk=bk+1
      if(bk.gt.10000) then
      goto 164
      endif
      zz2=zz2+l1
      if(zz2.gt.300) then
      goto 164
      else
      goto 165
      endif
  164 zz2=zz2-l1
      tz=abs(zz2-zz1)
      write(2556,*)'tz=',tz
      ttxy=tx*ty*tz
      write(2556,*)'ttxy=',ttxy


      nt=nt+1
      Thvol(k,nt)=tx+ty+tz
```

```fortran
17 nkk2=nkk2+3
if(nkk2.le.nkk) then
goto 12
endif
!Add all volumes!
tvv=0

do nt2=1,nt
write(2002,*)'nt=',nt2,thvol(k,nt2)
tvv=thvol(k,nt2)+tvv
enddo
113 tv(k)=tvol(k)+tvv
cc(k)=nt
1115  write(2001,*)'k=',k,tv(k),cc(k)
13 k=k+1
write(2555,*)'k=',k
 if(k.le.fk) then
goto 1
endif
stop
end
```

Curriculum Vita
Hyen Chung Chun

Education

1992 - 1996	Yeonsei University, Seoul, Korea
	BA in Geology
1996 - 1998	Yeonsei University, Seoul, Korea
	BA in Urban Engineering

2000 - 2003   Rutgers, the State University of New Jersey, New Brunswick, New Jersey

Master in environmental sciences (degreed conferred 2004)

Thesis Topic: Size and management effects on entropy of soil aggregate   structure

Adviser: Dr. Daniel Gimenez

2004 – Present   Rutgers, the State University of New Jersey, New Brunswick, New Jersey

Ph.D. in environmental sciences (expected, 2008)

Thesis Topic: Characterization of soil structures under elevated CO_2 / temperature and simulation of three dimensional pore structure
Adviser: Dr. Daniel Gimenez

Publications
Chun, H.C., D. Gimenez, and S.W. Yoon (2008) Properties of Intraggregate Pores: Aggregate Size and Soil Management Effects (submitted)
Chun, H.C., D. Gimenez, L. Ziska, K. George, and R. Heck (2008) Characterization of Changes in Soil Structure along an Urban-Ls CO_2 / Temperature Gradient (Manuscript in preparation)

Presentation
Chun, H.C. & K. Lee. 2001. Transport of DNAPL in Groundwater System. Environmental Management and Technology Conference and Exhibition, Atlantic City, New Jersey.
Chun, H.C., D. Gimenez, L. Ziska, K. George & R.Heck. 2006. Characterization of Changes in Soil Structure along an Urban-Ls CO_2 / Temperature Gradient. American Society of Agronomy Annual Meeting, Indianapolis, Indiana.

Gimenez, D. , R. R Filgueira, S.W. Yoon & H.C. Chun. 2006. Fractal Models of Soil Water Retention: How Good are They?. 18th World Congress of Soil Science, Philadelphia, Pennsylvania.

Gimenez, D., S. W. Yoon, H.C. Chun & Heck, R. 2006. Testing Fractal Models of Soil Water Retention. American Society of Agronomy Annual Meeting, Indianapolis, Indiana.

Gimenez, D., H.C. Chun, L. Ziska & R. Heck. 2007. Water Retention Properties along a Carbon Dioxide/Temperature Gradient. ASA-CSSA-SSSA International Annual Meetings. New Orleans, Luisiana.

Chun, H.C., D. Gimenez, L. Ziska & R. Heck. 2007. Three Dimensional Distribution of Mm Scale Porosity in Soils Under Elevated CO_2 and Temperature Conditions. ASA-CSSA-SSSA International Annual Meetings. New Orleans, Luisiana. (Oral presentation)